National Aeronautics and Space Administration

HELIOPHYSICS MISSION CONCEPT STUDY FOR THE 2022–2033 DECADAL SURVEY

30 November 2022

Exploring the Heliosphere from the Solar Interior to the Solar Wind

FIREFLY

Nour E. Raouafi
Principal Investigator
Johns Hopkins Applied Physics Laboratory
nour.raouafi@jhuapl.edu

James D. Kinnison
Design Study Lead
Johns Hopkins Applied Physics Laboratory
jim.kinnison@jhuapl.edu

www.nasa.gov

Data Release, Distribution & Cost Interpretation Statements

This document is intended to support the 2024–2033 Solar and Space Physics Decadal Survey.

The data contained in this document may not be modified in any way.

Cost estimates described or summarized in this document were generated as part of a preliminary concept study, are model-based, assume an APL in-house build, and do not constitute a commitment on the part of APL.

Cost reserves for development and operations were included as prescribed by the NASA ground rules for the Mission Concept Studies in Support of Heliophysics Decadal Survey, dated Jan 2022. Unadjusted estimate totals and cost reserve allocations would be revised as needed in future more-detailed studies as appropriate for the specific cost-risks for a given mission concept.

Acknowledgments

The Johns Hopkins Applied Physics Laboratory would like to thank all of the Firefly team members, the National Academies of Sciences, Engineering, and Medicine Solar and Space Physics Decadal Survey 2024–2033, and the NASA Heliophysics Science Division for supporting this study.

ROLE	NAME	AFFILIATION
SCIENCE TEAM		
Leadership	Nour E. Raouafi, Study Lead	Johns Hopkins Applied Physics Laboratory
Science	Angelos Vourlidas	Johns Hopkins Applied Physics Laboratory
	George C. Ho	Johns Hopkins Applied Physics Laboratory
	Glenn M. Mason	Johns Hopkins Applied Physics Laboratory
	Juliana T. Vievering	Johns Hopkins Applied Physics Laboratory
	Sofiane Bourouaine	Johns Hopkins Applied Physics Laboratory
	Vamsee K. Jagarlamudi	Johns Hopkins Applied Physics Laboratory
	J. Todd Hoeksema	Stanford University
	Jeffrey S. Newmark,	NASA GSFC
	Nicholeen M. Viall	NASA GSFC
	Adam Szabo	NASA GSFC
	Thomas E. Berger	University of Colorado Boulder
	Donald M. Hassler	Southwest Research Institute
	Lisa A. Upton	Southwest Research Institute
	Marta Casti	Catholic University of America & NASA GSFC
	Anthony W. Case	CFA Smithsonian Astrophysical Observatory
	Susan T. Lepri	University of Michigan
	Marco Velli	University of California Los Angeles
	Manolis K. Georgoulis	Academy of Athens Res. Ctr. For Astronomy & Applied Math
	John M. Laming	Naval Research Laboratory
ENGINEERING TEAM		
Design Study Lead/MSE	Jim Kinnison	Johns Hopkins Applied Physics Laboratory
Project Management	Andy Santo	Johns Hopkins Applied Physics Laboratory
RF/Communications	Mike O'Neil	Johns Hopkins Applied Physics Laboratory
Harness Design	Kyle Norman	Johns Hopkins Applied Physics Laboratory
Scheduling	Dewey Barlow	Johns Hopkins Applied Physics Laboratory
Operations	Josh Albers	Johns Hopkins Applied Physics Laboratory
	James Hudson	Johns Hopkins Applied Physics Laboratory
Propulsion	Stewart Bushman	Johns Hopkins Applied Physics Laboratory
	Seth Kijewski	Johns Hopkins Applied Physics Laboratory
Avionics	Adam Mizes	Johns Hopkins Applied Physics Laboratory
Radiation Design & Mitigation	Jamie Porter	Johns Hopkins Applied Physics Laboratory
Thermal Engineering	Eric Wallis	Johns Hopkins Applied Physics Laboratory
Scheduling	Dewey Barlow	Johns Hopkins Applied Physics Laboratory
Ground Support	Mike Furrow	Johns Hopkins Applied Physics Laboratory
	Adam Byerly	Johns Hopkins Applied Physics Laboratory
Flight Software	Musad Haque	Johns Hopkins Applied Physics Laboratory
MSE Support	Rafael M. Perez	Johns Hopkins Applied Physics Laboratory
Power Design	Neville/Butler	Johns Hopkins Applied Physics Laboratory
Flight Software	Michelle Chen	Johns Hopkins Applied Physics Laboratory
MSE Support	Debarati Chattopadhyay	Johns Hopkins Applied Physics Laboratory
Guidance Navigation & Control	David Carrelli	Johns Hopkins Applied Physics Laboratory
	Ian Whiting	Johns Hopkins Applied Physics Laboratory
Mechanical/Structure	Felipe Ruiz	Johns Hopkins Applied Physics Laboratory
Mission Design & Analysis	Jacob Englander	Johns Hopkins Applied Physics Laboratory
Cost Modeling	Ben Clare	Johns Hopkins Applied Physics Laboratory
Mission Design & Analysis	Jackson Shannon	Johns Hopkins Applied Physics Laboratory
Payload	Kim Slack	Johns Hopkins Applied Physics Laboratory
Integration & Test	Joe Pulkowski	Johns Hopkins Applied Physics Laboratory
LAYOUT & DESIGN TEAM		
Editing, Layout & Design	Marcie Steerman	Johns Hopkins Applied Physics Laboratory

FIREFLY

Exploring the Heliosphere from the Solar Interior to the Solar Wind

Magnetism is the primary force behind solar and stellar physics. The solar dynamo drives interplanetary space environments, influences the composition and evolution of planetary atmospheres, and determines the habitability of orbiting planets. But our studies of the Sun have always been limited to a single perspective – the ecliptic plane. Firefly offers a new perspective.

Firefly's unprecedented global coverage of the Sun and inner heliosphere provides the observations required to finally resolve long-standing questions in solar and stellar physics.

Firefly focuses on the global structure and dynamics of the Sun's interior, the generation of solar magnetic fields, deciphering the origins of the solar cycle, the conditions leading to the explosive activity, and the structure and dynamics of the corona as it drives the heliosphere.

Mission Concept Science Objectives

Firefly closes long-standing knowledge gaps in heliophysics. Its constellation of spacecraft acquires both remote sensing and in situ observations of the heliosphere from Jupiter to the top of the sun.

- Understand how surface and subsurface flows and toroidal magnetic field instabilities produce the cyclic solar dynamo – the root cause of solar activity.
- Understand the conditions leading to solar explosive activity and the role of large-scale magnetic field connections.
- Determine how conditions in the solar wind vary with latitude and longitude in response to changing global solar conditions and throughout the solar cycle.
- Understand how energetic particles are accelerated and transported through the heliosphere.

Understanding the Sun & Its Environment

Firefly provides diverse and complementary observations across multiple disciplines, bringing together a diverse group of scientists and engineers to view the heliosphere as a system.

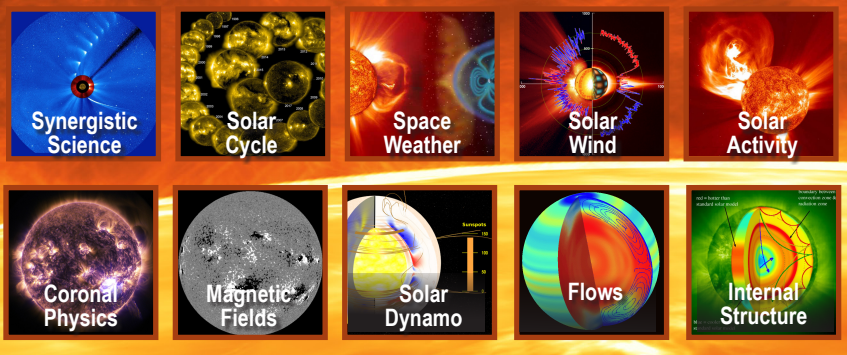

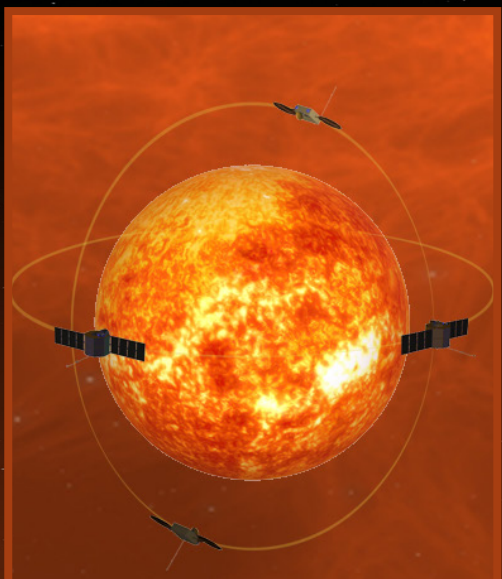

4-Spacecraft Constellation Provides Unprecedented, Near Global Coverage of the Sun

Firefly's innovative mission concept is designed to close long-standing knowledge gaps in heliophysics. A four-spacecraft constellation provides both remote sensing and in situ observations of the Sun and heliosphere from a full 4π-steradian field-of-view.

With two spacecraft in a polar orbit (~180° apart) and two in an elliptical orbit (90°–120° apart), Firefly observes the heliosphere from the Sun's interior, to the photosphere, through the corona, and into the solar wind ... simultaneously from multiple vantage points, providing continual global coverage over much of the solar cycle.

FIREFLY DESIGN STUDY

Designed to Be NASA's Next Heliophysics Flagship Mission

- Firefly encompasses an entire solar cycle and stretches from the far reaches of Jupiter to a first-ever view of the solar pole regions.
- Firefly offers an opportunity to study the Sun as a model star, providing a valuable analog for studying distant stars.
- Firefly is multi-disciplinary, addressing pressing heliophysics topics and offering opportunities to study astrophysical phenomena from the solar interior through the atmosphere to the inner Heliosphere.

	Phase A–D (FY25$K)	Phase E–F (FY25$K)	Total (FY25$K)
Total w/o Reserves	1800	251	2051
Reserves	740	63	803
Total w Reserves	2540	314	2854
Total w/o LV	2226	314	2540

Solar-Electric Propulsion Enables the "Impossible" Orbit

- Launch in early- to mid-2030s (polar S/C on Falcon Heavy Expendable; elliptic S/C on Falcon-9 ASDS)
- The elliptic S/C launch together using lunar gravity assists with phasing loops to transfer to STEREO-like orbits 120° behind and ahead of Earth (chem propulsion only).
- The polar S/C launch together using solar electric propulsion to arrive at final orbit with 180° of separation for simultaneous observation of both poles of the Sun.
- Establishes 10-year science mission, with 2 years in heliocentric science orbits

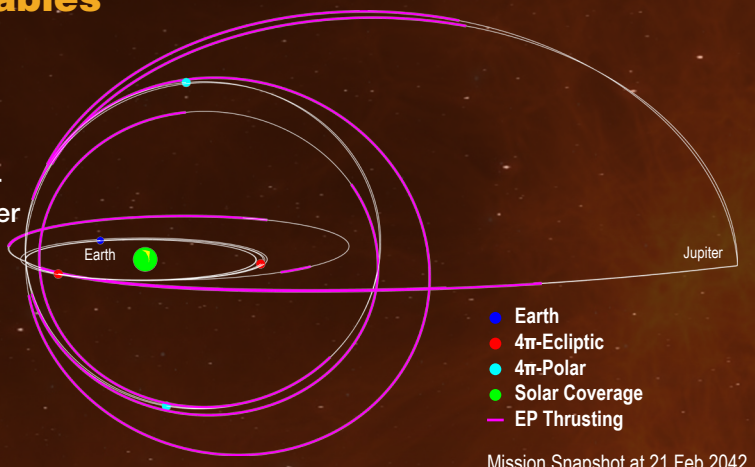

Mission Snapshot at 21 Feb 2042

Payloads Optimized for Science & Cost

Mission architecture supports a full instrument complement on each of the four S/C, but all instruments are not required to achieve science objectives. By tailoring the payload for each spacecraft, Firefly reduces cost and schedule risk, while accomplishing all mission objectives.

	Ecliptic-A	Ecliptic-B	Polar-A	Polar-B
Doppler Vector Magnetograph	✓	✓	✓	✓
EUV Imager/Solar Irradiance	✓	✓	✓	
White Light Coronagraph	✓	✓	✓	✓
Heliospheric Imager	✓			
Fluxgate Magnetometer	✓	✓	✓	✓
Faraday Cup	✓	✓	✓	✓
Solar Wind Composition (SPICES)			✓	
Solar Energetic Particle Suite (SIS+EPT-HET)	✓	✓	✓	

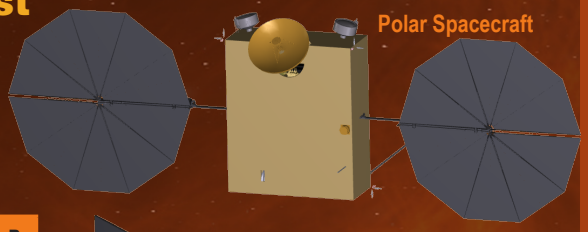

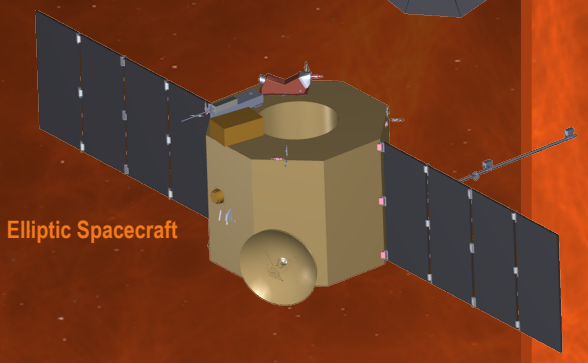

Spacecraft Characteristics

Modular spacecraft design and common subsystem elements facilitate manufacturing and integration of four spacecraft.

	Ecliptic Spacecraft (ea)	Polar Spacecraft (ea)
Design Life	15 years	15 years
Structure	Aluminum, Aluminum Honeycomb	Aluminum, Aluminum Honeycomb
Thermal	Passive w/ louvers, heat pipes & thermostatically controlled heaters	Passive w/ louvers, heat pipes & thermostatically controlled heaters
Estimated ΔV	515–659 m/s	
Attitude Control	3-axis. 60 arcsec about pitch and yaw, and 432 arcsec about roll relative to sun center	
Power	Rigid Deployed 5.0 m^2 Multi-Junction GaAs	Flexible Deployed 91.0 m^2 Multi-Junction GaAs LILT Cell
Comms	Hybrid X-band (uplink and downlink) and Ka-band (downlink only) for high data volume and access when Ka-band is not available.	

Graphic Cover i
Acknowledgments iii
Fact Sheet iv
Executive Summary 1
1. Scientific Investigation 2
1.1. Relevance to the Solar Terrestrial Probes Science Investigation 2
1.2. Science Motivation 2
1.3. Mission Concept Science Objectives 4
1.3.1. OBJECTIVE 1: Understand how surface and subsurface flows, and toroidal magnetic field instabilities produce the cyclic dynamo, the root cause of solar activity 4
1.3.2. OBJECTIVE 2: Understand solar magnetic eruptions and the role of large-scale magnetic field connections in triggering eruptions 8
1.3.3. OBJECTIVE 3: Determine how conditions in the solar wind vary with latitude and longitude in response to changing global solar conditions and throughout the solar cycle 10
1.3.4. OBJECTIVE 4: Understand where and how energetic particles are accelerated and transported through the inner heliosphere 12
1.4. Synergistic Science 13
1.4.1. Support for Human Exploration 13
1.4.2. High Risk, High Reward Science: the Solar Gravity Modes 13
1.4.3. Cross-Disciplinary Science 14
1.4.4. Make Headway in Exploration, Innovation & Inclusiveness 15
1.5. Mission Concept Science Traceability 15
1.6. Science Closure 18
1.6.1. OBJECTIVE 1: Understand how surface and subsurface flows, and toroidal magnetic field instabilities produce the cycle dynamo, the root cause of solar activity. 18
1.6.2. OBJECTIVE 2: Understand solar magnetic eruptions and the role of large-scale magnetic field connections in triggering eruptions. 19
1.6.3. OBJECTIVE 3: Determine how conditions in the solar wind vary with latitude and longitude in response to changing global solar conditions throughout the solar cycle. 19
1.6.4. OBJECTIVE 4: Understand where and how energetic particles are accelerated and transported through the inner heliosphere. 20
2. High-Level Mission Concept 21
2.1. Overview 21
2.1.1. Mission Architecture 21
2.1.2. Environments 22
2.2. Concept & Technology Maturity 22
2.3. Key Trades 22
2.3.1. Payload Optimization 23
2.3.2. Flight System Development Optimization 23
3. Technical Overview 24
3.1. Instrument Payload Description 24
3.1.1. Doppler Vector Magnetograph 24
3.1.2. Extreme Ultraviolet Imager 25
3.1.3. White-Light Coronagraph 26
3.1.4. Solar Irradiance 26
3.1.5. White-Light Heliospheric Imager 27

3.1.6. Fluxgate Magnetometer 27
3.1.7. Faraday Cup 28
3.1.8. Solar Wind Composition 29
3.1.9. Energetic Particle Suite 30
3.2. Flight System 30
3.2.1. Firefly-Ecliptic 32
3.2.2. Firefly Polar 37
3.2.3. Spacecraft Resources 41
3.3. Mission Design & Concept of Operations 44
3.4. Ground System 49
3.5. Risk List 50
4. Development Schedule & Constraints 51
5. Mission Life-Cycle Cost 58
5.1. Introduction 58
5.2. Mission Ground Rules & Assumptions 58
5.3. Cost Benchmarking 59
5.4. Methodology & Basis of Estimate 59
5.4.1. WBS 1, 2, 3 Project Management, Systems Engineering, Mission Assurance (PMSEMA) 59
5.4.2. WBS 4 Science 59
5.4.3. WBS 5 Payload 59
5.4.4. WBS 6 Spacecraft 60
5.4.5. WBS 7 & 9 Mission Operations (MOps) and Ground Data Systems (GDS) 61
5.4.6. WBS 8 Launch Vehicle & Services 61
5.4.7. WBS 10 System Integration & Testing (I&T) 61
5.4.8. Deep Space Network (DSN) Aperture Fees 61
5.4.9. Confidence & Cost Reserves 61
5.5. Enhancement & De-Scope Options 62
5.5.1. Enhancement 3 63
5.5.2. Enhancement 2 63
5.5.3. Enhancement 1 64
5.5.4. Descope 1 64
5.5.6. Descope 2 65
5.5.7. Descope 3 65
5.5.8. Descope 4 66
5.5.9. Descope 5 66
Appendix A. Mission Design Analysis 67
A.1 Physical Models 67
A.2 FF-P Launch Flexibility 67
A.2 FF-E Launch Flexibility 68
A.3 FF-E Rideshare Opportunity 68
Appendix B: Acronyms & Abbreviations 69
Appendix C: Institutions Involved in the Mission Concept Study 75
Appendix D: References 76
Appendix E: Additional Details 80

Executive Summary

Magnetism is paramount to most, if not all, solar and stellar physics phenomena and how stars interact with planetary environments, particularly those residing in the habitable zone. Magnetic fields are generated by dynamo processes in the interior and at the surface. They trigger activity that can crucially affect the composition and the physical and chemical evolution of planetary atmospheres and consequently the habitability of these planets. The Sun is the ideal target to understand stellar magnetism due to its proximity and the extensive observations gathered over the last few decades. Nonetheless, the current single viewpoint of observations from the Sun-Earth line or within the ecliptic plane is a severe obstacle, limiting the instantaneous coverage of the solar magnetic surface, including access to the solar poles, which are critical for deciphering the solar dynamo, the consequent evolution of solar magnetic fields, and the solar cycle.

Firefly is an innovative mission concept designed to close long-standing knowledge gaps in heliophysics. A constellation of spacecraft will provide both remote sensing and in situ observations of the Sun and heliosphere from a full 4π-steradian field of view. This mission implements a holistic observational philosophy that extends from the Sun's interior, to the photosphere, through the corona, and into the solar wind, simultaneously with multiple spacecraft at multiple vantage points, optimized for continual global coverage over much of a solar cycle. The mission constellation includes two spacecraft in the ecliptic plane and two flying as high as ~70º solar latitude. The overarching goal of the Firefly mission concept is ***to understand the global structure and dynamics of the Sun's interior, the generation of solar magnetic fields, the origin of the solar cycle, the causes of solar activity, and the structure and dynamics of the corona as it creates the heliosphere.***

To advance the scientific knowledge needed to characterize the heliosphere, the Firefly mission concept has defined four fundamental science objectives: (**1**) *Understand how surface and sub-surface flows, and toroidal magnetic field instabilities produce the cyclic solar dynamo, the root cause of solar activity*; (**2**) *Understand the conditions leading to solar explosive activity and the role of the large-scale magnetic field roles*; (**3**) *Determine how conditions in the solar wind vary with latitude and longitude in response to changing global solar conditions and throughout the solar cycle*; and (**4**) *Understand how and where energetic particles are accelerated and transported through the heliosphere*.

The primary mission design requirement is to achieve complete coverage of the entire solar sphere for >80% of the prime mission. To meet this, we adopt the pragmatic philosophies of SOLPEX, Solaris, SPOC, and STEREO and rely on proven launch capabilities and mission design approaches to envision the following mission concept.

Firefly consists of two pairs of spacecraft, each carrying remote-sensing (Doppler magnetograph, EUV coronal imager, WL coronagraph, and heliospheric imagers) and in situ (particles and fields package) payloads. One pair, referred to as 'Firefly Polar' (hereafter FF-P), uses a Jupiter gravity assist to reach a highly inclined (~70 degrees relative to the ecliptic) orbit near 1 AU. The FF-P spacecraft use solar electric propulsion to circularize their orbits and increase their relative phasing by ~180 degrees. The second pair, referred to as 'Firefly Ecliptic' (hereafter FF-E), is launched into near-circular orbits at 1 AU. Each spacecraft will be parked between 90 – 120 degrees relative to the Sun-Earth line, with one placed ahead of the Earth and the second placed behind. The combined observations of the four spacecraft provide nearly continuous global coverage of the photospheric magnetic field, the solar corona, and local heliospheric conditions, while enabling both global and local helioseismology measurements throughout the solar convective zone.

1. Scientific Investigation

1.1. Relevance to the Solar Terrestrial Probes Science Investigation

The science objectives of the Firefly mission concept are to understand the global structure and dynamics of the Sun's interior, the generation of solar magnetic fields through the dynamo processes, the origin of the solar cycle, the causes of solar eruptive activity, and the structure and dynamics of the corona as it creates the heliosphere. The Firefly science goals are central to the Solar Terrestrial Probes (STP) program-level science objective "Understand the fundamental physical processes of the complex space environment throughout our solar system, which includes the flow of energy and charged material, known as plasma, as well as a dynamic system of magnetic and electric fields." The continuous and near-simultaneous observations from multiple vantage points will substantially expand our knowledge of the solar environment and thus greatly advance our capabilities to predict solar magnetic activity and space weather. Firefly science goals are essential to the STP program-level science objective "Develop the capability to predict the extreme and dynamic conditions in space in order to maximize the safety and productivity of human and robotic explorers."

1.2. Science Motivation

Magnetism is paramount to most, if not all, solar and stellar physics phenomena and how stars interact with planetary environments, particularly those residing in the habitable zone. Magnetic fields are generated by dynamo processes in the convection zone and produce activity that can crucially affect the physical and chemical evolution of planetary atmospheres and consequently the habitability of these planets [Lüftinger et al. 2015; Gallet et al. 2017]. The Sun is the only star available for revealing the mechanisms of stellar magnetism thanks to its proximity to Earth. Nonetheless, observing the Sun from only a single viewpoint is a severe obstacle, limiting our ability to ascertain global dynamics. In particular, from our vantage point in the ecliptic, we cannot observe the solar poles, which are critical for deciphering how meridional and differential rotational flows power the solar dynamo and the consequent evolution of solar magnetic fields. For a detailed overview on the benefit of solar observations from multiple viewpoints [Gibson 2018].

In spite of decades of ground- and space-based observations of the Sun, there are major gaps in our understanding of how it generates its cyclic magnetic fields, which in turn create instabilities impacting the whole heliosphere. Examples of these knowledge gaps (Exhibit 1) include, *but are not limited to:*

1. **Convection Zone Flows.** At least three major gaps exist in observations of the solar subsurface flows that are critical to understanding the solar dynamo
   - **a.** A "polar gap" exists above about 60° in latitude in which both the magnetic field and the plasma flows as a function of depth remain impossible to observe from our sole vantage point in the ecliptic plane (Exhibit 1a).
   - **b.** The variable longitudinal structure and the dynamics of zonal flows, including their variations over the cycle, cannot be fully observed from a single viewpoint.
   - **c.** The structure of meridional circulation, in particular whether there is a single cell or multiple cells in latitude, longitude, depth and time, remains unknown, again because we cannot resolve the critical high-latitude regions from the ecliptic plane.
2. **Magnetic Fields.** Magnetic fields are the primary inner boundary condition of the corona and the heliosphere. Magnetic field measurements from a single view point cannot provide data on the full disk. They are accurate only up to about 60° from the disk center (Exhibit 1b). Thus global "synoptic" maps of the magnetic field (Exhibit 1c) that are used to drive coronal magnetic field and solar wind models are stitched together from daily observations of a limited portion of the Sun, producing a fictional construct that has major errors, particularly during solar maximum. In

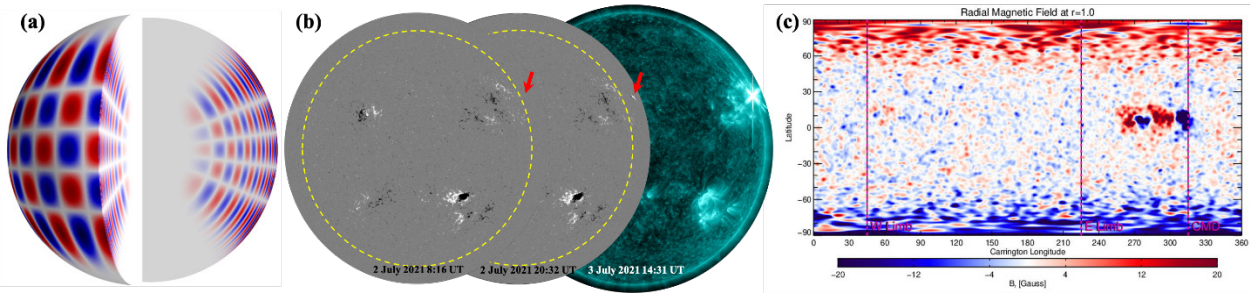

Exhibit 1. *Example of the Major Knowledge Gaps in Our Understanding of the Sun and the Heliosphere. (a) SOHO/MDI helioseismic measurement of a solar global oscillation mode; global modes are insensitive to conditions at high latitudes. (b) Example of the failure of Sun-Earth line magnetograms to capture a newly emerging active region near the limb. This active region emerged within 12 hours and produced an X1.5-class flare that could not be forecast due to lack of magnetic field data for the active region. The yellow dashed line shows the S/N limit for magnetogram data away from disk center. (c) Photospheric radial magnetic field daily-update "synoptic map" built using measurements taken over a 27-day "Carrington Rotation" (CR) during CR 2217 and 2218. Note that the polar regions are extrapolated and distorted due to low signal-to-noise above 60° latitude and lack of visibility [courtesy Cooper Downs, PSI]*

addition, the critical unobserved polar regions must be extrapolated from noisy high-latitude data leading to systematic errors that propagate to coronal field and solar wind models (Exhibit 1c). Synoptic maps cannot, by definition, include: the evolution of active regions that have rotated to the far side of the Sun, newly emerged far-side active regions, or complete and accurate polar field measurements.

3. **Continuity.** To understand the physical processes leading to the formation of complex sunspot active regions and filaments prone to eruption, continuity of observations is essential to following the evolution of magnetic structures and the buildup of energy in the solar corona. This is not possible from single vantage point observations. Earth-based observations capture only about one third of the Sun's activity belts at any one time, leading to many critical events that cannot be fully analyzed. Exhibit 1b provides an excellent example of these events as flux emergence started just outside the 60° circle where magnetic field measurements are reliable, resulting in an X-class flare about a day later. In addition, one of the most tantalizing findings of multi-viewpoint imaging is the evidence for long-range, interhemispheric, interactions between eruptive events occurring over the span of hours to days across a full solar hemisphere. Another example is the 23 Jul 2012 "Carrington Event"-level eruption that took place out of view of our Sun-Earth line instruments but was luckily captured by the STEREO-A spacecraft about 125° from the Sun-Earth line.
4. **Structure & Evolution of the Heliosphere.** Conditions in the solar wind vary with latitude and longitude in response to changing global solar conditions, but the exact links to the global magnetic field are not understood. The role of the polar fields in structuring the large-scale dipolar magnetic field of the Sun is critical to understanding how the global solar magnetic field structures the heliosphere, from interplanetary space, past the Kuiper belt and Oort cloud, and to the heliopause interface with interstellar space. Until we can fully measure the solar magnetic field over at least a solar cycle, we will not be able to link solar variability to observed changes in the distant heliosphere.

The following sections outline a new mission concept that will overcome the challenges discussed above and lead to major discoveries in heliophysics.

Exhibit 2. Firefly Mission Objectives.

1. **Understand how surface and sub-surface flows, and toroidal magnetic field instabilities produce the cyclic solar dynamo, the root cause of solar activity.**
   a. How do the solar differential rotation and meridional flow evolve through the solar cycle?
   b. What is the non-axisymmetric flow structure of the solar polar regions?
   c. Is surface flux transport of active region magnetic fields sufficient to explain the evolution of polar magnetic fields over the solar cycle?
2. **Understand the conditions leading to solar explosive activity and the role of the large-scale magnetic field connections.**
   a. How does non-potential complexity of the magnetic field transfer from the photosphere to the corona, and how does that lead to solar eruptions?
   b. What are the triggers and the processes at the origin of the coronal eruptive activity?
   c. How does the solar spectral irradiance (SSI) vary with latitude and over the solar cycle?
3. **Determine how conditions in the solar wind vary with latitude and longitude in response to changing global solar conditions and throughout the solar cycle.**
   a. How does the 4π solar wind originate from its sources and moves out to the heliosphere?
   b. How does the corona drive the inner heliosphere through the solar cycle?
   c. What are the mechanisms for accelerating the thermal and suprathermal solar wind? How do solar wind structures evolve throughout the heliosphere?
4. **Understand how energetic particles are accelerated and transported through the inner heliosphere.**
   a. How are energetic particles accelerated and transported throughout the inner heliosphere, particularly at the high solar latitudes?
   b. How are energetic particles transported to the high solar latitudes, and how are CIRs electrons transported to the polar latitudes?
   c. What are the physical processes at the origin of the CIRs' energetic particle acceleration, and where does that occur?

1.3. Mission Concept Science Objectives

Firefly is an innovative mission concept designed to close long-standing knowledge gaps in heliophysics. A constellation of spacecraft will provide both remote sensing and in situ observations of the Sun and heliosphere, sampling the full 4π-steradians of the solar surface. It implements a holistic observational philosophy that extends from the Sun's interior, to the photosphere, through the corona, and into the solar wind simultaneously, with multiple spacecraft at multiple vantage points, optimized for continuous global coverage over much of a solar cycle. The mission constellation includes two spacecraft off the Sun-Earth line in the ecliptic plane and two orbiting out of the ecliptic at ~70º solar latitude. The overarching goal of the Firefly mission concept is ***to understand the global structure and dynamics of the Sun's interior, the generation of solar magnetic fields, the origin of the solar cycle, the causes of solar activity, and the structure and dynamics of the corona as it creates the heliosphere***. To advance the scientific knowledge needed to characterize the heliosphere, the Firefly mission concept has the following science objectives:

In the remainder of this section, we summarize the Firefly science objectives and discuss how the mission design will enable us to address these objectives.

1.3.1. OBJECTIVE 1: Understand how surface and subsurface flows, and toroidal magnetic field instabilities produce the cyclic dynamo, the root cause of solar activity

The cyclic solar dynamo remains one of the most enigmatic aspects of the Sun. Despite decades of research and a general consensus that the Sun's dynamo operates through inductive fluid motions in the convection zone [Charbonneau 2020], we have an incomplete picture of the global-scale motions that drive it, both in the interior and at the surface. Model approaches vary, but all models have to account for

observed flows and field characteristics (e.g., Dikpati [2014]). For example, global-scale magnetohydrodynamic (MHD) models based on Babcock-Leighton flux transport can currently produce 11-year sunspot activity cycles by tuning unmeasured flow parameters such as turbulent diffusivity and differential rotation in the convection zone. However, these models are unable to predict critical details of the solar activity cycle, such as the timing of the sunspot maximum, the north-south asymmetry in activity, and longitudinal flux emergence sites.

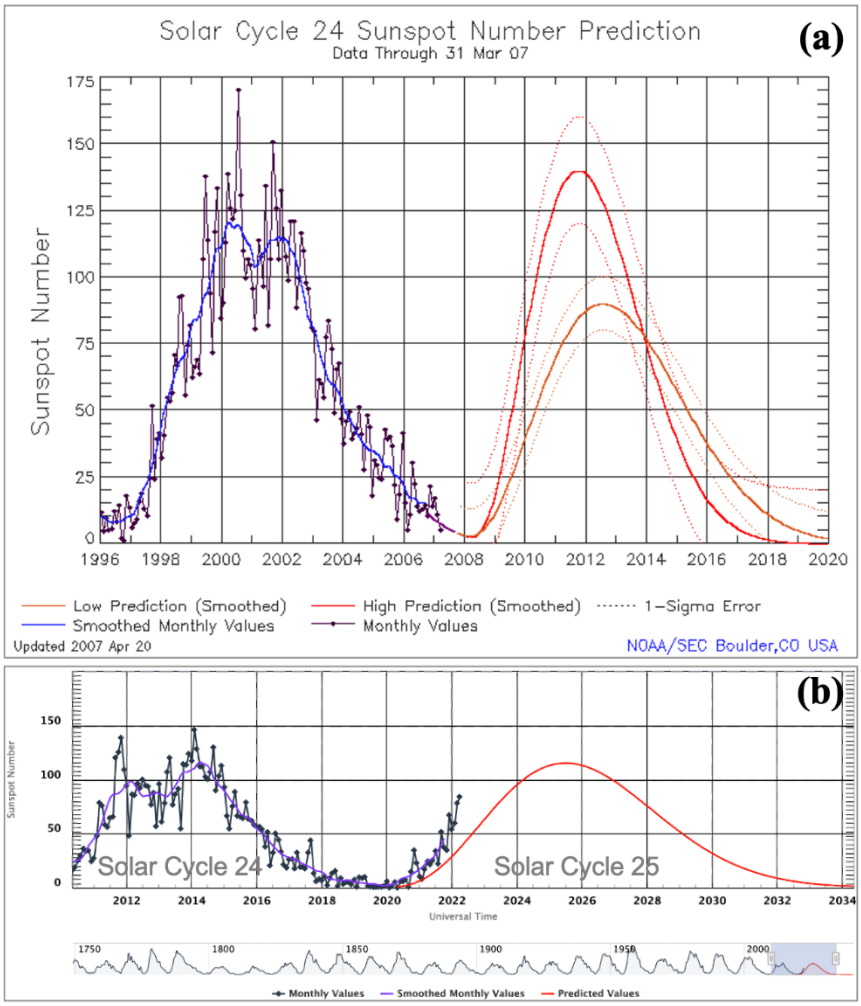

***Exhibit 3**. Consensus predictions of the Solar Cycles 24 (a) and 25 (b). The differences between the predictions and the real data are significant. Unless we obtain extensive coverage observations of the Sun from within and outside the ecliptic plane (particularly the solar polar region), solar cycle prediction will remain unreliable. Source: NOAA/SWPC.*

Predictions of Solar Cycle 24 (Exhibit 3a) ranged from a strong with a maximum sunspot number range 120–160 to a weak cycle with sunspot number range 80–100 cycle with an average of 140 and 90 sunspots, respectively. As Solar Cycle 24 unfolded, it was more toward the latter prediction with a higher sunspot number at the maximum (~114). The predicted timing of the solar cycle maximum also differed from the real one by about a year. Solar Cycle 25 is also anticipated to be a weak one. However, the cycle's rising phase is higher than predicted (Exhibit 3b). It is not clear whether this will significantly deviate from the prediction as the cycle progresses toward the maximum. The seemingly unreliable predictions may be related to the models. But in point of fact, we do not possess the data needed to understand how the solar cycle works. Relying on single vantage point observations, particularly from the ecliptic, will not solve this problem.

A major goal of long-term space weather forecasting is to accurately and precisely predict the timing and magnitude of oncoming activity cycles. But these goals will remain unmet until we develop data-assimilative, non-axisymmetric, global dynamo models, along with the necessary measurements of surface and subsurface flows to feed such models.

Major gaps exist in our observations of the solar surface and subsurface flows that are critical to understanding the solar dynamo (Section 1.2). Time variations in speed and profile of the Sun's global meridional circulation play a crucial role in determining the solar cycle properties (e.g., amplitude, phase, duration, etc.) For instance, the unusually long and deep minimum between Solar Cycles 23 and 24 was modeled by Dikpati [2010] as the result of a change from a latitudinal two-cell meridional flow in Solar

Cycle 22 to a one-cell flow in Cycle 23 (Exhibit 4a), and by Nandy [2011] as a temporal change of meridional flow speed during the declining phase of each cycle. Knowing the variation of the profile and speed of the meridional circulation during the solar cycle would significantly improve our understanding of the solar dynamo and prediction of the next solar cycle.

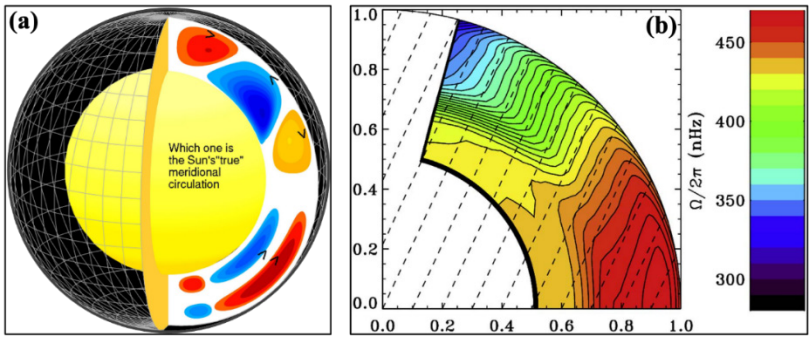

Exhibit 4. *(**a**) The structure of the meridional circulation in radius and in depth is debated. The meridional circulation may or may not include counter cells at high latitude, a shallow return flow or a return flow at the base of the convection zone, and these may change over the cycle. Source: NCAR/HAO. (**b**) Solar differential rotation in the upper meridional plane, in and below the convection zone, as a function of latitude and depth. The rotation rate is averaged in longitude and time from 1995 to 2009. The polar gap is evident. From Thompson et al. [2003].*

Perhaps the largest gap in our knowledge of the solar dynamo is that neither the meridional circulation nor differential rotation have been measured in the solar polar regions. The SO/PHI instrument on the Solar Obiter mission will improve on the current measurements as the spacecraft will be about 30° out of the ecliptic. However, the remote sensing observations are limited to short windows that might not provide the necessary temporal coverage. This "polar gap" is due to ***all*** surface magnetic and helioseismic measurements to date being from an Earth-based vantage point, i.e., confined to the ecliptic plane. From Earth, each pole can only barely be seen during half of the year due to the inclination of the ecliptic to the solar rotation axis, but even these measurements are located outside of the 60° accuracy zone (Exhibit 4b) and are plagued by low signal to noise (S/N). Exhibit 3b shows a longitudinally averaged helioseismic map of internal solar differential rotation [Thompson 2003] with a clear polar gap due to the fact that global modes are insensitive to high-latitudes. Higher-resolution local helioseismology measurements do not help: the high line-of-sight (LOS) angles to the solar poles from the ecliptic still impose low S/N conditions on local helioseismology. Helioseismic measurements from a single platform orbiting over the solar poles can fill the near-surface layers of this polar gap, but measuring deeper flows over the solar cycle will require coordinated Doppler measurements from multiple polar vantage points over significant fractions of a solar cycle.

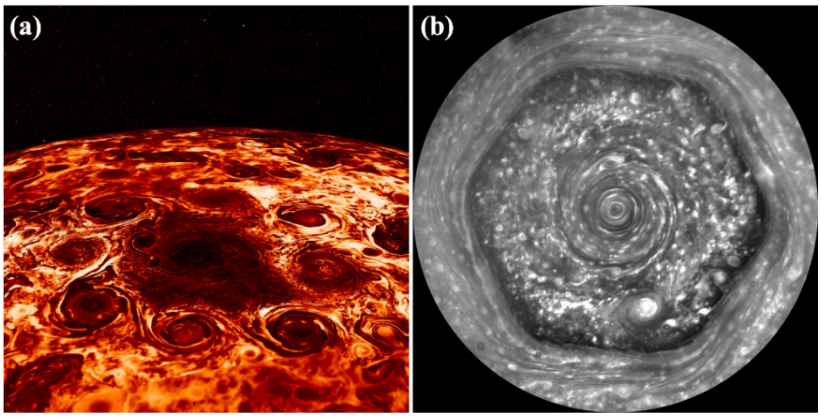

Exhibit 5. *(a)* Jupiter's north pole shows the central cyclone encircled by eight cyclones, as seen by NASA's Juno mission on 2 Feb 2017. The composite infrared image is derived from observations by the Jovian Infrared Auroral Mapper (JIRAM). (b) *View from NASA's Cassini mission is the highest-resolution view of the unique six-sided jet stream at Saturn's north pole known as "the hexagon."* ***These views were not possible before Juno's and Cassini's passes above the Jovian and Saturn poles.***

Similarly, magnetic field measurements depend largely on LOS polarization and are severely degraded far from disk center due to projection, inclination, and solar atmospheric effects, although some preliminary measurements have been achieved [Tsuneta 2008]. These preliminary measurements showed surprising hints of strong-field regions near the poles where current models predict only weak network fields. Are these strong field regions the signatures of complex polar vortex flows like those seen on gas giant planets (Exhibit 5)? Ecliptic-plane observations alone cannot answer this critical question. If polar flows on the

Sun turn out to be as complex as those seen on Jupiter and Saturn (e.g., Gibson et al. [2018]), it would have a revolutionary impact on solar dynamo models since these models depend critically on the structure and magnitude of polar flows.

Rossby waves, long theorized but only recently observed [Löptien 2018; Hathaway & Upton 2021], are essential to convection zone dynamics and are thought to be the primary mechanism for removing kinetic energy at the largest scales. Disturbances in the differential rotation or in Rossby waves may provide a physical mechanism for detecting fluctuations in the toroidal field that correspond to "nests" to the locations where active regions (ARs) are likely to emerge [Dikpati et al. 2017]. Recent observations [Hathaway & Upton 2021] (Exhibit 6) indicate that large vortical structures are present on the Sun, but the limits of ecliptic observations prevent these vortices from being fully resolved. Similarly, determining the structure of non-axisymmetric zonal flows and of the subsurface meridional return flows requires that we gain multiple viewpoints from both in and out of the ecliptic plane. ***Observing from a single orbit near the equatorial plane is simply insufficient to discern the global magnetic field and plasma flow structure of our complex, variable, non-axisymmetric, magnetically active star.***

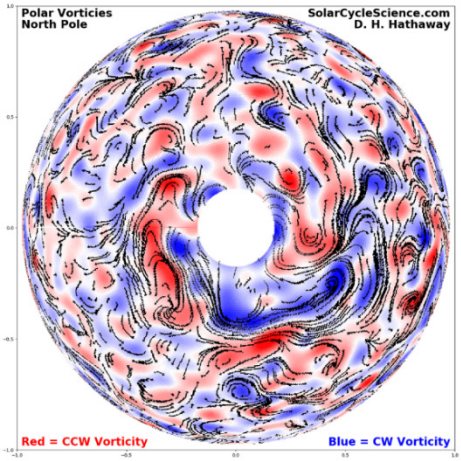

Exhibit 6. *Giant cellular flow patterns as seen from above the north pole. The right-handed and left-handed vorticity are shown in red and blue, respectively, along with the flow tracers in black. The streaklines indicate the flow direction. From Hathaway & Upton [2021].*

The Firefly mission concept includes a solar polar orbiting component to regularly (~2 month-long pass/pole/year) capture the helioseismology observations required to finally fill the "polar gap." Together with magnetic imaging, these observations will reveal the time-varying structure and dynamics of flows and magnetic fields at the polar regions of the Sun and throughout the convection zone by using simultaneous ecliptic plane observations. The Firefly mission will continuously observe the entire Sun over timescales on the order of a solar cycle, greatly advancing our understanding of the solar dynamo and paving the way towards predictive models of the solar magnetic cycle.

Firefly will address the following questions regarding solar interior structure and flows:

- How do the solar differential rotation and meridional flow evolve through the solar cycle?
- What is the flow structure of the solar polar regions?
- Is surface flux transport of active region magnetic fields sufficient to explain the evolution of polar magnetic fields over the solar cycle?

Objective 1 Science Closure

Firefly would measure:

- The meridional circulation and the differential rotation as a function of latitude and depth, and determine their relationship to polar vortical convective motions as the solar cycle evolves. Use this information to constrain and exclude solar dynamo models.
- The magnetic flux transport over the solar cycle as a function of latitude, longitude, and depth by measuring the distribution and strength of magnetic fields and flows. Use this information to understand how the polar magnetic fields seed the following solar cycle

1.3.2. OBJECTIVE 2: Understand solar magnetic eruptions and the role of large-scale magnetic field connections in triggering eruptions

Solar magnetic eruptions are the most powerful explosions in the solar system, releasing 25,000 times more energy in several hours than consumed on Earth over an entire year. Solar magnetic eruptions are the progenitors of flares, coronal mass ejections (CMEs; e.g., Webb & Howard [2012]), and solar energetic particle (SEP) events, all of which drive space weather impacts to Earth- and space-based technology. CMEs are particularly dangerous as they drive geomagnetic storms that can destabilize and damage the electric power grid, potentially causing long-term black outs and mass casualties. Solar prominences demarcate energy storage in pre-eruptive magnetic structures in the corona and are thus precursors of CMEs, but the triggering of prominence eruptions to form CMEs remains a mystery.

Previous studies [Forbes 2000] identified the key role played by the solar magnetic field in the release of magnetic energy that drives flares and CMEs. Numerical MHD simulations of eruptions (e.g., Kliem & Török [2006]; Fan & Gibson [2007]; Archontis & Török [2008]; Archontis & Hood [2012]; Amari et al. [2014]) rely on the pre-eruption coronal magnetic field configuration to study its evolution until triggering, which is modeled as either an ideal MHD instability or numerical reconnection. Unfortunately, the magnetic field extrapolation from the photosphere to the corona is an ill-posed problem with many valid and significantly differing solutions [De Rosa et al. 2009]. Thus models based on force-free coronal field extrapolations may be far from reality for any given active region magnetic configuration. Even if coronal magnetic field measurements [Raouafi et al. 1999, 2002; Raouafi 2005, 2011] can be used to address such limitations [Savcheva et al. 2013; Malanushenko et al. 2014; Gibson et al. 2016; Dalmasse et al. 2019], modeling limb eruptions (which although they may not produce Earth-directed CMEs, can still produce X-class flares and SEP events) is still impossible because the LOS angle to the limb precludes measurement of the underlying active region.

Modeling and understanding CMEs is also severely hindered by single observations from the Sun-Earth line. CME 3D reconstruction and basic parameter evaluation have been attempted using 2D plane-of-sky projected observations [Gopalswamy et al. 2009; Rouillard 2011; Webb & Howard 2012; Sterling 2018], but such methods suffer from LOS integration effects, causing loss of information and ambiguity (e.g., Burkepile et al. [2004]; Schwenn et al. [2005]). A further step has been made by STEREO and SOHO combined observations (illustrated in Exhibit 7), demonstrating the advantage of having multiple viewpoints to obtain information about source region location, CME orientation, and propagation direction [Temmer et al. 2009; Lee et al. 2013]. Nevertheless, information about longitudinal structures is still missing, and we cannot determine how these structures interact with neighboring solar coronal field and solar wind structures or how they evolve in the inner heliosphere.

To address these issues, observation of the Sun from strategically chosen multiple simultaneous viewpoints is essential. A "4π view field" enables monitoring of the birth-to-death evolution of solar active regions, which is critical since many large eruptions occur shortly after new flux emerges

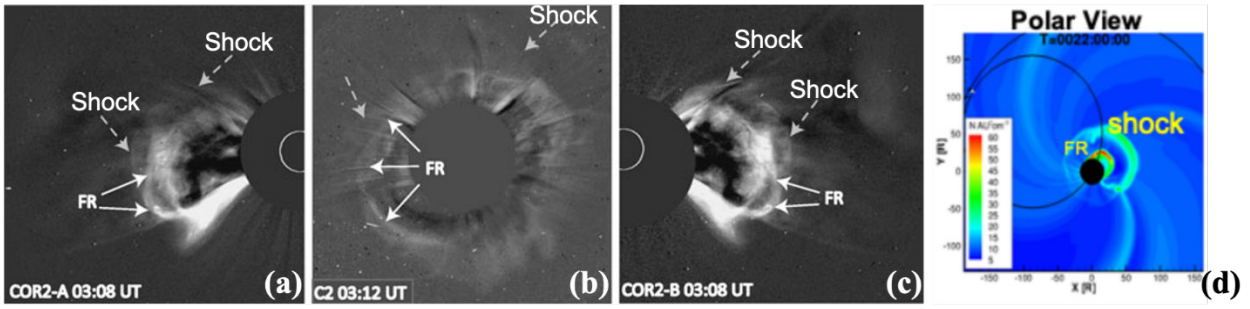

Exhibit 7. *(**a-c**) CME imaged by three coronagraphs in quadrature. The shock sheath and the magnetic flux rope driver can be discerned but the true extent of the shock and accurate CME directions can only be obtained by a polar perspective as shown in (**d**). Sources: (a-c) adapted from Vourlidas et al. [2013]; (d) MHD simulation, courtesy N. Lugaz.*

[Feynman & Martin 1995]. Multiple viewpoints can also address vector magnetic field ambiguities and enable tomographic and/or stereoscopic methods [Kramar et al. 2006, 2016; Aschwanden et al. 2015], yielding information on magnetic energy, helicity, and field line topology.

A polar vantage is particularly powerful for resolving longitudinal structure and avoiding center-to-limb projection effects that severely impact the quality of photospheric boundary conditions for high-latitude structures such as coronal holes that drive high speed streams (HSS) in the solar wind. The interaction of CMEs with solar wind HSS structures can alter the sheath region fields, significantly influence the arrival time at Earth of weaker CMEs, and change the ensuing geomagnetic storm characteristics. HSSs and the associated corotating interaction regions (CIRs) can also drive their own geomagnetic storms, sometimes more powerfully than CME impacts. Without an accurate measurement of polar fields, we cannot properly model global coronal magnetic fields and hence all models of the solar wind that might inform CME-solar wind interaction investigations are inaccurate. Finally, from the poles, the more accurately determined LOS magnetic field component is well aligned with *Bz*, the North-South component of the CME field in GSE coordinates, which is known to determine the strength of the geomagnetic storm following a given CME impact. Coronal spectropolarimetric measurements from even a small-aperture telescope in a solar polar orbit could potentially provide critical information about the geoeffectiveness of Earth-directed CMEs [Gibson et al. 2020].

One of the most tantalizing findings of multi viewpoint imaging is the evidence for long-range interactions between eruptive events occurring over the span of hours to days across a full solar hemisphere [Schrijver & Title 2011]. The subject of 'sympathetic' flaring and remote triggering of flares or eruptions has been discussed for decades, but is seriously hampered by a single viewing angle, so we depend largely on models for our current understanding of global interactions [Török et al. 2011; Titov et al. 2012, 2017]. Relatedly, although we know CMEs exhibit rotation, deflection, and deceleration during eruption, we cannot observe longitudinal structure and dynamics from the ecliptic, limiting our understanding of the CME's evolution as it traverses the heliosphere.

With the unique combination of observations from above and in the ecliptic plane, Firefly will provide critical observations for better understanding the physics behind solar magnetic eruptions while also informing the global coronal field models that drive all solar wind models.

In addition, monitoring the solar spectral irradiance (SSI) variability allows us to determine solar influence on global climate change. SSI, with its variation on different timescales, is crucial to our understanding not only of the Sun-Earth Connection but also of the Sun as a star. While SSI has been measured continuously from space since 1978, it has always been from the ecliptic near-Earth viewpoint. Even long-term trends are controversial because composite time series have been constructed from six different long-term experiments, which for some time periods, suffered from uncertain and contradictory calibrations. Firefly will provide full coverage of the Sun from which to characterize the various contributions to the Sun's radiative output at all latitudes and longitude simultaneously. The 4π-steradian SSI measurements will additionally provide the solar cycle variability of the solar luminosity as well as aid in our interpretation of the irradiance measurements of Sun-like stars whose polar orientations are unknown and whose activity cycles are apparently quite different than the Sun's. Firefly will fly the same instrumentation over a significant part of the solar cycle, providing continuity across timescales while reducing calibration issues.

In this context, with the unique combination of observations from within and outside the ecliptic plane, the Firefly mission will provide valuable observations for a better understanding of the physics behind the release of magnetic structures from the solar corona and for providing boundary conditions to the existing models.

Firefly will address the following specific science questions:

- How does non-potential complexity of the magnetic field transfer from the photosphere to the corona, and how does that lead to solar eruptions?
- What are the triggers and the processes at the origin of the coronal eruptive activity?
- How does the solar spectral irradiance (SSI) vary with latitude and over the solar cycle?

Objective 2 Science Closure

Firefly would provide continuous, multi-viewpoint data flow (e.g., magnetic fields, EUV and white-light imaging, and spectral irradiance measurements) from the Firefly constellation together with advanced modeling will result in a continuous flow of physical quantities, including velocities, magnetic free energy, and relative helicity to constrain the triggers of solar flares and CMEs and the propagation of the associated disturbances through the inner heliosphere.

1.3.3. OBJECTIVE 3: Determine how conditions in the solar wind vary with latitude and longitude in response to changing global solar conditions and throughout the solar cycle

So far, there has only been one mission to explore the solar wind out of the ecliptic plane. The Ulysses mission revealed how high-speed streams fill the heliospheric volume above the poles at solar minimum (Exhibit 8a, c), how this state is disrupted at solar maximum (Exhibit 8a), and how MHD turbulence and wave-particle interactions in collisionless plasma regimes differ greatly from those in the ecliptic [Goldstein et al. 1995; Marsden 2001]. However, Ulysses only provided three relatively short polar passes and lacked a magnetogram to enable field-line mapping of the solar wind back to the surface. The low-density polar regions are better for exploring such connections because the field-lines do not experience as much stochastic mixing from, e.g., corotating stream interactions and Coulomb collisions. These effects give rise to substantial ambiguity when attempting to map small-scale structures in solar-wind streams back to their origins in the corona [Elliott et al. 2012; Cranmer et al. 2017]. The Firefly mission will have transformative potential to improve our knowledge of how the solar magnetic field connects different coronal regions to the high-latitude, often high-speed, wind that can influence speeds and structures in the ecliptic.

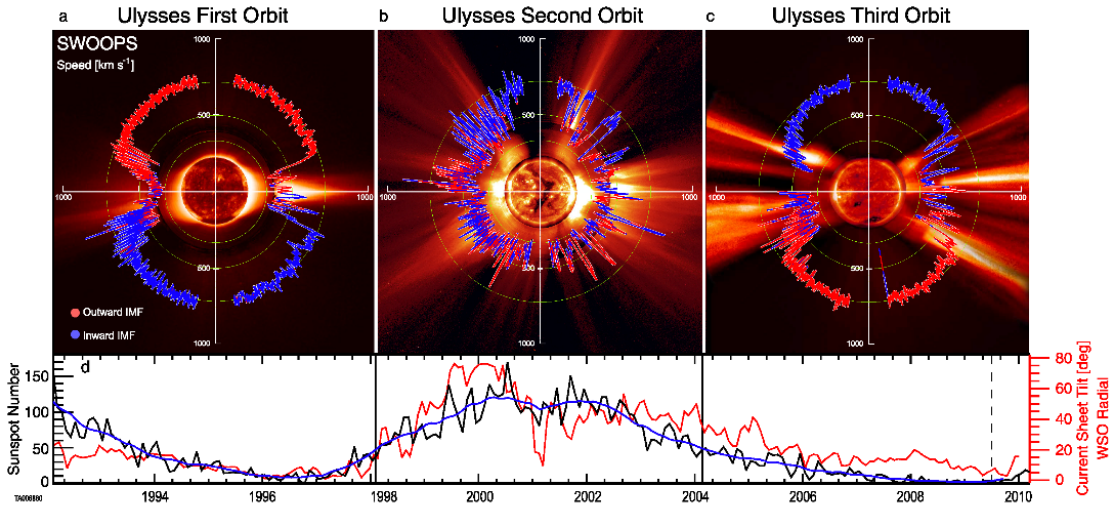

Exhibit 8. *Solar wind speed as a function of heliographic latitude illustrating the relationship between the structure of the solar wind and coronal structure at solar minimum (a, c) and solar maximum (b). Ulysses SWOOPS solar wind data are superposed on composite solar images obtained with the SOHO EIT and LASCO C2 instruments and with the Mauna Loa K-coronameter. (d) Solar cycle evolution. Adapted from McComas et al. [2008].*

Global MHD models of the solar wind depend on photospheric magnetic-field maps as a lower boundary condition. The ability to augment existing magnetograms – obtained from vantage points along the Sun-Earth line – with data from other viewpoints will greatly improve the accuracy of these simulations and forecasts (e.g., Pevtsov et al. [2016]; Gibson et al. [2018]). The models have long been hindered by unobserved polar fields, and different observatories tend to correct for the lack of data in different ways [Riley et al. 2014; Poduval et al. 2020]. The lack of reliable polar magnetic-field data at the solar surface is also one of the reasons that the so-called "open-flux problem" (i.e., the mismatch between measured heliospheric magnetic flux and that extrapolated from existing photospheric field data) remains unsolved [Linker et al. 2017, Riley et al. 2019]. Thus, the continuous full-surface coverage of Firefly provides ground-truth data that will improve our knowledge of Sun-to-heliosphere connections.

The ability to view equatorial coronal holes at disk-center, and to detect their in situ impacts at Earth, has been crucial for understanding how the solar wind accelerates, expands super-radially, and produces geoeffective high-speed stream activity (e.g., Verbanac et al. [2011]; Bale et al. [2019]; Karna et al. [2020]). Observations of polar coronal holes from above will also lead to new insights on coronal heating and solar wind acceleration. Because polar coronal hole wind fills a much larger volume of the heliosphere than equatorial hole wind, similar remote/in situ observation synergy for polar streams will reveal a larger missing piece of the solar wind acceleration puzzle.

It is impossible to establish the structure of the young solar wind from single viewpoint measurements. The available measurements from missions such as SDO, STEREO, SOHO, etc., provide the latitudinal structure of the flow. Its longitudinal structure has always been inferred from coronal and heliospheric models (e.g., PFSS, LFF, NLFF, and MHD), but validation is lacking. Measuring the longitudinal evolution of the solar wind is crucial to understanding its evolution in its acceleration zone (i.e., the corona) and beyond the breakdown of the corotation. In addition, Ulysses data indicated that the momentum flux modulates over the solar cycle, which might affect the whole structure of the heliosphere. However, these data are very sparse and from a single point. Models suggest that the heliospheric structure breathes in and out as a function of the solar cycle, but we do not have the data to verify that.

Firefly will address the following specific science questions:

- How does the solar wind originate from its sources and moves out to the heliosphere?
- How does the corona drive the inner heliosphere through the solar cycle?
- What are the mechanisms for accelerating the thermal and suprathermal solar wind? How do solar wind structures evolve throughout the inner heliosphere?

Objective 3 Science Closure

Firefly will provide a polar view of the evolving solar wind for the first time by imaging the corona and the solar wind from high latitudes in both EUV and white light, and contemporaneous in situ measurements (velocity distributions of the solar wind and its composition) from four different locations. The 4π-steradian observations together with appropriate modeling will determine the longitudinal structure of the solar wind and track evolving structures below and above the boundary of the corotation breakdown. This data will also enable the determination of the modulation of the momentum and energy fluxes in all solar wind regimes and for the whole solar cycle.

1.3.4. OBJECTIVE 4: Understand where and how energetic particles are accelerated and transported through the inner heliosphere

High-energy charged particles (e.g., GCRs and SEPs) are the most hazardous space weather phenomena. In the modern space exploration era, there have been no astronauts beyond LEO during the few extreme Solar Energetic Particle (SEP) events that have occurred. But this will certainly not be the case in the future and we currently lack any predictive skill in determining if and when an SEP event will occur in connection with any given solar magnetic eruption.

The energization of the SEPs occurs at the Sun during solar eruptive activity (e.g., flares; Exhibit 8bD) and also in the heliosphere in CME shock fronts (Exhibit 9c) and within the co-rotating interaction regions (CIRs; Exhibit 8e). Although the acceleration and transport of energetic particles in the heliosphere has been studied extensively (e.g., Reames [1999]; Mewaldt [2006]; Lee et al. [2012]; Raymond et al. [2012]; Drake & Swisdak [2012]; Giacalone [2010]), there are still many open questions. Using only data acquired in the ecliptic and within 1 AU has proven to be insufficient to answer these questions. For instance, it has been assumed for decades that CIR energetic particles are accelerated by shock waves beyond 2 AU. The Ulysses mission and earlier Pioneer-10/11 missions showed CIR intensities peaking at several AU.

We know very little about the SEP environment out of the ecliptic plane. Ulysses measurements created more open questions than answers due to the sparsity of the acquired data. CIR electrons have been observed during the Ulysses three polar passes at very high latitudes. The sporadic measurements did not fully illustrate the physical processes at the origins of these particles and how they are transported from (or to?) the solar polar regions. Additionally, CIRs with well-developed shocks are very rare at Earth since the shocks tend to form between 2 and 3 AU. Several spacecraft (e.g., Mariner II, Voyager I & II, Cassini, etc.) have crossed regions believed to be CIR shocks. However, these missions did not spend sufficient time to sample that environment and provide the data necessary to characterize the energization processes of the CIR energetic particles. During the cruise phase (5–6 years), the FF-P spacecraft will fly multiple times through the region between 2 AU and 5 AU. It will spend a significantly longer time there, which will provide sufficient data to shed light on the physical processes at the origin of the particle acceleration in CIRs.

Acceleration and transport of energetic particles out of the ecliptic is also poorly understood. The only measurements above the solar polar regions were collected by Ulysses during the three polar flybys. Although these flybys were so distant in time as they occurred over a time interval of about 12 years (i.e., over a solar cycle), the data obtained led to several open questions. For instance, it is not clear how

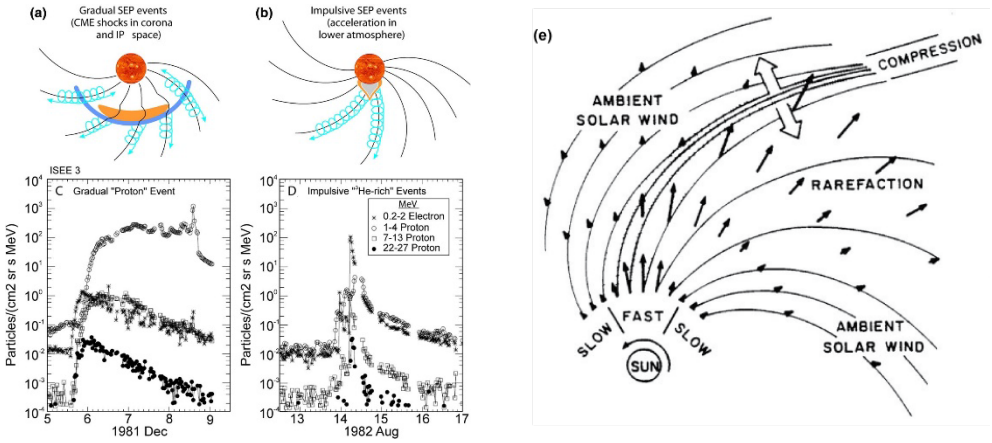

Exhibit 9. *(a,C) SEP events produced by a large-scale CME-driven shock wave accelerating the SEPs and populating the interplanetary magnetic field (IMF) lines over a large longitudinal area. These events are typically known as gradual events. (b,D) impulsive events produced by a solar flare that populates only those IMF lines well-connected to the flare site. (From Desai & Giacalone [2016]). (e) Schematic illustration of a CIR where energetic particles are presumably accelerated by shock waves beyond ~2 AU (from Pizzo [1978]).*

CIR energetic electrons are transported to the solar polar regions and how the accelerations and transport of particles from flares and CMEs vary with latitude.

Firefly will address the following specific science questions:

- How are solar energetic particles accelerated and transported throughout the inner heliosphere, particularly in the solar polar regions?
- What are the physical processes of CIR energetic particle acceleration, and do they differ from CME shock acceleration mechanisms?
- How are energetic particles transported to high solar latitudes, and how are CIRs electrons transported to the polar latitudes?

Objective 4 Science Closure

Firefly will fill this gap with continuous data over an extensive range of latitudes and longitudes and nearly a solar cycle. This will allow for constraining models of energetic particle acceleration and transport (e.g., shock wave acceleration, cross-field diffusion, magnetic field meandering, etc.). FF-P will spend sufficient time at and beyond 2 AU and at different latitudes to provide the necessary data to close open questions and assumptions about the acceleration of CIR energetic particles.

1.4. Synergistic Science

1.4.1. Support for Human Exploration

Space weather is a critical aspect of how the Sun influences its surroundings, notably planetary environments. The importance of space weather, and the need for reliable predictions of solar activity and its impacts on the Earth, can only grow in the future. Solar explosive events (i.e., flares and CMEs) drive space weather that causes hazardous conditions for humans in space and the ever-growing number of spacecraft, especially the Global Positioning Systems (GPS). The far-reaching impact of space weather can extend to the ground. The geomagnetically induced currents (GIC) in technological systems could cause damage to power grids and disruption of power distribution, increased corrosion in oil and gas pipelines, and degradation of radio communications [Pirjola et al. 2000]. Air travel at high latitudes could also be affected dramatically as space weather could lead to the disruption in high frequency (HF) communications, satellite navigation system errors, and radiation hazards to humans and avionics.

Firefly would provide full coverage of the solar surface and corona, which is essential to follow the evolution of magnetic systems from emergence to eruptions. These observations are critical for coming to terms with predictions of solar activity and for reliable modeling of the heliosphere and solar wind, which is a prerequisite for a reliable space weather forecast. With 4π-steradian coverage of the solar surface, we will no longer need to use outdated magnetic field measurements (i.e., synoptic maps built over a whole solar rotation; Ex. 1) as a boundary condition for our coronal and heliospheric models. In addition, the most impactful events to the Earth's environment are halo CMEs (i.e., events propagating toward the Earth). Observations from the Sun-Earth line do not provide the necessary information on the propagation and evolution of these structures, making predicting their effects a problematic task. Spacecraft such as STEREO help to some extent, but we are still faced with the limiting viewpoint from the ecliptic. A top-down view from high solar latitude is necessary to solve this problem and also to figure out the 3D structure of the CME material and its true propagation path. Firefly would provide beacon data for a near-real-time space weather forecasting.

1.4.2. High Risk, High Reward Science: the Solar Gravity Modes

Helioseismology, which measures the solar pressure modes (*p*-modes), has been used to successfully characterize the solar interior structure and dynamics in the convection zone and the outer part of the deep interior radiative zone (e.g., Howe [2009]; Basu [2016]). Recently, inertial, Rossby, or r-, modes, driven

by the Coriolis force, have been observed and exploited as probes of the deeper interior [Gizon, et al. 2021] However, several extremely important questions about the deep solar interior remain, for example the structure and rotation of the solar nuclear energy-generating core. Gravity modes, driven by the buoyancy force, are the only known probes for studying the core and radiative-zone structure and dynamics. These modes remain challenging to observe, but they are essential for advancing our understanding of the Sun–Earth system. Today, knowledge of the internal dynamics from acoustic modes concerns mainly the convection zone containing 2% of the solar mass. Solar gravity modes (*g*-modes) are buoyancy waves trapped below the convection zone in the solar radiative zone and have been *very* difficult to detect at the surface. Therefore, the quest for detecting solar *g*-modes has attracted considerable attention in the past, with several reported detections. Unfortunately, none of the reported detections have been confirmed so far [Appourchaux et al. 2010]; Appourchaux & Pallé 2013, Appourchaux & Corbard 2019].

The Global Oscillations at Low Frequencies (GOLF) instrument and the Luminosity Oscillations Imager (LOI) package of the Variability of solar IRradiance and Gravity Oscillations (VIRGO) instrument on board SOHO were designed to search for and study the solar gravity modes. The detection of these modes proved a difficult task for two main reasons: a mechanism failure early in the life of GOLF, and the amplitude of the solar *g*-modes turns out to be *significantly* less than was expected before the launch of SOHO. Today we face two challenges that limit the *g*-mode detection and their use as diagnostics of the solar core: (1) their minute surface velocity imprint and (2) the presence of solar noise in the range of frequencies where *g*-modes are expected to be found, which contributes to poor signal/noise. The next generation of instruments dedicated to gravity modes must address these points to observe more quickly (i.e., within a few years) with better sensitivity.

A new generation of instruments that are more sensitive, and particularly having one or two instruments off the Sun–Earth line (to very significantly reduce the noise background) on FF-E, should significantly advance our knowledge of solar *g*-modes, and enable their use to probe the otherwise accessible solar core.

Investigating solar *g*-modes is a high risk (they have not been unambiguously identified yet), but high reward (direct knowledge of the structure and dynamics of the solar core is critical for progress). This would also provide full coverage of the entire solar interior.

1.4.3. Cross-Disciplinary Science

The Firefly constellation offers ample opportunities for cross-disciplinary science from viewpoints not accessible before. It will provide significant insight into the dust structure of the zodiacal cloud, near-Earth hazardous objects, comets, and objects inside 1 AU. The down-view of the solar system from high altitudes outside the ecliptic plane is critical to these research topics. For instance, cometary physics will benefit significantly from the multiple viewing observations from Firefly. Previous observations could only offer a single viewpoint, which often suffers from effects (e.g., projection effects, timeliness, and continuity of the observations) that curtail access to important information about these solar system bodies reminiscent of the formation time of the solar system. Observations from multiple vantage points inside and outside of the ecliptic plane will better determine the orbits of these bodies, the three-dimensional structure of the cometary environment, and its interaction with the solar wind. The science of the sungrazing comets will particularly benefit from continuous observations. These comets are typically eclipsed at crucial times close to the Sun. Substantial evolution (e.g., evaporation, coma fragmentation, etc.) occurs there, and frequently we do not have access to these critical developments. The Firefly observations will allow us to monitor comets continuously through their voyage around the Sun. Stealth asteroids are a hazard to us, and their early detection is critical for our safety. The changing observation geometries of the Firefly mission might provide important insight into that. In addition, observing the solar planetary system from different viewpoints offers essential information about the phasing of the planets. This is essential for our understanding of the exo-planetary system around other stars.

1.4.4. Make Headway in Exploration, Innovation & Inclusiveness

The Firefly mission concept represents a departure from the conventional exploration approaches of the Heliosphere in so many ways. This new approach is driven by our need for new observing paradigms of our star –the Sun—and its Heliosphere to solve phenomena with multi-scale temporal and spatial aspects. Such phenomena will remain the primary long-standing open questions in solar and stellar exploration until we can observe the Sun and its environment as a whole.

- **Sun as a Model Star:** the Sun is the only star we can observe up close and in many details. It is the model star to observe how it evolves and interacts with its planetary environment. It is also the only star in the universe we can study as a whole using multi-vantage point observations to characterize multi-scale phenomena pertinent to stellar research.
- **Timeliness:** since the dawn of time, we (humans) have largely observed the Sun from a single viewpoint and generally within the ecliptic. The only exceptions to that are Ulysses (a polar mission with in situ measurement only) and STEREO (i.e., two drifting spacecraft in the ecliptic). Single viewpoint observations are very limiting considering the magnetized and active nature of the Sun. We cannot understand major and challenging astrophysical phenomena (e.g., the solar dynamo, solar cycle, solar activity, space weather, etc.) unless we have full coverage of the Sun. In this context, a mission like Firefly is overdue.
- **Breaking New Frontiers in Heliophysics Exploration:** Firefly will provide long overdue observations needed to understand how the Sun works and to be able to predict its activity and impact on the interplanetary environment.
- **Mission Lengthiness – Multi-Scale Phenomena:** the Firefly mission is a long-term mission by design and necessity. The prime science phase covers a whole solar cycle, unprecedented in heliospheric exploration. Observing an entire solar cycle (length of the Firefly Phase E) is essential to understanding multi-scale phenomena. These observations will provide data to characterize and predict phenomena such as the solar eruptive activity (i.e., short term) and solar magnetism, the solar dynamo, and the solar cycle (i.e., long term).
- **Inclusiveness & Diversity:** Firefly is, by design, an inclusive mission in numerous ways.
  - **Multi-Disciplinarily:** Firefly objectives cover astrophysics phenomena from the solar interior through the atmosphere to the inner heliosphere. This will involve scientists and engineers with diverse expertise and background.
  - **Heliospheric System:** Firefly would provide diverse and complementary observations across multiple disciplines. These data together with modeling will allow us to get insight of the inner heliosphere as a system.
  - **Partnership:** Firefly development would benefit greatly from including various national and international agencies and institutions. For instance, Firefly Ecliptic and Firefly Polar could be developed in two or more different institutions or agencies.
  - **Future Generation:** Firefly would also be a fertile ground to involve early-career scientists, particularly students from underrepresented communities. We envision that the projects and payload development should include students at all stages.
  - **Citizen Science:** the Firefly broad-ranging scientific scope and the data variety and significant volume will a fertile ground for Citizen Science projects, particularly in the era of artificial intelligence and big data. We envision to engage the public and entice them to get involved in the Firefly science.

1.5. Mission Concept Science Traceability

Exhibit 10 maps the science questions, the measurements, payload, and the mission requirements to accomplish the science objectives of the Firefly mission. Firefly's comprehensive instrument payload satisfies the objectives laid out in the science traceability matrix.

Exhibit 10. *Science Traceability Matrix.*

Coverage	Science Objectives	Science Questions	Measurements	Observation Requirements	Instruments	Mission Requirements
Solar Interior Photosphere Corona Solar Wind & Heliosphere	Understand how surface and sub-surface flows, and toroidal magnetic field instabilities produce the cyclic solar dynamo, the root cause of solar activity.	How do the solar differential rotation and meridional flow evolve through the solar cycle?	The differential rotation and meridional flows over the entire (4π) solar sphere from the surface down to the tachocline (including the key unexplored polar regions) and over a significant part of the solar cycle.	**Doppler Velocity Measurements (Local & Global Helioseismology)** Getting to the tachocline: multi-view points Field of view: Full disk Sensitivity: <10 m/sec (surface flows) Spatial resolution: 1 arcsec for FF-E & 4 arcsec for FF-P Temporal resolution: 1-min full disk. Velocity resolution: ~20 m/s per pixel per min Temporal coverage: near continuous in the ecliptic for global HS; continuous in ~12-hr intervals for out-of-ecliptic measurements and local HS. Line following: GONG-like line following to compensate for large radial velocity variations over 4π-polar orbit regime. **Continuum Imaging to Enable Correlation Tracking of Surface Flows** Spatial resolution: 1 arcsec (need to see granulation) Temporal resolution: 1 min **Full-Disk Vector Magnetic Fields From Four View Points** Spatial resolution: 1 arcsec Cadence: B_LOS: 60 sec (B_LOS) & ~10-15 min (vec. ***B***). Spectral line: 547 nm. Spectral resolution: 2–4-line samples for B_{LOS}; 6–10-line samples for vec-***B*** (for filtergraph method); see sensitivity for GONG-like technique. Weak field sensitivity: ~2 Gauss (LOS) Transverse ***B*** sensitivity: 10-20 Gauss Line following: GONG-like line following to compensate for large radial velocity variations over 4π-out orbit regime. **Solar Spectral Irradiance (SSI)** Field of view: full solar disk from each view point; Resolution: 1 pixel (the Sun as a star); Cadence: 1-5 min Wavelengths range: 170–340 Å (Opt. 1 − 100–200 Å) **EUV Imaging** Field of view: ±3 R_{SUN} from the Sun's center; Resolution: 1–2 arcsec; Cadence: 1-5 min; Wavelengths: 304 Å & 171 Å **White-Light Coronagraph Imaging** Field of view: 2.5-15 R_{SUN}; Resolution: 30 arcsec; Cadence: 1 min; Wavelength range: 4000-7000 Å *Option: polarization capability* **White-Light Heliospheric Imaging** Field of view: 4° – 24° (~16-96 R_{SUN}) Resolution: 30 arcsec Cadence: 15-30 min Wavelength range: 4000-7000 Å **Solar Wind Magnetic Fields** B magnitude range: 0–1000 nT Cadence: 20 sec synoptic & up to 8-Hz (shock science) **Thermal Solar Wind Plasma** Pointing: subsolar point SW speed: <1000 km/s Cadence: 1 min synoptic - 8 Hz (shock science) **Solar Wind Composition** VDFs of ions (mXq+): 4He+, C1-1+, O1-2+; SW dominant ions; suprathermal and tail ions; (interstellar and inner source PUI) Speed range: 200-2000 km/sec E/q range: 0.5-130 KeV/e Field of view: 30 deg x 6 deg Angular resolution: 6 deg x 6 deg Energy resolution (ΔE/E): 0.1 Pointing: sunward Geo. factor (cm2-sr eV/eV): 1.e-05 Identified ions: 4He2+, 3He2+, 4He1+, 3He1+, C1-6+, 14N1-7+, 16O1-8+, 22Ne1-10+, 22Ne1-10+, Mg1-12+, Si1-14+, S1-6+, F2-20+ **Energetic Particles & Cosmic Rays** Electrons: 10 keV – 10 MeV Ions: 10 keV/nuc – 300 MeV/nuc	Doppler Vector Magnetograph Extreme Ultraviolet Imager Total Solar Irradiance White-light Imaging – Coronagraph (Mini-COR) White-light Imaging – Heliospheric Imager (HI+) Magnetometers Faraday Cup Solar Wind Composition Solar Energetic Particle Suite SolO/EPD-EPT/HET (x2 to cover the whole sky) SolO/EPD-SIS	All spacecraft are 3-axis stabilize (no spinning spacecraft) 4***π*** solar coverage: >80% over the 2–3 yr after reaching the final orbit -- Coverage is defined as being within 60 degrees of center from each view point (i.e., spacecraft) 4π-out: minimum inclination 60°, desired inclination >80° 4π-in: ±90 degree to ±120 degree longitude from the Earth Perihelia: ~1 AU At least 1-2 solar rotations above 60-degree latitude Time accuracy: 100 ms across constellation ~1 polar pass/pole/year Mission duration: 10 yr Two launches: one for FF-E (2 spacecraft); and one for FF-P(2 spacecraft) Ellipticity: (4***π***-out): 2/1 (final orbits) Propulsion FF-E: chemical (electric propulsion if affordable) FF-P: electric propulsion Communication: Ka-band Autonomy & onboard processing Power FF-E: solar arrays FF-P: solar arrays
		What is the non-axisymmetric flow structure of the solar polar regions?	The size and morphology of the vortical/convective flows at the solar polar regions.			
		Is surface flux transport of active region magnetic fields sufficient to explain the evolution of polar magnetic fields over the solar cycle?	**B** over the entire (4π) solar sphere, and over a significant part of the solar cycle.			
	Understand the conditions leading to solar explosive activity and the role of the large-scale magnetic field connections.	How does the solar spectral irradiance (SSI) vary with latitude and over the solar cycle?	TSI over the wavelength range Opt. 1 − 100-200 Å Opt. 2 − 170-340 Å			
		How does non-potential complexity of the magnetic field transfer from the photosphere to the corona, and how does that lead to solar eruptions?	Full-sphere photospheric **B** dynamics EUV imaging			
		What are the triggers and the processes at the origin of the coronal eruptive activity?	**B** on active region scales and below Global EUV imaging on faster time scales.			
	Determine how conditions in the solar wind vary with latitude and longitude in response to changing global solar conditions and throughout the solar cycle.	How does the 4π solar wind originates from its sources and moves out to the heliosphere?	Longitudinal expansion of the solar wind from the coronal base to the Alfvén critical boundary and beyond, where co-rotation breaks down.			
		How does the corona drive the inner heliosphere through the solar cycle?	Photospheric ***B*** Coronal imaging in situ ***B***, ***V***, *n*, *T*, etc.			
		What are the mechanisms for accelerating the thermal and suprathermal solar wind? How do solar wind structures evolve throughout the heliosphere? What is the global, large-scale structure of the inner heliosphere (inside 1 AU)? How do stream boundaries evolve?	Solar wind velocity distribution of ions (mXq+) of (a) low-q ions, (b) solar wind dominant minor ions, and (c) suprathermal and tail ions [(d) interstellar and inner source pick up ions].			
	Understand how energetic particles are accelerated and transported through the heliosphere.	How are solar energetic particles accelerated and transported throughout the heliosphere, particularly at the solar polar regions?	The energetic particle environment throughout the heliosphere and over a significant part of the solar cycle. Photospheric magnetic fields EUV and white-light imaging In situ magnetic fields			
		What are the physical processes at the origin of the CIRs' energetic particle acceleration, and where does that occur?				
		What is the magnetic connectivity of SEP particles to the Sun?				
		How are energetic particles transported to various solar latitudes, and how are CIRs electrons transported to the polar latitudes?				

The science objectives complement each other. The inter-dependency of these objectives on the science measurements are shown in Exhibit 11.

Modeling is an integral part of all the science objective of Firefly.

Science Objectives	Science Questions	$V_{Doppler}$	B_{PH}	EUV Imaging	WL Imaging	SW Plasma	SW Comp	B_{SW}	Energetic Particles	Modeling
Understand how surface and sub-surface flows, and toroidal magnetic field instabilities produce the cyclic solar dynamo, the root cause of solar activity.	How do the solar differential rotation meridional flow evolve through the solar cycle?	R	R		C					
	What is the non-axisymmetric flow structure of the solar polar region?	R	R	C	C					
	Is surface flux transport of active region magnetic fields sufficient to explain the evolution of polar magnetic fields over the solar cycle?	R	R	C	C			R		R
Understand the conditions leading to solar explosive activity and the role of the large-scale magnetic field connections.	How does non-potential complexity of the magnetic field transfer from the photosphere to the corona, and how does that lead to solar eruptions?		R	R	R					R
	What are the triggers and the processes the origin of the coronal eruptive activity?		R	R	R					R
Determine how conditions in the solar wind vary with latitude and longitude to changing global solar conditions and throughout the solar cycle.	How does the 4π solar wind originate from its source and move out to the heliosphere?		R	R	R	R	R	R		R
	How does the corona drive the inner heliosphere through the solar cycle?		R	R	R	R	R	R		R
	How do solar wind structures evolve throughout the heliosphere do (perturbed vs non-perturbed)?		R	R	R	R	R	R		R
Understand how energetic particles are accelerated and transported through the heliosphere.	How are solar energetic particles accelerated and transported throughout the heliosphere, particularly at the solar polar regions?		R	R	R				R	R
	What are the physical processes at the origin of the CIRs' energetic particle acceleration, and where does that occur?		R		C	R		R	R	R
	How are energetic particles transported to the solar latitudes and how are CIR electrons transported to the polar latitudes?		R	C	R			R	R	R

Exhibit 11. *Required (R) and complementary (C) measurements to accomplish the Firefly science objectives.*

1.6. Science Closure

1.6.1. OBJECTIVE 1: Understand how surface and subsurface flows, and toroidal magnetic field instabilities produce the cycle dynamo, the root cause of solar activity.

To close Objective 1, we must fill major gaps in our observations of the solar surface and subsurface flows, and polar magnetic fields that are critical to understanding the solar dynamo. A "polar gap" exists above about 60 degrees in latitude in which both surface magnetic fields and plasma flows are poorly measured or unobservable from the ecliptic plane. Additionally, the depth structure of meridional circulation, particularly whether there is a single cell or multiple cells structured in latitude, longitude, depth, and time remains unknown. ***Firefly will characterize***

1. ***meridional circulation and the differential rotation as a function of latitude and depth, and determine their relationship to polar vortical convective motions as the solar cycle evolves. This information will be used to constrain and exclude solar dynamo models.***

2. ***magnetic flux transport over the solar cycle as a function of latitude, longitude, and depth by measuring the distribution and strength of magnetic fields and flows. This information will be used to understand how the polar magnetic fields seed the following solar cycle.***

1.6.2. OBJECTIVE 2: Understand solar magnetic eruptions and the role of large-scale magnetic field connections in triggering eruptions.

Solar Spectral Irradiance. Monitoring the solar spectral irradiance (SSI) variability allows us to determine solar influence on global change. SSI, with its variation on different timescales, is crucial to our understanding not only of the Sun-Earth Connection, but also of the Sun as a star. While SSI has been measured continuously from space since 1978, it has always been from the ecliptic near-Earth viewpoint. Even long-term trends are controversial because composite time series have been constructed from six different long-term experiments, which for some time periods, suffered from uncertain and contradictory calibrations. ***Firefly will provide full coverage of the Sun from which to characterize the various contributions to the Sun's radiative output at all latitudes and longitude simultaneously. The 4π-steradian SSI measurements will additionally provide the solar cycle variability of the solar luminosity as well as aid in our interpretation of the irradiance measurements of Sun-like stars whose polar orientations are unknown and whose activity cycles are apparently quite different that the Sun's. Firefly will clarify why SSI variability is ~1/3 of the variation observed in other Sun-like stars. Also, Firefly will fly the same instrumentation over a significant part of the solar cycle, providing continuity to across timescales while reducing calibration issues.***

Complexity of the Magnetic Field Transfer & Processes at the Origin of Coronal Eruptions. It is essential to understand the physical processes leading to the formation of complex structures prone to eruption (e.g., flares, CMEs, and jets) and the processes by which energy flows into the corona and heats and accelerates the solar wind plasma. Continuity of observations is essential to following the evolution of magnetic structures and the buildup of energy and helicity in the corona, the rates of emergence and cancellation of photospheric magnetic fields, and quantify sympathetic eruptive activity – something impossible from a single viewpoint. ***The continuous, multi-viewpoint data flow (e.g., magnetic fields, EUV, and white-light imaging) from the 4π constellation, together with advanced modeling, will result in a continuous flow of physical quantities, including velocities, magnetic free energy, and relative helicity to constrain the triggers of solar flares and CMEs and the propagation of the associated disturbances through the inner heliosphere.***

1.6.3. OBJECTIVE 3: Determine how conditions in the solar wind vary with latitude and longitude in response to changing global solar conditions throughout the solar cycle.

4π Solar Wind Origination & Movement. It is impossible to establish the complete structure of the solar wind from single viewpoint measurements. The available measurements from missions such as SDO, STEREO, SOHO, etc., provide the latitudinal structure of the flow. Its longitudinal structure has always been inferred from coronal and heliospheric models (e.g., PFSS, LFF, NLFF, and MHD), but validation is lacking. Measuring the longitudinal evolution of the solar wind is crucial to understanding its evolution in its acceleration zone (i.e., the corona) and beyond the breakdown of the corotation.***Firefly will provide a polar view of the evolving solar wind for the first time by imaging the corona and the solar wind from high latitudes in both EUV and white light. The 4π observations together with appropriate modeling will determine the longitudinal structure of the solar wind and track evolving structures below and above the boundary of the corotation breakdown.***

How Does the Corona Drive the Inner Heliosphere. Ulysses' data indicated that the momentum flux modulates over the solar cycle, which might affect the whole structure of the heliosphere. However, these data are very sparse and from a single point. Models have shown that the heliospheric structure breathes in and out as a function of the solar cycle. But we do not have the data to verify that. ***Firefly will provide contemporaneous measurements from four different locations. Together with the remote sensing observations and modeling, this data will allow determining the modulation of the momentum and***

energy fluxes in all solar wind regimes and for the whole solar cycle, and the possible asymmetry of the heliosphere.

1.6.4. OBJECTIVE 4: Understand where and how energetic particles are accelerated and transported through the inner heliosphere.

We know very little about the SEP environment at higher latitude. Ulysses' measurements created more open questions than answers due to the sparsity of the acquired data. CIR electrons have been observed during the Ulysses three polar passes at very high latitudes. The sporadic measurements did not fully understand the physical processes at the origins of these particles and how they are transported to the solar polar regions. Additionally, CIRs with well-developed shocks are very rare at Earth orbit. It has been assumed that at some distance between 2 AU and 3 AU, the density gradient on both sides of the CIR becomes large, and a pair of shocks develop. Several spacecraft (e.g., Mariner II, Voyager I & II, Cassini, etc.) have crossed the region where the CIR shocks are believed to form. However, these missions did not spend sufficient time to sample that environment and provide the data necessary to characterize the energization processes of the CIR energetic particles. ***Firefly will fill this gap with continuous data over an extensive range of latitudes and longitudes and nearly a solar cycle. This will allow constraining models of energetic particle acceleration and transport (e.g., shock wave acceleration, cross-field diffusion, magnetic field meandering, etc.). FF-P will spend sufficient time at and beyond 2 AU and at different latitudes to provide the necessary data to close open questions and assumptions about the acceleration of CIR energetic particles.***

2. High-Level Mission Concept

In support of the Solar and Space Physics (Heliophysics) 2024 Decadal Survey, an experienced team of engineers and scientists led by the Johns Hopkins Applied Physics Laboratory (APL) have developed a mission concept that implements the science objectives discussed in Section 1. The mission concept presented here is the result of trade studies that optimized the mission with regard to factors such as science objectives, concept study requirements, space environment and engineering constraints, and risk. Section 2 of this concept study report presents an overview of the Firefly concept; detailed information on the flight system is given in Section 3. An Appendix to the Firefly concept study report provides details of the mission design analysis.

2.1. Overview

2.1.1. Mission Architecture

The concept study was developed using APL's Concurrent Engineering (ACE) Laboratory, which fosters real-time interaction between scientists, instrument developers, and flight system engineers. This interaction allows the team to focus quickly on trades and critical factors in the design to arrive at a concept representing a mission point design at Concept Maturity Level (CML) 4, understand trades and development to be conducted in subsequent mission phases, and identify mission-level risks and mitigations.

Development of the concept for Firefly began with a trade of mission architectures involving the number of spacecraft, chemical vs electric propulsion mission design, and coverage of the Sun, among other factors. After the high-level architecture was determined, more detailed concepts for the individual flight systems, mission design, and concept of operation were developed. The result of this process is a well-defined, feasible mission that accomplishes science goals at reasonable cost and with low schedule risk. We, therefore, recommend Firefly as the best concept for providing full, continuous study of the Sun. Mission and spacecraft design features of the Firefly mission concept include:

- Mission architecture consisting of four spacecraft of two types – Firefly-Ecliptic (FF-E) spacecraft, flying in the ecliptic plane, and Firefly-Polar (FF-P) spacecraft, flying in an orbit inclined with respect to the ecliptic by 60–70 deg to observe the Suns poles.
- FF-E Spacecraft: Two smaller spacecraft (FF-EA and FF-EB)1 launched together using use lunar gravity assists with phasing loops to transfer to STEREO-like orbits 120-deg behind and ahead of the Earth. The spacecraft achieve the desired orbit with chemical propulsion only.
- FF-P Spacecraft: Two larger spacecraft (FF-PA and FF-PB) launched together on a Falcon Heavy Expendable launch vehicle to Jupiter for a gravity assist to change orbit plane. Each spacecraft uses solar electric propulsion to arrive at the final orbit with 180 deg of separation to provide simultaneous observation of both pole of the Sun.
- Payload on each spacecraft to perform remote imaging (Doppler Vector Magnetograph, Extreme Ultraviolet Imager, White-Light Coronagraph, White-Light Heliospheric Imager, Solar Irradiance) and in-situ measurements (Fluxgate Magnetometer, Faraday Cup, Solar Wind Composition, Solar Energetic Particle Suite). Payload complement on each spacecraft is optimized to meet science objectives at minimum cost.
- Two launches in the early to mid-2030s to support simultaneous science phase for all four spacecraft.
- Modular spacecraft design and maximal common subsystem elements to facilitate manufacturing and integration/test of four spacecraft.
- Ground system capable of supporting the operation of all four spacecraft, collecting and distributing science data, and analysis of data products.
- Cost: $2.2B in FY22 dollars, excluding launches.

[1] "A" and "B" stand for "Ahead" and "Behind".

2.1.2. Environments

The FF-E spacecraft are launched into the near-Earth environment and use lunar gravity assists and chemical propulsion to reach final orbit at 1 AU leading and following the Earth. The environments experienced by these spacecraft are typical of other Sun-observing spacecraft, especially STEREO spacecraft, which flew in virtually the same orbit. Particularly, the thermal, mechanical, and radiation environments do not impose significant challenges to the flight design. Electromagnetic cleanliness will be required, with the requirements consistent with previous missions such as STEREO and Parker Solar Probe.

The FF-P spacecraft eventually also arrive at a relatively benign 1 AU orbit, but to get there, a Jupiter gravity assist is needed to change the orbit plane. The spacecraft described in Section 3 are designed to meet the range of environments (thermal, radiation, solar illumination, etc.) over the full mission trajectory. In particular, the FF-P spacecraft are designed to meet the radiation requirements of the Jupiter flyby with the typical margins of safety; the total ionizing dose requirement, for example, is 60 krads (Si) including a safety factor of 2. Electromagnetic cleanliness will also be required consistent with previous missions such as STEREO and Parker Solar Probe.

2.2. Concept & Technology Maturity

The study was conducted at CML 4, point design to subsystem-level mass, power, performance, cost, risk. The outcome of the study was the evaluation of the trade space and the development of a point design that achieves the mission goals. Where the information needed for CML 5 (initial concept implementation) was available, the information is included in the trade space, point design, and this study report.

The team considered the technology readiness levels (TRLs) for spacecraft subsystems and payload in the mission study of the Firefly concept. The project can be executed with minimal technology development. All spacecraft components are TRL 6+ except for elements of the NEXT-C electric propulsion system and the SPICES instrument which are at TRL4-5. The remaining strawman payload is based on previously flown instruments and fully meet the requirements for Firefly. In other words, the mission could be flown now. Instrument and spacecraft subsystem TRL assessments are discussed in Section 3.

2.3. Key Trades

The study team assessed options for all major design decisions and selected the best approach for the mission concept using a combination of mission performance requirements and engineering judgement of the technical benefit, cost, schedule, and risk trade-offs. Major system and subsystem design decisions are described in Exhibit 12.

Area	Trade Options	Results
Development Optimization	Single Institution vs. Multiple Institutions*	• Spacecraft subsystems for FF-E and FF-P are substantially the same, with multiple copies of the same design for many components. • Two pairs of identical spacecraft offer the option to separate the development to two different institutions if cost and schedule is favorable. Non-US institutions could be included in a Phase A trade to optimize manufacturing plan. • Baseline for this report is development of all spacecraft at a single institution.
	Single Agency *vs.* Multiple Agencies*	• Two pairs of identical spacecraft offer the option to separate the development to two different space agencies (e.g., NASA and ESA) if cost and schedule is favorable. • Baseline for this report is development of all spacecraft at a single institution.
Payload	Optimize Instrument Selections & Cost/Schedule	• Tailored payloads for each of the four spacecraft to meet science objective while reducing cost and schedule.
Data Return	Antenna Size, RF Power, Frequency Band, Data Collection Plan	• Telecommunications designs for FF-E and FF-P spacecraft due to need to communicate at Jupiter for FF-P. • Hybrid X-Band (uplink and downlink) and Ka-Band (downlink only) system provides high data volume and access to spacecraft when Ka-Band is not available.
Solar Arrays	Size, Solar Cell Selection	• Solar array size and cell choice tailored for different FF-E and FF-P trajectories. • Low Intensity, Low Temperature (LILT) solar cells chosen for FF-P to provide power at Jupiter.
Trajectory	Multiple Options for Trajectory In Primary Science Phases	• Trajectory chosen to minimize radiation exposure and meet science objectives, especially solar disk coverage requirements.

Exhibit 12. *Major Trades Considered.*

** The payload instruments will naturally be developed at different institutions.*

2.3.1. Payload Optimization

The most significant trade is in the area of payload optimization. While the mission architecture supports a full instrument complement on each of the four spacecraft, this choice drives the cost and schedule, while a full complement on each spacecraft is not required to meet the science objectives. By individually tailoring the payload for each spacecraft, the team was able to reduce cost and schedule risk, while accomplishing the mission objectives. Exhibit 13 gives the tailored payloads for each spacecraft for the baseline option (i.e., option 6 in Exhibit 14).

Instrument	FF-EA	FF-EB	FF-PA	FF-PB
Doppler Vector Magnetograph (DVM)	✓	✓	✓	✓
EUV Imager/Solar Spectral Irradiance (EUV/SSI)	✓	✓	✓	
White Light Coronagraph (WLC)	✓	✓	✓	✓
White Light Heliospheric Imager (WL HI)	✓			
Fluxgate Magnetometer (FGM)	✓	✓	✓	✓
Faraday Cup (FC)	✓	✓	✓	✓
Solar Wind Composition (SWC)			✓	
Solar Energetic Particle Suite (EPS)	✓	✓	✓	

Exhibit 13. *Baseline (option 6 in Exhibit 14) payload for each Firefly spacecraft.*

Because the mission architecture supports a full complement of instruments on all spacecraft, this baseline design could be enhanced by adding instruments as cost and schedule are made available. In addition, further descopes exist by reducing the number of spacecraft to three or by deselecting additional instruments, at the cost of reduced science objectives. Exhibit 14 provides a summary of the payload for each of the nine options. Section 5 includes a discussion of possible enhancements and descopes to the baseline design, with impacts on cost given for each option.

	Option	Instrument Quantities Over 4 Spacecraft								
		Qty S/C	DVM	EUVI/SSI	WLC	WL HI	FGM	FC	SWC	EPS
	1	3	3	2	3	—	3	3	—	3
	2	4	4	2	4	—	4	4	—	3
	3	3	3	3	3	—	3	3	—	3
	4	4	4	3	4	—	4	4	—	3
	5	3	3	3	3	1	3	3	1	3
BASELINE ▶	**6**	**4**	**4**	**3**	**4**	**1**	**4**	**4**	**1**	**3**
	7	4	4	4	4	1	4	4	1	3
	8	4	4	4	4	1	4	4	1	4
	9	4	4	4	4	2	4	4	4	4

Exhibit 14. *Payload summary for each option of the Firefly mission concept.*

2.3.2. Flight System Development Optimization

The mission architecture is designed to lower manufacturing risks, especially cost and schedule risks, while accomplishing the science objectives. This means that all four spacecraft are substantially the same, only differing where needed to meet the requirements imposed by the Jupiter gravity assist for the FF-P spacecraft, and in the selection of instruments for each spacecraft instrument complement to optimize cost. The baseline concept takes advantage of savings in making multiple copies of components and sharing non-recurring costs among the four spacecraft.

Another option is to recognize that the spacecraft could be produced in pairs at different institutions, reducing the risk of schedule conflicts, especially in integration and test facilities, along with delays to later spacecraft as earlier ones are produced. If desired, one pair of spacecraft could be built by a foreign contributor, sharing cost across multiple agencies. We recommend that a detailed study be carried out in Phase A to determine the lowest risk, lowest cost approach to manufacturing the four spacecraft.

3. Technical Overview

The overall mission architecture is described in Section 2: two FF-E spacecraft and two FF-P spacecraft, where the instrument complement for each is tailored to accomplish the science objectives of the mission while optimizing the mission cost and schedule. In Section 3, we describe each instrument, the design of each type of spacecraft, trajectories and concept of operations for each spacecraft type, and discuss mission risks.

3.1. Instrument Payload Description

The Firefly mission includes instrument types accommodated on FF-E and FF-P spacecraft as shown in Exhibit 13. Most of the instruments are based on heritage instruments from previous heliospheric missions such as STEREO, Solar Orbiter and SOHO, with a few exceptions – the Doppler Vector Magnetograph is a newer design with smaller optics than previously flown, and the Solar Irradiance instrument and Faraday Cup have simplified optical designs compared to the heritage instruments. The payload accommodation includes a single Data Processing Unit (DPU) per spacecraft that provides data processing and compression capabilities for the imaging instruments, as well as a 4-meter magnetometer boom per spacecraft to accommodate the Fluxgate Magnetometer Assembly.

	Mass			Average Power (Full Science Mode)		
	CBE (kg)	% Cont.	MEV (kg)	CBE (W)	% Cont.	MEV (W)
Imaging Instruments						
Doppler Vector Magnetograph (DVM)	19.0	15	21.9	17.0	15	19.6
Extreme Ultraviolet Imager (EUVI)	18.0	10	19.8	25.0	10	27.6
White-Light Coronagraph (WLC)	3.0	15	3.45	3.5	15	4.03
Solar Spectral Irradiance (SSI)**	3.5	15	4.03	3.0	15	3.5
White-Light Heliospheric Imager (HI+)	15.0	10	16.5	14.0	15	15.4
In-Situ Instruments						
Fluxgate Magnetometer Assembly	3.8	10	4.18	7.2	10	7.9
Faraday Cup	6.2	15	7.13	4.1	15	4.7
Solar Wind Composition	13.14	15	15.11	23.2	15	26.7
Solar Energetic Particle Suite	10.40	10	11.44	10.3	15	11.33
Total Payload Mass: FF-EA	78.9	12.7	89.0	84.1	13.1	95.1
Total Payload Mass: FF-EB	63.9	12.2	71.7	70.1	13.7	79.7
Total Payload Mass: FF-PA	73.5	12.8	83.0	93.3	14.0	106.4
Total Payload Mass: FF-PB	32.0	14.4	36.6	31.8	4.4	36.2

Exhibit 15. *Payload Mass & Power Table.*[*]
** Does not include payload accommodation mass.*
*** Packaged with the Extreme Ultraviolet Imager.*

Exhibit 15 shows the Firefly payload mass and power table. Instruments are grouped into two suites – imaging, and in-situ particles and fields.

3.1.1. Doppler Vector Magnetograph

The Doppler Vector Magnetograph (DVM) provides solar photospheric magnetic field images and Doppler velocity images using an instrument design and observing method based on the highly successful GONG instrument, which has been operating for over 20 years [Harvey et al. 1995, 1996]. The solar vector magnetic fields are critical for understanding the sources of the solar variability, such as for eruptive events related to

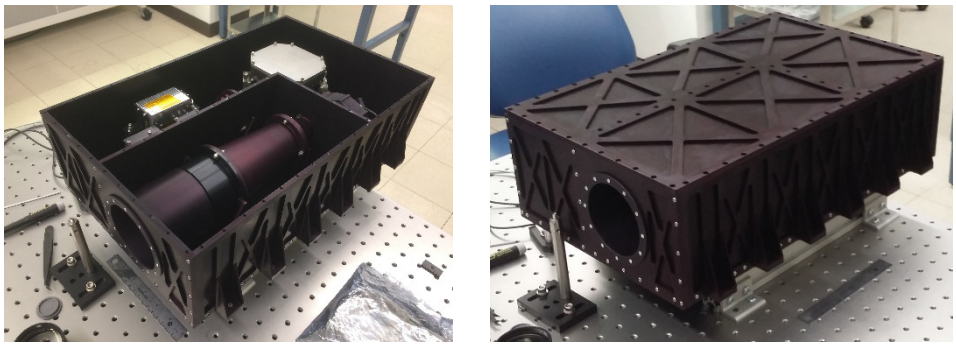

Exhibit 16. *Photographs of the Compact Doppler Magnetograph (CDM) prototype that has successfully undergone TRL 6 promotion. CVM is essentially the same system with additional optical element*

magnetic reconnection. The Doppler velocity images are important for helioseismology studies to explore the interior of the Sun, such as for rising magnetic fields of emerging active regions on the Sun. The instrument is a straightforward modification of the Compact Doppler Magnetograph (CDM) that was promoted to TRL 6 in early 2022 (Exhibit 16), and has three main differences from the GONG design to reduce size and complexity – a liquid crystal variable retarder replacing the rotating waveplate, a narrowband (~2 Å) interference filter replacing the birefringent filter, and the use of three adjacent spectral lines near 5476 Å in place of the GONG 6768 Å line to increase signal-to-noise and provide relative immunity from LOS Doppler shifts introduced by the spacecraft velocity relative to the Sun. This approach provides the advantage of higher sensitivity in B and v measurements for a given SNR compared to other single line instruments. See Exhibit 17 for the Doppler Vector Magnetograph specifications.

Item	Value	Units
Type of instrument	Doppler Vector Magnetograph	
Number of channels	One:Fe I/Ni I 5476 Å	Å
Size/dimensions (for each instrument)	43 × 28 × 18	cm × cm × cm
Instrument average science data rate **without** contingency	202.02	kbps
Instrument average science data rate contingency	25	%
Instrument average science data rate **with** contingency	252.53	kbps
Instrument Fields of View (if appropriate)	32 × 32	arcmin × arcmin
Pointing requirements (knowledge)	60	arcsec
Pointing requirements (control)	60	arcsec
Pointing requirements (windowed stability)	2	arcsec/sec

Exhibit 17. *Doppler Vector Magnetograph Summary.*

3.1.2. Extreme Ultraviolet Imager

EUV is a rebuild of the Sun-Earth Connection Coronal and Heliospheric Investigation (SECCHI) EUV telescope [Howard et al. 2008] on the STEREO mission, with slight modifications to reduce its size and complexity. EUV full disk imagers have a long heritage, from SOHO/EIT in the 1990s to the GOES/SUVI suite currently in use. Similar to the other EUV imagers, EUVI is a normal incidence Ritchey-Chrétien telescope with the image plane at the Cassegrain focus (2ry mirror in Exhibit 19). For this application, we envision the following straightforward changes to the flight-proven EUV design – reducing magnification to 2 arcs/pixel, coating the mirror for 2 wavelengths (171 and 195 A) instead of four, using updated multi-layer coatings, replacing the recloseable door with a shutter, and replacing the CCD detector with a CMOS detector. These changes will result in a lower mass and power design with better capability to image structures at the edge of the field of view. In addition, E-UV will use the same configuration as the SunCET Cubesat flight program and accommodate the Solar Irradiance (SSI) instrument in the same instrument housing.

Item	Value	Units
Number of channels	Ultraviolet Imager	
Size/dimensions (for each instrument)	2: 171/304	Å
Instrument average science data rate **without** contingency	90 x 30 x 25	cm × cm × cm
Instrument average science data rate contingency	301.85	kbps
Instrument average science data rate **with** contingency	25	%
Instrument Fields of View (if appropriate)	377.31	kbps
Pointing requirements (knowledge)	1.5	degrees
Pointing requirements (control)	60	arcsec
Pointing requirements (windowed stability)	60	arcsec
Number of channels	1	arcsec/ 10 sec

Exhibit 18. *Extreme Ultraviolet Imager Summary.*

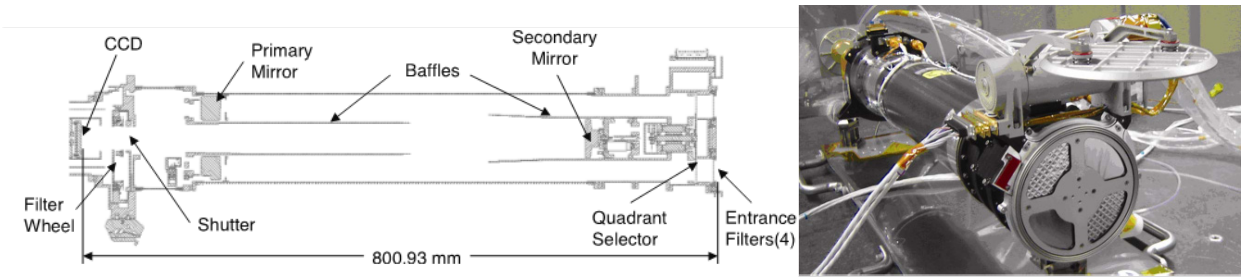

Exhibit 18. *Left: STEREO/EUVI cross section showing the main components. Right: The EUVI telescope prior to integration into the SECCHI suite. The door is open and reveals the thin Al entrance filters. The bottom left and top right filters are mesh based filters, the others are polyimide backed supported on a coarse grid. From Howard et al [2008].*

3.1.3. White-Light Coronagraph

The mini-COR WLC is a miniaturized coronagraph used to study the extended solar corona. This miniaturized design has thus far been proposed for CubeSats [Korendyke, et al. 2015], reducing the size and power compared to heritage coronagraphs on STEREO and SOHO. The design (Exhibit 20) can be accommodated in the available volume on the Firefly spacecraft by enabling a post-launch door deployment, similar to COR2 or COR1 coronagraphs. We envision that EUVI and mini-COR will be accommodated together in a common structure, similar to the SOHO/LASCO concept in order to reduce mass. See Exhibit 21 for WLC specifications.

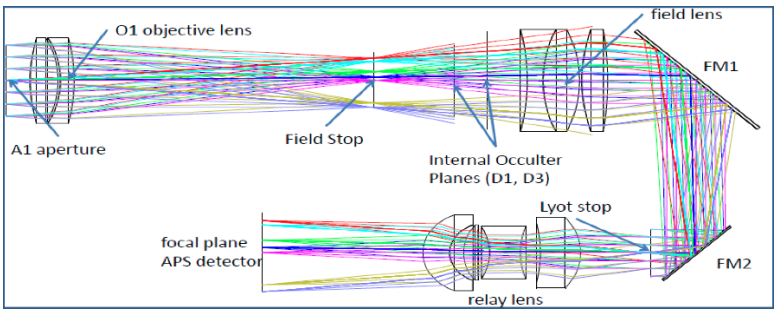

Exhibit 20. *The optical design of miniCOR white-light coronagraph. From Korendyke et al. [2015].*

Item	Value	Units
Type of instrument	Coronagraph	
Number of channels	1: 450-750	nm
Size/dimensions (for each instrument)	66 × 41 × 29	cm × cm × cm
Instrument average science data rate **without** contingency	39.81	kbps
Instrument average science data rate contingency	25	%
Instrument average science data rate **with** contingency	49.77	kbps
Instrument Fields of View (if appropriate)	10	degrees
Pointing requirements (knowledge)	60	arcsec
Pointing requirements (control)	60	arcsec
Pointing requirements (stability)	10	arcsec/20 sec

Exhibit 21. *White Light Coronagraph (WLC) Summary.*

3.1.4. Solar Irradiance

The Solar Spectral Irradiance (SSI) instrument studies the variation in solar output of light energy. The SSI irradiance spectrograph channel is a high-heritage off-Rowland circle design based on the SDO/EVE Multiple EUV Grating Spectrographs A2 (MEGS-A2) channel [Crotser et al. 2007]. It provides the full-Sun solar irradiance from 170–340 Å at 1 Å spectral resolution. This EUV range is important for overlapping with the EUVI bands for calibration purposes. SI observes Fe IX through Fe XVI emission lines that often experience coronal dimming during CMEs. It has a simplified optical design compared to previously flown irradiance instruments such as the one on Solar Dynamics Observatory, and a similar design is expected to be flown on Cubesats in the next few years (SunCET: Mason et al [2022]). Solar

Item	Value	Units
Type of instrument	Solar irradiance (μW/m²/Å)	
Number of channels	170-340	Å
Size/dimensions (for each instrument)	10x10x5	cm × cm × cm
Instrument average science data rate **without** contingency	2.13	kbps
Instrument average science data rate contingency	25	%
Instrument average science data rate **with** contingency	2.66	kbps
Instrument Fields of View (if appropriate)	N/a	degrees
Pointing requirements (knowledge)	N/a	degrees
Pointing requirements (control)	N/a	degrees
Pointing requirements (stability)	N/a	deg/sec

Exhibit 22. *Solar Irradiance Instrument Summary.*

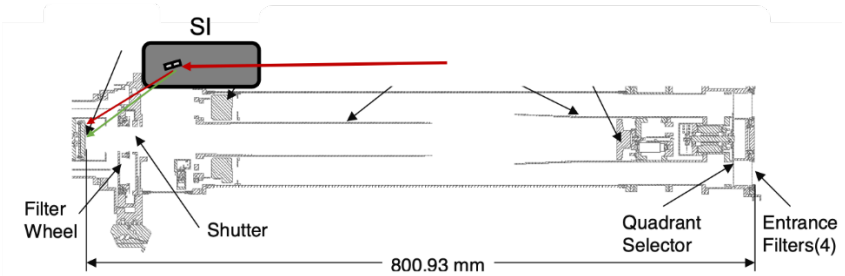

Exhibit 23. *Detail from the EUVI optical design in Exhibit 18 shows the approximate location of the SSI grating. This configuration adds spectroscopic capability to the imager with the simple addition of a grating (and its mounting hardware) and taking advantage of unused detector imaging area.*

irradiance instrument data will be continuously downlinked from the Firefly spacecraft to support space weather monitoring during the prime mission.

For this study, we accommodate SI (Exhibit 23) as a separate structure that sits on top of the nominal EUV box, and the SI and EUVI tubes have a hole to allow the dispersed light from SSI to enter the EUV focal plane array and illuminate the unused imaging area of the EUVI detector. See Exhibit 22 for the Solar Irradiance instrument specifications.

3.1.5. White-Light Heliospheric Imager

The White-Light Heliospheric Imager (HI+, Exhibit 24) measures density fluctuations in the heliosphere by observing the solar wind. HI+ is similar in design and performance requirements to the SoloHI instrument [Howard et al. 2019] currently operating on the Solar Orbiter mission.

The design modifications for HI+ relative to SoloHI are – changes to the mounts and radiators, redesign of forward baffle assembly (to account for lack of Solar Orbiter heat shield which acted as a baffle), replacement of the detector with a monolithic back-illuminated detector to increase throughput. These changes are relatively simple, straightforward tasks. See Exhibit 25 for details on the White Light Heliospheric Imager.

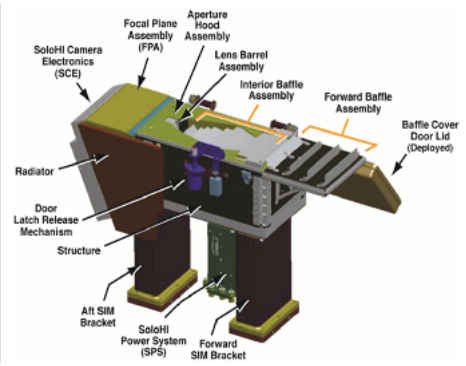

Exhibit 24*. The SoloHI instrument on board the Solar Orbiter mission. From Howard et al. [2019].*

Item	Value	Units
Type of instrument	Heliospheric Imager	
Number of channels	1: 450–760	nm
Size/dimensions (for each instrument)	66 × 41 × 29	cm × cm × cm
Instrument average science data rate **without** contingency	5.09	kbps
Instrument average science data rate contingency	25	%
Instrument average science data rate **with** contingency	6.36	kbps
Instrument Fields of View (if appropriate)	40	degrees
Pointing requirements (knowledge)	300	arcsec
Pointing requirements (control)	300	arcsec
Pointing requirements (stability)	15	deg/sec

Exhibit 25. *White Light Heliospheric Imager Summary.*

3.1.6. Fluxgate Magnetometer

The fluxgate magnetometer measures the in-situ vector magnetic field in the solar wind. The instrument has a long heritage, having flown on multiple missions. The Fluxgate Magnetometer includes two magnetometer units accommodated on a 4-m boom. The design of the triaxial fluxgate magnetometer units is the same as the IMAP magnetometer design, with one unit at the end and another midway along the length of the boom.

Item	Value	Units
Type of instrument	Fluxgate Magnetometer	
Number of channels	N/A	N/A
Size/dimensions (for each instrument)	11 × 6.6 × 8.6	cm × cm × cm
Instrument average science data rate **without** contingency	0.35	kbps
Instrument average science data rate contingency	25	%
Instrument average science data rate **with** contingency	0.43	kbps
Instrument Fields of View (if appropriate)	N/A	N/A
Pointing requirements (knowledge)	N/A	N/A
Pointing requirements (control)	N/A	N/A
Pointing requirements (stability)	N/A	N/A

Exhibit 26. *Fluxgate Magnetometer Summary.*

The required measurement range is 0–1000 nT for the magnetic field magnitude, with a cadence 20 sec for the synoptic mode and up to 8 Hz for shocks. See Exhibits 26 and 27 for details.

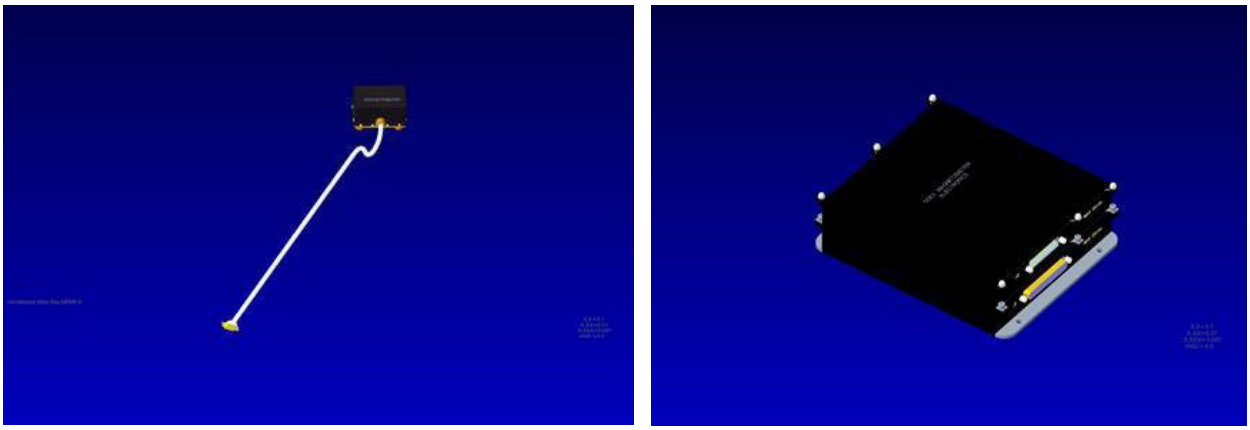

Exhibit 27. *Magnetometer Sensor (left) & Instrument Electronics Box (right).*

3.1.7. Faraday Cup

The Faraday Cup (Exhibit 28) instrument measures solar plasma distribution. This instrument is a simpler redesign of the Solar Probe Cup (SPC) on the Parker Solar Probe mission, as the complexity and materials needed to operate close to the Sun are not required in Firefly's environment at 1 AU. The modification to the PSP/SPC instrument includes the structure that is made of aluminum rather other materials required for the hot environment near the Sun. The instrument has been proposed in the payload of the MIDEX HelioSwarm mission (https://eos.unh.edu/helioswarm/mission), and it is expected that the instrument will be developed to TRL 7 in the next few years. The performance of the HelioSwarm Faraday cup satisfy the requirements of the Firefly mission.

The required measurement range is <100 km/s for the the solar wind speed, with a cadence 1 minute for the synoptic mode and up to 8 Hz for shocks. The instrument will point sunward. See Exhibit 29 for instrument characteristics.

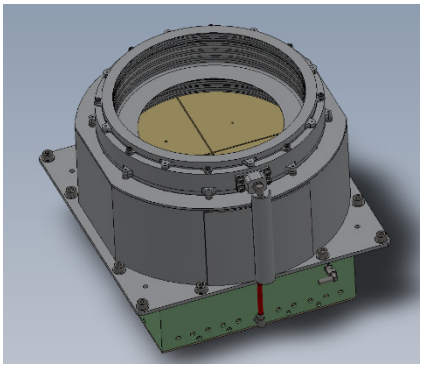

Exhibit 28*. Faraday Cup Assembly.*

Item	Value	Units
Type of instrument	Faraday Cup	
Number of channels		
Size/dimensions (for each instrument)	Sensor: 10.5 high × 20 dia Electronics: 16.5 × 17.7 × 7	cm × cm × cm
Instrument average science data rate **without** contingency	2.54	kbps
Instrument average science data rate contingency	25	%
Instrument average science data rate **with** contingency	3.18	kbps
Instrument Fields of View (if appropriate)	±20	degrees
Pointing requirements (knowledge)	0.25	degrees
Pointing requirements (control)	2	degrees

Exhibit 29. *Faraday Cup Summary.*

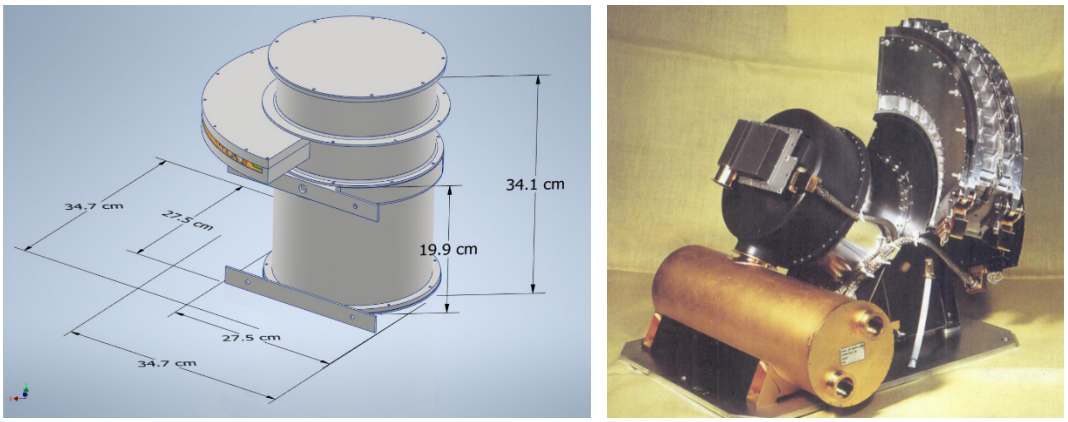

Exhibit 30. *(Left) SPICES Sensor Assembly. (Right) The ACE/SWICS Experiment (from Gloeckler et al. [1992]).*

3.1.8. Solar Wind Composition

The solar wind composition instrument SPICES (Exhibit 30) measures the elemental and ion-charge composition, the temperature and speed of all major solar wind ions from hydrogen (H) through iron (Fe). These measurements are essential to determine the dominant mechanisms for creating and accelerating thermal and non-thermal particles in the solar wind. It covers a speed range of 200–2000 km/sec and an energy range of 0.5–130 keV/e. The instrument combines an electrostatic analyzer with post-acceleration, followed by a time-of-flight (TOF) and energy measurements.

SPICES will measure the velocity distribution functions (VDFs) of solar the wind ions (mXq+): $^{4}He^{+}$, $^{4}He^{2+}$, $^{3}He^{2+}$, $^{4}He^{1+}$, $^{3}He^{1+}$, $C^{1\text{-}6+}$, $^{14}N1^{-7+}$, $^{16}O1^{-8+}$, $^{22}Ne^{1\text{-}10+}$, $Mg^{1\text{-}12+}$, $Si^{1\text{-}14+}$, $S16^{+}$, $F^{2\text{-}20+}$; suprathermal and tail ions; (interstellar and inner source PUI), within the speed range of 200–2000 km/sec, the E/q range of 0.5–130 KeV/e, and a time resolution of 2 minutes. The instrument has a field of view (FOV) and an angular resolution of 70° × 8° and 6° × 6°, respectively. The energy resolution (ΔE/E) is 0.1. SPICES will point sunward and has a geometric factor of $1.e^{-05}$ cm^{2}-sr eV/eV.

Item	Value	Units
Type of instrument	Solar Wind Composition	
Number of channels	N/A	
Size/dimensions (for each instrument)	34.7 × 34.7 × 34.1[a] 27.5 × 27.5 × 19.9[b] 15 × 20 × 8[c]	cm × cm × cm
Instrument average science data rate **without** contingency	15	kbps
Instrument average science data rate contingency	25	%
Instrument average science data rate **with** contingency	18.75	kbps
Instrument Fields of View (if appropriate)	70 × 8	degrees
Pointing requirements (knowledge)	6 × 6	degrees
Pointing requirements (control)	1–5	degrees
Pointing requirements (stability)	1–5	degrees

Exhibit 31. *Solar Wind Composition Summary.*
a – Sensor Assembly (SA); b – Available Spacecraft Interior Space; c – Electronic Box

SPICES combines the heritage from ACE/SWICS, Ulysses/SWICS and Solar Orbiter/HIS. SPICES development has been supported by NASA contract 80GSFC20C0052 to build the high voltage power supply required for the -50 kV post acceleration and the supporting mechanical and thermal design. The electrostatic analyzer design and testing was supported by internal funding from the University of Michigan. The TOF telescope electronics and non-post acceleration power supplies derive heritage from SO/HIS and Messenger/FIPS, Huygens Gas Chromatograph Mass Spectrometer (GCMS), Cassini, Comet Nucleus Tour (CONTOUR/NGIMS), Lunar Atmosphere and Dust Environment Explorer Neutral Mass Spectrometer (LADEE/NMS), and MAVEN/NGIMS.

Full instrument level system integration and environmental testing are required to reach TRL6. Instrument characteristics are provided in Exhibit 31.

3.1.9. Energetic Particle Suite

The Energetic Particle Suite measures the flux and composition of high-energy particles accelerated at flares sites, CME-driven shock waves, CIRs, SIRs, and cosmic rays. The suite is composed of multiple sensors with sunward and anti-sunward look directions. For FF-E spacecraft, the instruments are aligned with the Parker spiral at about 45 deg from the Sun-spacecraft line. For FF-P, instruments with multi-view directions, such as the instruments on STEREO, are preferred since the Parker spiral is not well-known at high solar latitudes.

Item	Value	Units
Type of instrument	Energetic Particle Suite	
Number of channels	N/A	
Size/dimensions (for each instrument)	EPT: 14 × 17 × 14 HET: 13 × 24 × 14 SIS: 10 × 40 × 30	cm × cm × cm
Instrument average science data rate **without** contingency	2.0	kbps
Instrument average science data rate contingency	25	%
Instrument average science data rate **with** contingency	2.5	kbps
Instrument Fields of View (if appropriate)	EPT: 4[a] HET: 4[a] SIS: 2[b]	
Pointing requirements (knowledge)	EPT: 30 HET: 43 SIS: 22	degrees
Pointing requirements (control)	1–5	degrees
Pointing requirements (stability)	1–5	degrees

Exhibit 32. *Energetic Particles Suite Summary*
[a] sunward, anti-sunward, north, & south; [b] sunward & anti-sunward

The energetic particle suite is TRL 9 and has been flown on multiple missions. The suite considered for this study is similar to the Solar Orbiter Energetic Particle Detector. The suite includes three detectors: the Electron Proton Telescope-High-Energy Telescope (EPT-HET) and the Suprathermal Ion Spectrograph (SIS). Rodríguez-Pacheco et al. [2020] provide the full details of the instrument suite specifications. The suite will provide electron and ion measurements within the 10 keV – 10 MeV and 10 keV/nuc – 300 MeV/nuc range, respectively.

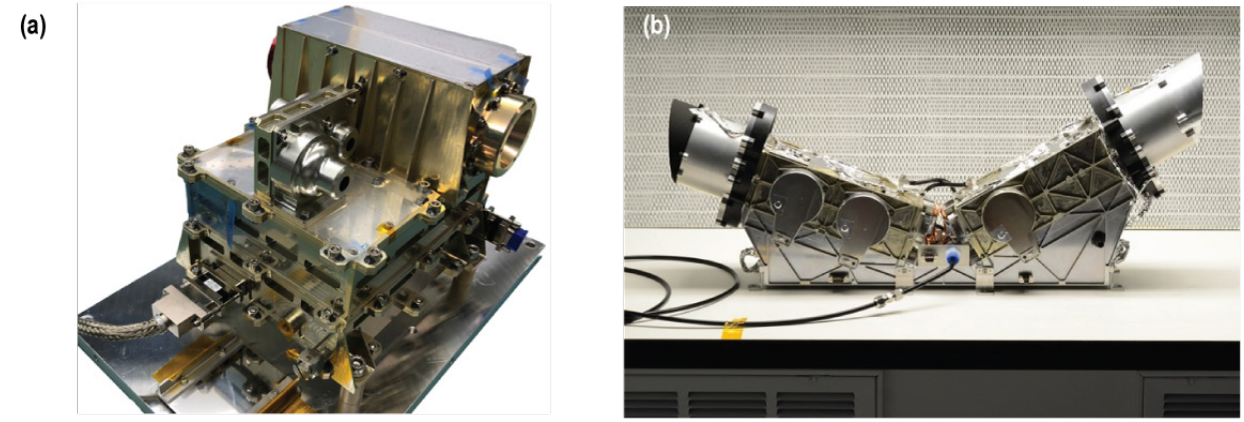

Exhibit 33. *(a) The EPT-HET unit. The EPT is on the left and the HET is the big telescope on the right. The lower part contains the electronics and power-supply. (b) The SIS flight model. All instruments are flying onboard of the Solar Orbiter mission. All three instruments have two view directions. From Rodríguez-Pacheco et al. [2020].*

3.2. Flight System

The mission architecture uses two different types of spacecraft: FF-E, designed to operate in the ecliptic plane, and FF-P which will use a Jupiter gravity assist to incline the orbit to approximately 65 degrees with respect to the ecliptic to allow for observation of the Sun's polar regions. These two spacecraft types have many elements in common; they differ only where required to allow for operation near Jupiter.

As described in Section 2, two FF-E and two FF-P spacecraft will be flown in the baseline mission. Each of these will include a tailored set of instruments, however, each spacecraft, and the mission as a whole, can accommodate a full complement of instrument on any or all spacecraft. To achieve this, we have included, for example, a full set of interfaces in the spacecraft avionics design, design of the downlink to

Flight System Element	FF-E Spacecraft	FF-P Spacecraft
General		
Design Life	15 years	15 years
Structure		
Structures Material (aluminum, exotic, composite, etc.)	Aluminum, Aluminum Honeycomb	Aluminum, Aluminum Honeycomb
Number Of Articulated Structures	None	None
Number Of Deployed Structures	Magnetometer Boom	Magnetometer Boom, Solar Array Panels
Aeroshell Diameter, m	N/A	N/A
Thermal Control		
Type Of Thermal Control Used	Passive "Thermos bottle" approach with louvers, heat pipes and thermostatically controlled heaters	Passive "Thermos bottle" approach with louvers, heat pipes and thermostatically controlled heaters
Propulsion		
Estimated ΔV Budget, m/s	See Section 3.3	See Section 3.3
Propulsion Type(S) & Associated Propellant(S)/Oxidizer(S)	Monopropellant Hydrazine	Monopropellant Hydrazine & Electric Propulsion
Number of Thrusters & Tanks	(4) 5-lbf thrusters (12) 1-lbf thrusters (1) diaphragm tank	Chem: 12 1-lbf thrusters, 1 diaphragm tank EP: 2 NEXT-C gridded ion thrusters, 2 xenon propellant tanks
Specific Impulse of Each Propulsion Mode, Seconds	Mission Average Isp = 215	Chem: Mission Avg Isp = 215 EP:
Attitude Control		
Control Method (3-axis, spinner, grav-gradient, etc.).	3-axis	3-axis
Control Reference (solar, inertial, Earth-nadir, Earth-limb, etc.)	Earth/Solar Nominal Solar – Safing Inertial - TCM	Earth/Solar Nominal Solar – Safing Inertial - TCM
Attitude Control Capability	60 arcsec about pitch and yaw, and 432 arcsec about roll, relative to the sun center	60 arcsec about pitch and yaw, and 432 arcsec about roll, relative to the sun center
Attitude Knowledge	Similar to control capability	Similar to control capability
Agility Requirements (maneuvers, scanning, etc.)	Requirement is to maintain Sun-pointing except for turns to accomplish TCMs.	Requirement is to maintain Sun-pointing except for turns to accomplish TCMs.
Articulation/#–Axes (solar arrays, antennas, gimbals, etc.)	HGA – 1 axis	HGA – 1 axis Solar Arrays – 1 axis NEXT-C thruster Gimbals – 2 axis
Sensor & Actuator Information (precision/errors, torque, momentum storage capabilities, etc.)	Reaction Wheels (4), Star Trackers (2), Sun Sensors (6) IMU (1) as described below	Reaction Wheels (4), Star Trackers (2), Sun Sensors (6) IMU (1) as described below
Command & Data Handling		
Flight Element Housekeeping Data Rate	<10 kbps	<10 kbps
Data Storage Capacity	256,000 Mbits	256,000 Mbits
Maximum Storage Record Rate	100 kbps	100 kbps
Maximum Storage Playback Rate	900 kbps	900 kbps
Power		
Type of Array Structure (rigid, flexible, body mounted, deployed, articulated)	Ridged Deployed	Deployed Flexible
Array Size, meters x meters	5.0^2m	91m^2
Solar Cell Type (Si, GaAs, Multi-Junction GaAs, concentrators)	Multi-Junction GaAs	Multi-Junction GaAs LILT Cell
Expected Power Generation at Beginning of Life (BOL) & End of Life (EOL)	1079W BOL, 865W EOL	1245W BOL Spacecraft, 22.5KW EP BOL Power, 1245W EOL Spacecraft
On-Orbit Average Power Consumption	769W	1028W
Battery Type (NiCd, NiH, Li-ion)	Lithium Ion	Lithium Ion
Battery Storage Capacity	55AH	112AH

Exhibit 34. *Flight System Element Characteristics Table.*

accommodate the data volume from a full complement of instruments, solar array sizing to power all instruments on each spacecraft, and propellant sufficient to achieve the mission with the mass of a full instrument complement. This design offers flexibility to enhance the mission as cost and schedule allow. In Exhibit 34, we first provide a full description of the FF-E spacecraft design, followed by description of those elements of the FF-P spacecraft design that differ from the FF-E design.

3.2.1. Firefly-Ecliptic

The FF-E spacecraft are 3-axis controlled spacecraft that incorporate all the functions needed to accomplish the Firefly science objectives, including communication functions with Earth, maneuvers, a stable platform for the science measurements, and powering of all systems. All electronics subsystems are redundant to accommodate the 15-year mission design life. Exhibit 35 shows the physical configuration of the FF-E spacecraft, while Exhibit 36 provides the system block diagram for FF-E.

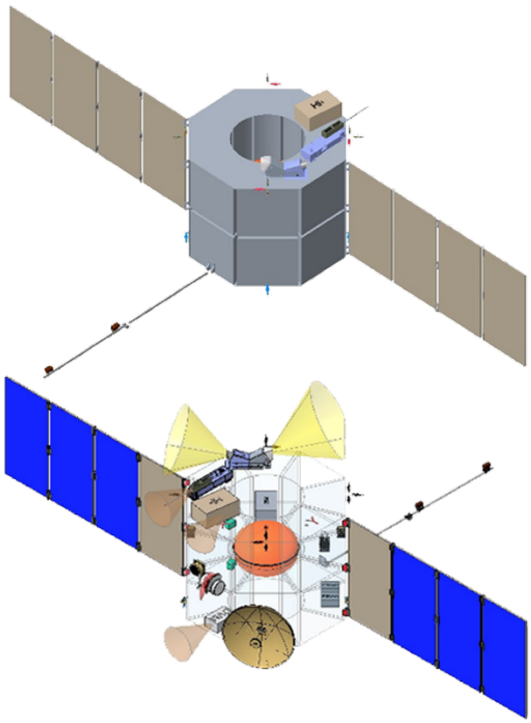

Exhibit 35. *Views of the FF-E spacecraft. The left figure shows the exterior as viewed from the anti-Sunward direction. The right figure gives a transparent view of the Sun-facing side to show instruments with fields of view and major structure.*

Structure. The FF-E spacecraft structure consists of an aluminum central cylinder, with aluminum honeycomb primary structural panels. The top, mid, and bottom decks have an octagonal planform, and eight spoke panels extend from the primary cylinder to the octagon's vertices. The primary structure is then closed out by eight rectangular panels, which mate to the mid-deck as well as adjacent panels. The central cylinder on each spacecraft serves as the interface to the propellant tank, and additionally provides the clamp-band interface for the launch vehicle separation system. As the two FF-E

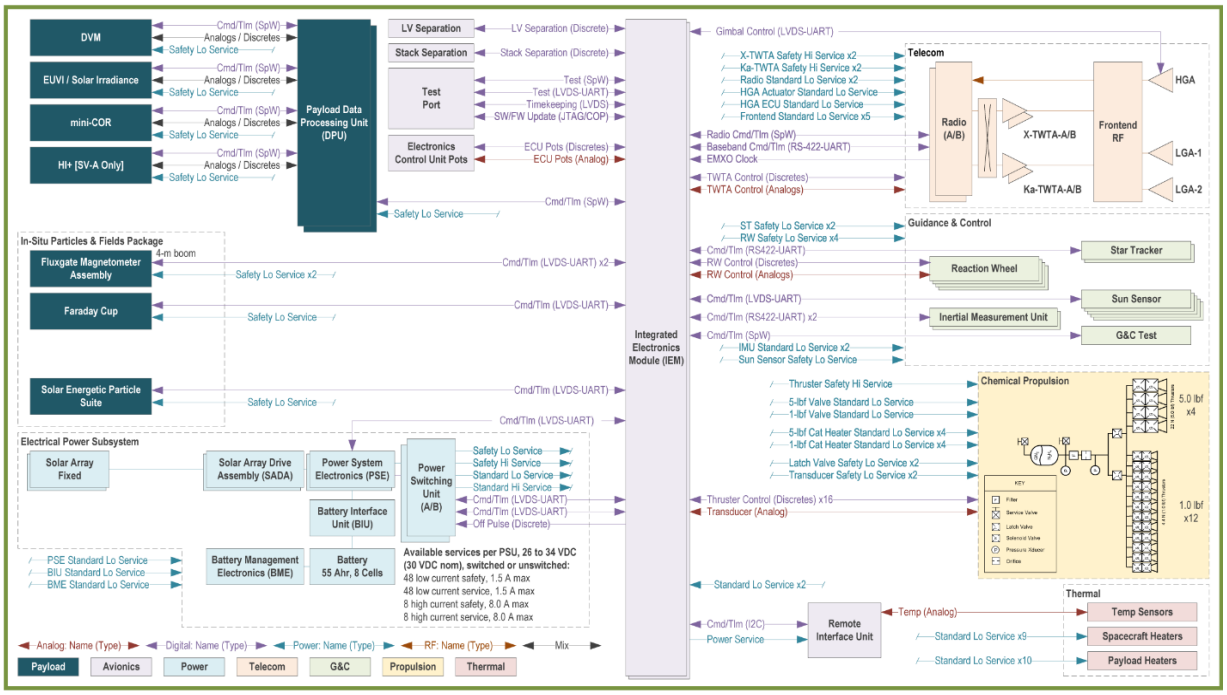

Exhibit 36. *FF-E Block Diagram.*

spacecraft are designed to launch stacked on a single launch vehicle (Exhibit 37), an additional separation system is located between the top and bottom spacecraft, and the primary cylinders are sized to react the combined base bending moment at the launch vehicle interface. The separation system is a commercially available clamp band system with high heritage in missions such as STEREO.

Instruments on spacecraft components are packaged to maintain clear FOVs and achieve desired pointing angles, with Sun pointing instruments located on the Sun-facing +X panels. The HGA is packaged on the panel adjacent to the central +X panel to take advantage of the orbital Sun-Earth angle and minimize the required range of motion. The deployable magnetometer boom located on the –X panels and +Y/-Y panels are used to support the stowed solar arrays. The stacked spacecraft assembly in the launch configuration fits within available 5-m fairings.

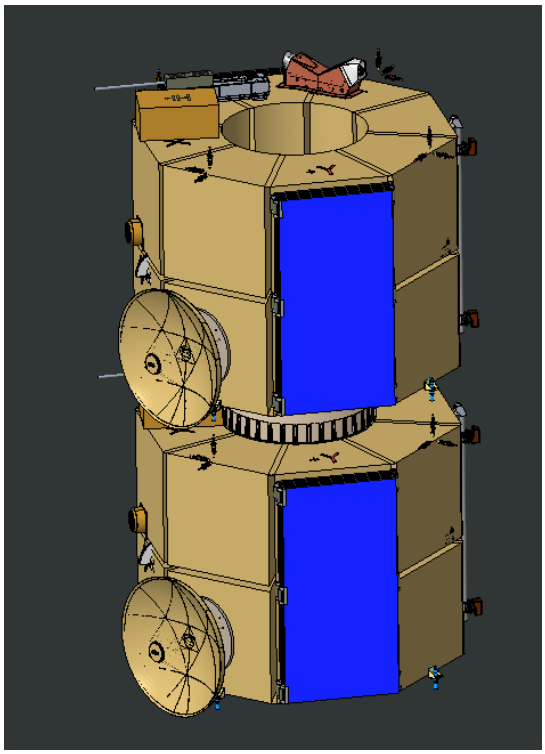

Exhibit 37. *Physical configuration of the FF-E spacecraft in launch.*

Propulsion. Each FF-E spacecraft will use a simple blowdown monopropellant system (Exhibit 38). Hydrazine propellant will be stored in a single 40.2-inch oblate-spheroid diaphragm tank, NGIS 80263, with flight heritage. Four 22 N (5 lbf) MR-106L thrusters and twelve 4.4 N (1.0 lbf) MR-111G thrusters provide ΔV and attitude control respectively. The remaining components, such as latch valves and pressure transducers, etc., will all be sourced from a catalog of options having extensive flight heritage on past missions. The 362 kg of propellant carried by each FF-E spacecraft will provide 830 m/s of ΔV capability. 10 kg of the total mass is allocated to attitude control usage.

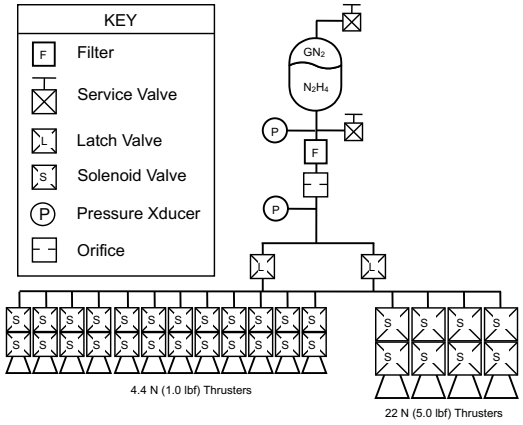

Exhibit 38. *FF-E Propulsion System.*

Power. The power system design for both FF-E spacecraft is identical. The power system consists of a redundant power system electronics box, two block redundant power switching units, two solar array wings, solar array diode box, battery management unit, and a single 55 Ah battery. The power system topology chosen is a battery on the bus peak power tracking system. The architecture isolates the solar array from the variations of the battery voltage and maximizes the solar array power output. The loads are directly connected the single 8-cell 55 Ah lithium-ion battery. The unregulated bus voltage varies between 24 V to 32 V, depending on the battery state of charge. The power system is sized to support the battery recharge post-G&C maintenance mode of operations at EOM, 546 W CBE +30% margin, 835 W total including battery recharge power. The 5 m^2 solar array develops an end of mission (EOM) power of 1011 W. The power system electronics has a maximum power processing capability of 1000 W, which meets the EOM power requirements by both spacecraft. The maximum battery depth of discharge is 62% from launch to solar array deployment without solar input.

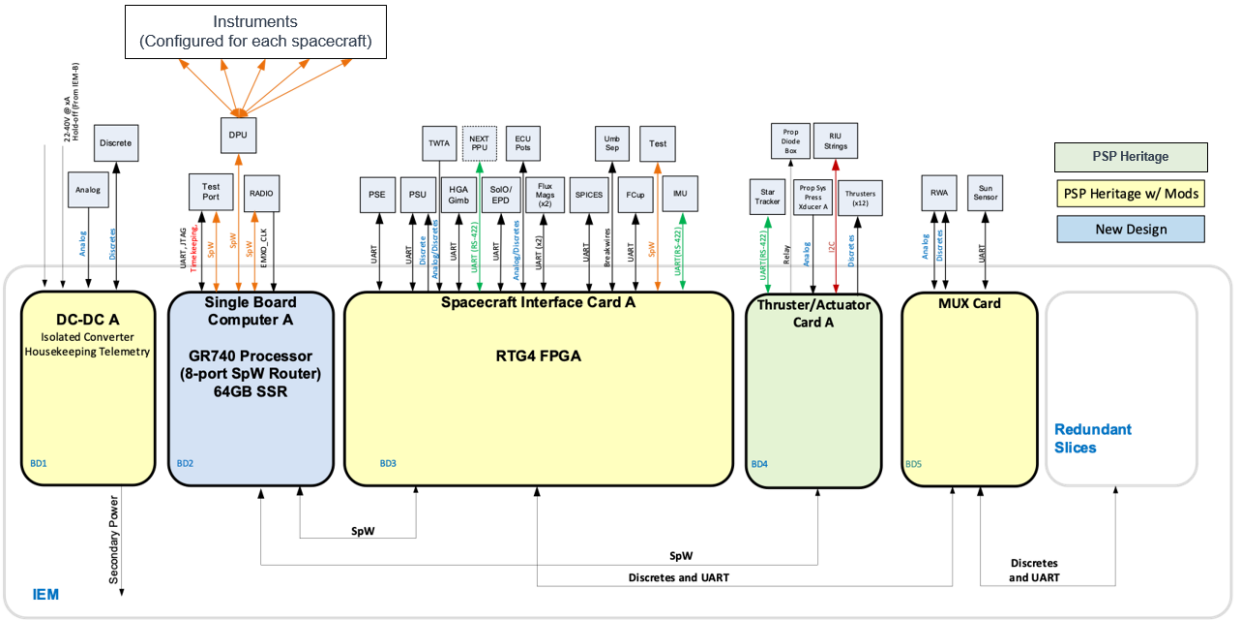

Exhibit 39. *Firefly Avionics Block Diagram.*

Avionics. The avionics subsystem (Exhibit 39) manages the spacecraft command and data handling requirements and is based on heritage designs from Parker Solar Probe (PSP) and Double Asteroid Redirection Test (DART). The single Integrated Electronics Module (IEM) box leverages a slice-based architecture similar to PSP flight system, using a multiplexer card (MUX) to join A and B sides of the IEM in order to achieve block redundancy. Other heritage-based components of the IEM include DC/DC converters, Spacecraft Interface Cards (SCIF), and a Thruster/Actuator Cards (TAC). The Single Board Computers (SBC) each provide 187 MB of SRAM, 8 MB of NOR flash for flight software code storage, 256 Gb of NAND flash for solid-state recorder (SSR) storage and a GR740 quad-core processor that operates at 250MHz and utilizes an eight-port SpaceWire router. The FF-E IEM will host four TACs to support the additional thrusters needed. The SCIF card will support interfaces that are tailored for the FF–E and FF–P spacecraft. The two strings of Remote Interface Units (RIUs) provide 240 analog channels for temperature sensing. Propulsion Diode Boxes (PDB) planned for Europa Clipper are used to mitigate electromagnetic interference that are caused by the thrusters firing. The IEM also provides the capability to disable individual cards when their functions are not needed to help save power.

Guidance & Control. The FF-E spacecraft control subsystem will assert three-axis attitude control at all times using two types of control actuators, 4 × 12 Nms momentum reaction wheels and 12 × 5 N chemical propellant thrusters. These hydrazine thrusters exist primarily to desaturate the momentum wheel speed but will also facilitate Trajectory Correction Maneuvers (TCM) controlled by the Reaction Control System (RCS) algorithm.

Attitude determination will be accomplished by blending angular rate measurements from a four-axis Inertial Measurement Unit (IMU), containing full internal redundancy, with attitude quaternion data from two orthogonally mounted Star Trackers. This configuration guarantees redundant measurements with a large sky coverage providing sufficient attitude knowledge to meet the pointing requirements. Attitude determination hardware is further augmented with 5 wide-angle Digital Sun Sensors (DSS) providing full 4π-steradian angular coverage for single star tracker and safe mode operations.

The attitude guidance will persistently point the scientific instrument boresight directly at the Sun, to maximize the fixed solar array output, facilitate scientific observation, and correct for any moments due to Center-of-Pressure (CP) to Center-of-Mass (CM) offsets resulting from solar radiation pressure (SRP). During science collection the pointing accuracy shall be within 60 arcsec about pitch and yaw, and

Component	Manufacturer & Model	TRL	Quantity (per S/C)	Unit Mass	Unit Power
Wheels	Rockwell Collins RSI12-75/60	9	4	4.85 kg	<90W Max <20W Nom 24-51VDC <3.75A
Star Tracker	Leonardo AA-STR	9	2	2.55 kg	<13W 22-35 VDC
Sun Sensor	Redwire (Formerly Adcole)	9	1(SSE) 5 (DSS)	1 x 1.45 kg (Max) 5 x 0.26 kg (Max)	< 6W 22-35 VDC
IMU	Northrop Grumman SSIRU	9	1 (Internally Redundant)	~8kg	< 48W

Exhibit 40. *Guidance and Control Instruments.*

432 arcsec about roll, relative to the sun center. The G&C subsystem shall ensure that the optical jitter over a 10 second window does not exceed 1 arcsec cross boresight and 40 arcsec about the boresight, while the optical smear over a 1 hour window shall not exceed 7.2 arcsec cross boresight and 1.1 arcmin about the boresight. Meeting the jitter requirement is an area of concern for the G&C team and implies either having a very rigid spacecraft (probably not feasible) or avoiding excess excitation of the structural modes. The large momentum storage capability of the wheels assists in this regard by minimizing the need for desaturation burns from the Attitude Control System (ACS) and/or allowing such burns to occur at times when science coverage may be available from other spacecraft. To prevent excitation of structural resonances due to wheel imbalance, certain wheel speed may need to be avoided.

Lastly, the flight control software is also responsible for articulation of the High Gain Antenna (HGA) through one rotational Degree-of-Freedom (DoF) using an electromechanical servo. During cruise phase of flight, the Sun-spacecraft-Earth geometry is highly variable, significantly minimizing the usability of the HGA, thus the Fanbeam and Low-Gain Antennae (LGA) will be responsible for communications. However, after the spacecraft has parked within its final orbit, such geometry will stabilize allowing the HGA to frequently close communications contact with Earth, which will require only about ±4º of HGA servo articulation without spacecraft attitude adjustments.

All G&C subsystem hardware should be TRL 9 and have significant flight heritage. The initial trades were performed using the list of hardware described in Exhibit 40.

Flight Software. The Flight Software (FSW) subsystem can be built with heavy reuse from legacy software that provides a reused common set of applications for command management, telemetry, formatting, data recording and playback, autonomy, file management, and application scheduling that can be used with minimal changes/updates. A description of the flight software design and heritage is given in Exhibit 41.

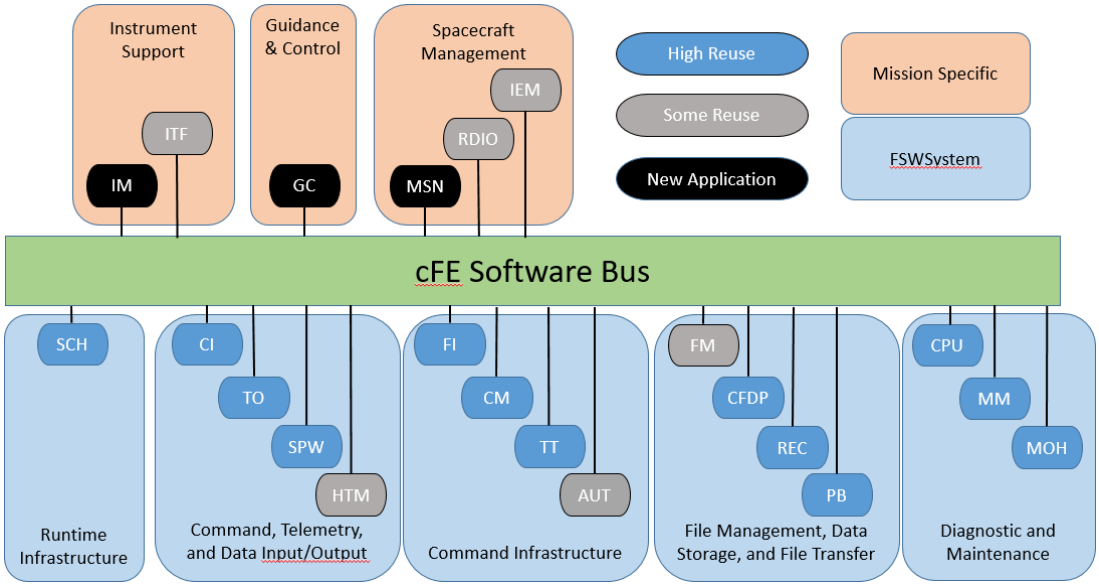

Exhibit 41. *The FSW Architecture Concept built on cFE applications. As shown, nearly all applications in flight software system can be reused entirely, while there are some mission specific apps that will be customized for Firefly, as is typical for any mission.*

Some unique components would be required for a mission like Firefly, but none that present any unsurmountable challenges from those normally solved during the FSW development for current missions. No major risks have been identified for this mission from a FSW perspective.

Thermal Control. The FF-E thermal design is enabled by its near constant solar distance, lack of eclipses and consistent, sun-relative spacecraft attitude. Each spacecraft is blanketed entirely in multi-layer insulation with the exception of the radiators and component/instrument penetrations. The spacecraft is oriented so that some surfaces are consistently non-sun facing offering flexibility in radiator placement. A majority of the spacecraft, including the propulsion system, is kept within temperature ranges via thermostats, heaters, and internal component heat dissipation coupled to the structure. The battery and sun-facing instruments require thermal isolation to stay within their temperature limits. K-core doublers or aluminum thermal ribs may be required to distribute heat in the final design, as is typical for many spacecraft.

Telecommunications. The telecommunications subsystem characteristics are driven by the large amount of data to be downlinked daily: 6.4 GB of compressed data per day, with 25% margin. For the FF-E spacecraft, a 1.0-m gimbaled HGA is paired with 100-W traveling-wave tube amplifiers (TWTAs) for both a Ka-band and X-band downlink. The HGA is dual-feed X- and Ka-band, so X-band downlink through the pointed HGA is available. Command uplink is X-band in all cases. The HGA requires 0.1-degree pointing accuracy to minimize losses. The mission profile results in approximately 30-degree Sun-Earth-Probe (SEP) angles during the science phase for all spacecraft, so the HGA is nominally pointed at this angle, while the gimbal allows it to track the Earth.

For housekeeping or periods of cruise where pointing cannot be maintained (such as launch and early operations, and maneuvers), the downlink will be X-band through two opposing low-gain antennas (LGAs). The mission also requires a continuous downlink for space weather data (low volume) at all times. When not included with the science data on the Ka-band link, it can be downlinked through the HGA at X-band.

Downlinking this required volume of data daily requires 10-hour passes with NASA's Deep Space Network (DSN) 34-m ground stations. Numerous mission phases and conditions were evaluated to ensure links close with sufficient margin for both FF-E. Exhibit 42 shows a summary of key rates.

Two key trades defined the telecommunications subsystem. First, NASA directs all new missions to baseline Ka-band downlinks, which inherently offer more gain. For Firefly, the required data volume makes this extra Ka-band gain necessary. This adds mass, complexity, and more accurate pointing, however, accommodating these are within the scope of this mission. Second, because two spacecraft are launched on one rocket (each for FF-E and FF-P), fairing profiles limit the size of the HGA. Further, the relatively close Sun range means the power system is capable of accommodating higher power downlink amplifiers, so the HGA size is minimized in favor of higher power TWTAs.

Telemetry, tracking, and control (TT&C) is provided through redundant Frontier Radios. The Frontier Radio has significant flight heritage on NASA's Van Allen Probes, Parker Solar Probe, and DART missions, as well as on the United Arab Emirates' Hope Mars mission; and, by the time Firefly would launch, NASA's Europa Clipper and Dragonfly missions. The next-generation version will employ major reuse of the software-defined radio (SDR) algorithms and processing while taking advantage of more

Mission Phase	Max Range (AU)	Frequency Band	Antenna	Pointing Accuracy	Min Max Uplink (bps)	Min Max Downlink (bps)
LEOPs	< 0.1	X	LGA1/2	± 90°	325	3,500
Cruise, no HGA pointing	0.4 to 1.76	X	LGA1	± 45°	62.5	75
Science, Space Weather	1.76	X	1.0-m HGA	± 0.1°	2,000	312,500
Science, 6.4 GB/day (+25%)	1.76	Ka	1.0-m HGA	± 0.1°	2,000	1,666,667

***Exhibit 42**. FF-E Critical Links and Data Rates.*

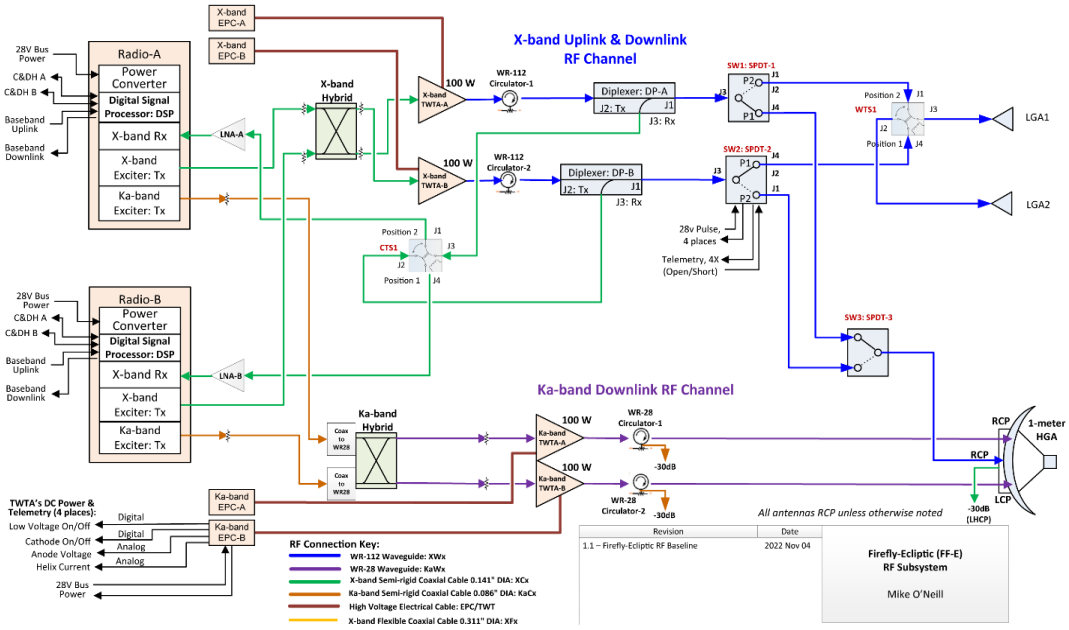

Exhibit 43. *FF-E Telecommunications Subsystem.*

advanced modern hardware. All other components have flight heritage except for the 150-W Ka-band TWTA which a vendor has in development based on flight heritage designs, with tested engineering models. It will have flight heritage by the time Firefly development would be underway. A block diagram details the subsystem in Exhibit 43. Just two items indicate the difference between the FF-E and FF-P subsystems (TWTA power and HGA size).

3.2.2. Firefly Polar

In many areas, the design of the FF-P spacecraft is identical to the FF-E spacecraft. In this section, only the subsystems that are different are described. Exhibit 44 gives the physical configuration of the FF-P spacecraft, while Exhibit 3-45 gives the block diagram.

Structure. The FF-P spacecraft structure takes the shape of rectangular prism, and also employs aluminum honeycomb panels. Two vertical stringer panels and three distinct mid-decks are close out by forward, rear, and side panels. The vertical stringer panels run from the base deck to the upper middeck, and serve as locations for launch vehicle separation nut system as well as the primary load path for the spacecraft. The three propellant tanks are packaged on the central middeck, and struts are used to provide a structural load path down to the launch vehicle interfaces.

Instruments on the FF-P spacecraft are also packaged to allow for unobstructed fields of view. The +X panel on the FF-P spacecraft is sun pointing, and has provisions to mount or

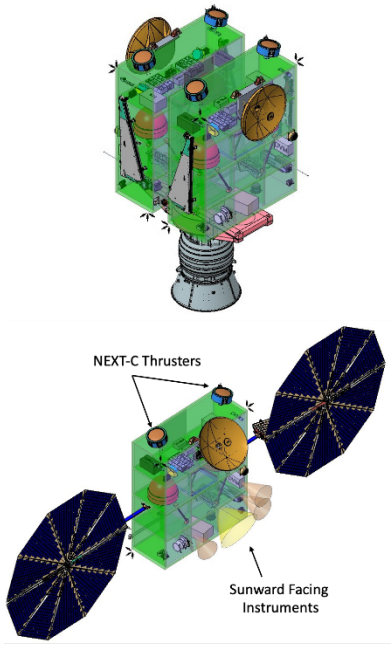

Exhibit 44. *Physical configuration of the FF-P spacecraft in launch configuration (top) and fully deployed for science operations (bottom).*

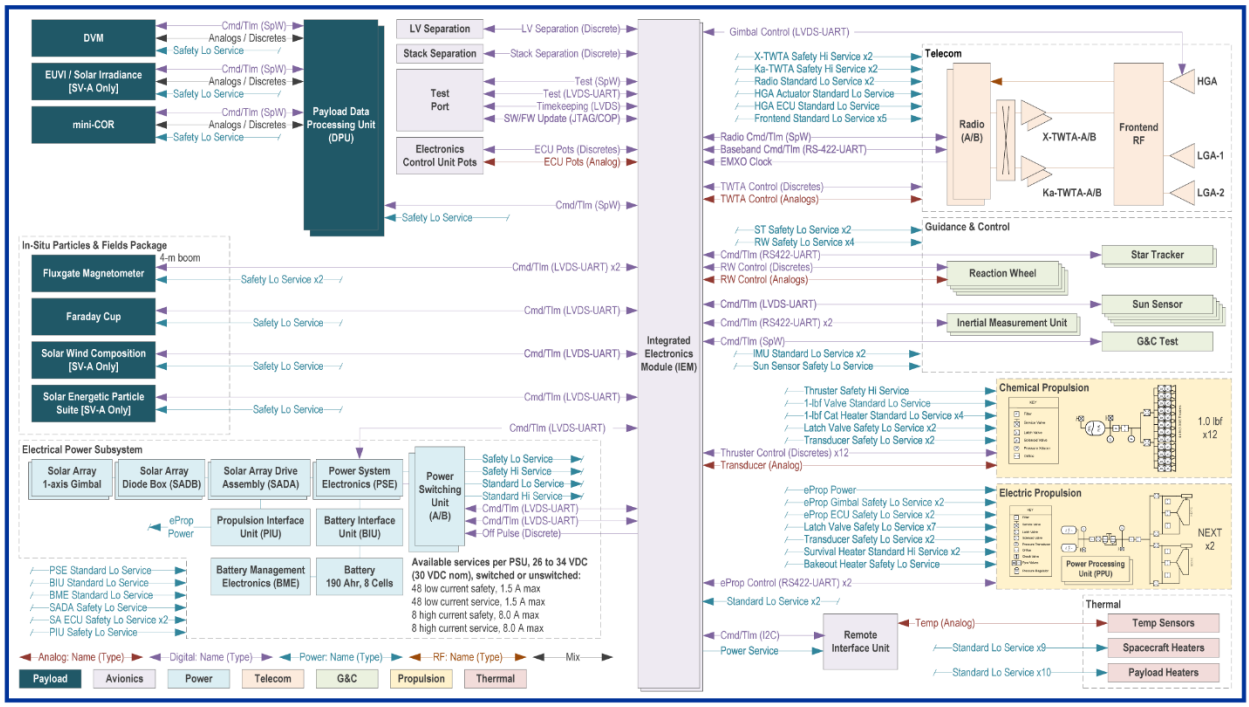

Exhibit 45. *FF-P Block Diagram.*

accommodate the fields of view of sun pointed instruments. The deployable Solar Arrays are installed to the ±Y panels, while the outside face of the top deck is used to package the dual electric propulsion thrusters and gimbal assemblies. The HGA is stowed to point in the +X direction, and uses a gimbal to point it about the Y-axis in flight. The deployable magnetometer boom is packed on the –X panel to avoid any instrument fields of view when deployed. The two FF-P spacecraft are designed to mount side by side on a dispenser table, and the combined assembly is compatible with available 5-m fairings as well.

Propulsion. Each FF-P spacecraft will have a chemical and electric propulsion (EP) system. The EP system will be the primary source of delta-V, with the chemical system acting as support to provide momentum dump capability and compensation for any offset in the EP engine thrust vector relative to the spacecraft center of mass.

The chemical system on FF-P will be a blowdown monoprop system, similar to FF-E but of smaller size. The chemical system is required to provide 20 m/s ΔV along with 43 kg of propellant for momentum dumps and other attitude control functions for a total propellant load of 60.7 kg. The hydrazine will be stored in a single ATK 80512-in spherical diaphragm tank. Twelve 4.4 N (1 lbf) MR-111G thrusters are all that's needed to provide the necessary system capability.

The EP system will feature two NEXT-C gridded ion engines, with one acting as primary and the other redundant. Each NEXT engine requires its own power-processing unit (PPU) which will provide the appropriate power and voltage. The NEXT-C PPU flown on the APL mission DART had only three throttle levels qualified. The Firefly

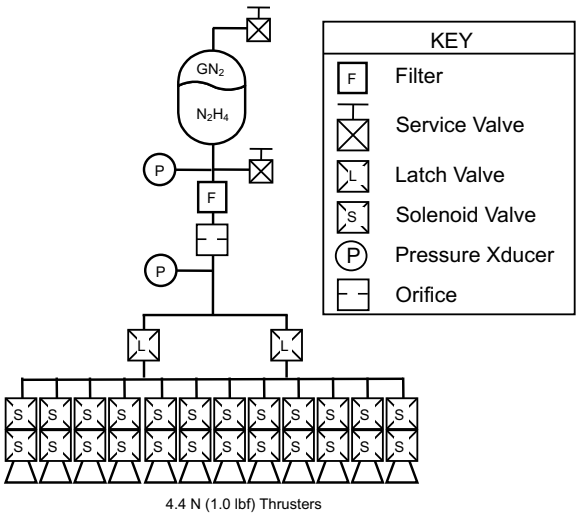

Exhibit 46. *FF-P Chemical Propulsion System.*

mission design will require additional throttle levels to achieve the necessary performance from the engine. This will require ground testing of the PPU at each needed throttle level for flight, and will increase TRL to 6; this testing will be completed by PDR. To provide a measure of control of the thrust vector, the engines will each be mounted on a gimbal. As there is no existing gimbal for NEXT-C, one will need to be designed and built for the mission. Xenon propellant will be stored in two ARDE 4790 30-inch diameter tanks. A total of 531 kg of xenon will be loaded onto the spacecraft and pressurized to approximately 2600 psi. Remaining components will be selected from APL flight heritage options.

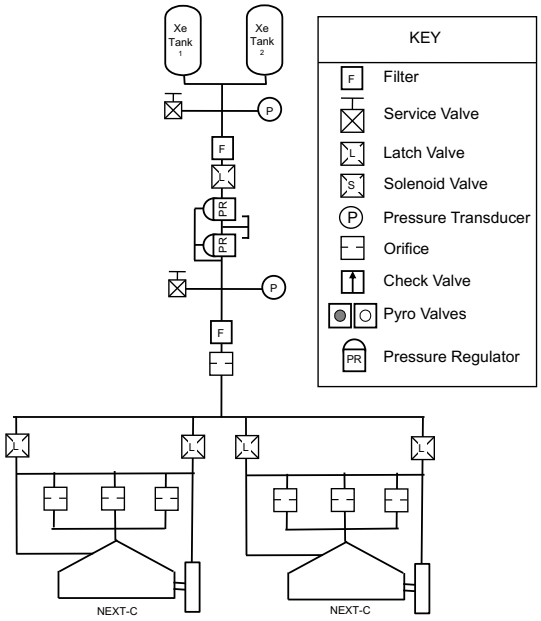

Exhibit 47. *FF-P Electric Propulsion System.*

Power. The power system designs for both FF-P spacecraft are identical. The power system consists of a redundant power system electronics box, two block redundant power switching units, two solar array wings, solar array junction box, propulsion interface unit, battery management unit, and a single 112 Ah battery. The power system topology chosen is a battery on the bus peak power tracking system. The architecture isolates the solar array from the variations of the battery voltage and maximizes the solar array power output. The loads are directly connected the single 8-cell 112 Ah lithium-ion battery. The unregulated bus voltage varies between 24 V to 32 V, depending on the battery state of charge. The power system is sized to support the downlink at Jupiter mode of operations at end of mission (EOM), 799.7 W CBE +30% margin, 1077 W total power. The residual solar array power generated is used to operate the NEXT thruster at sun distances less than 2.0 AU. The 92-m^2 solar array provides power to operate the spacecraft at 5.137 AU. The EOM solar array power utilized by the spacecraft is 1445 W, which is limited by the power system electronics, and meets all EOM power requirements by both spacecraft. For this concept study, we have used solar arrays from Northrup Grumman similar to the arrays flown on the Lucy mission, however a Phase A trade will be carried out to define the optimum solar array architecture. The maximum battery DOD is 35% during from launch to sun pointing without solar input.

Guidance & Control. In general, the majority of the G&C subsystem for FF-P is identical to the FF-E spacecraft with key differences highlighted below.

The FF-P spacecraft utilizes two Electric Propulsion (EP) thrusters to perform protracted TCMs while employing a Thrust Vector Control (TVC) Assembly (TVCA). The TVCA for each thruster consists of a two degree of freedom servo control system that will manipulate the thrust vector line of action, and as a consequence, the spacecraft attitude. In addition to directional thrust, EP has the undesired effect of also generating a disturbance "swirl" torque, tending to spin the spacecraft around the thrust vector. The momentum wheels will gradually spin up to counter the swirl torque effects, requiring more frequent desaturation from the hydrazine thrusters. Lastly, in order to power the EP, each of the two solar arrays must articulate through one angular degree of freedom, using a Sun-tracking algorithm that maximizes solar flux.

Because the FF-P spacecraft will use a Jupiter gravity assist, the solar arrays are expected to be very large in order to power the spacecraft at ~5 AU. Fortunately, the EP will not be operated during science operations, so the more frequent desaturation events required because of EP operation should not adversely impact the jitter. However, the large solar arrays will lower the structural flexible mode frequencies, which will most likely require significantly longer to dampen out, an effect that is present

during science ops. Furthermore, the large solar array area will make the effects of CP to CM offsets more pronounced when operating at 1AU. Therefore, the large momentum storage capacity of the wheels become even more important to reduce the structural mode impacts on science ops. The detailed design of FF-P will address this issue, including the possibility of using instrument stabilization.

HGA articulation is similar to the FF-E spacecraft, using a one degree-of-freedom arrangement, but the angular extent required is significantly larger at ±40 degrees. During cruise flight the spacecraft attitude will be modified to close HGA contacts as using fan beam antennae would be impractical at the 5 AU range. This also requires the G&C algorithms to control each Solar Array about a single degree of freedom of articulation to consistently track the Sun during these events.

During science operations at 1 AU the attitude guidance will again persistently point the scientific instrument boresight directly at the Sun, but HGA contacts may require the spacecraft to be rolled about the Sun Line.

Thermal Control. The FF-P thermal design accommodates a range of solar input due to the need for a Jupiter gravity assist, followed by an elliptical science orbit at 1–2 AU. Each spacecraft is blanketed entirely in multi-layer insulation with the exception of the radiators and component/instrument penetrations. The spacecraft is oriented so that some surfaces are consistently non-sun facing offering flexibility in radiator placement. A majority of the spacecraft, including the propulsion system, is kept within temperature ranges via thermostats and heaters sized to accommodate the worst-case environment, and internal component heat dissipation coupled to the structure. The battery and sun-facing instruments require thermal isolation to stay within their temperature limits. K-core doublers or aluminum thermal ribs may be required to distribute heat in the final design, as is typical for many spacecraft.

Telecommunications. The telecommunications subsystem characteristics are driven by the large amount of data to be downlinked daily: 6.4 GB of compressed data per day, with 25% margin. For the FF-P, the increased Earth ranges necessitate a 1.4-m gimbaled high-gain antenna (HGA) with a 150-W Ka-band TWTA, while X-band links still close with the 100-W TWTA. The HGA requires 0.1-degree pointing accuracy to minimize losses. The mission profile results in approximately 30-degree Sun-Earth-Probe (SEP) angles during the science phase for all spacecraft, so the HGA is nominally pointed at this angle, while the gimbal (along with spacecraft orientation) allows it to track the Earth for pointing.

For housekeeping or periods of cruise where pointing cannot be maintained (such as launch and early operations, and maneuvers), the downlink will be X-band through two opposing low-gain antennas (LGAs). The mission also requires a continuous downlink for space weather data (low volume) at all times. When not included with the science data on the Ka-band link, it can be downlinked through the HGA at X-band. The HGA is dual-feed X- and Ka-band, so X-band downlink through the pointed HGA is also available for this or as a backup to the Ka-band link (with lower rates). Command uplink is X-band in all cases.

Downlinking this required volume of data daily requires 10-hour passes with NASA's Deep Space Network (DSN) 34-m ground stations. For FF-P, emergency operations at Jupiter range would require a

Mission Phase	Max Range (AU)	Frequency Band	Antenna	Pointing Accuracy	Min Max Uplink (bps)	Min Max Downlink (bps)
LEOP	< 0.1	X	LGA1/2	± 75°	2,000	10,000
Cruise, Emergency*	5.9	X	LGA1	± 30°	31.25	40
Cruise, Pointed, X	5.9	X	1.4-m HGA	± 0.1°	2,000	40,000
Cruise, Pointed, Ka	5.9	Ka	1.4-m HGA	± 0.1°	2,000	455,000
Science, Space Weather	3	X	1.4-m HGA	± 0.1°	2,000	160,000
Science, 6.4 GB/day (+25%)	3	Ka	1.4-m HGA	± 0.1°	2,000	1,666,667

Exhibit 48. *FF-P Critical Links and Data Rates.*
X-Band: 100-W TWTA; Ka-Band: 150-W TWTA
*Emergency assumes 70-m ground station

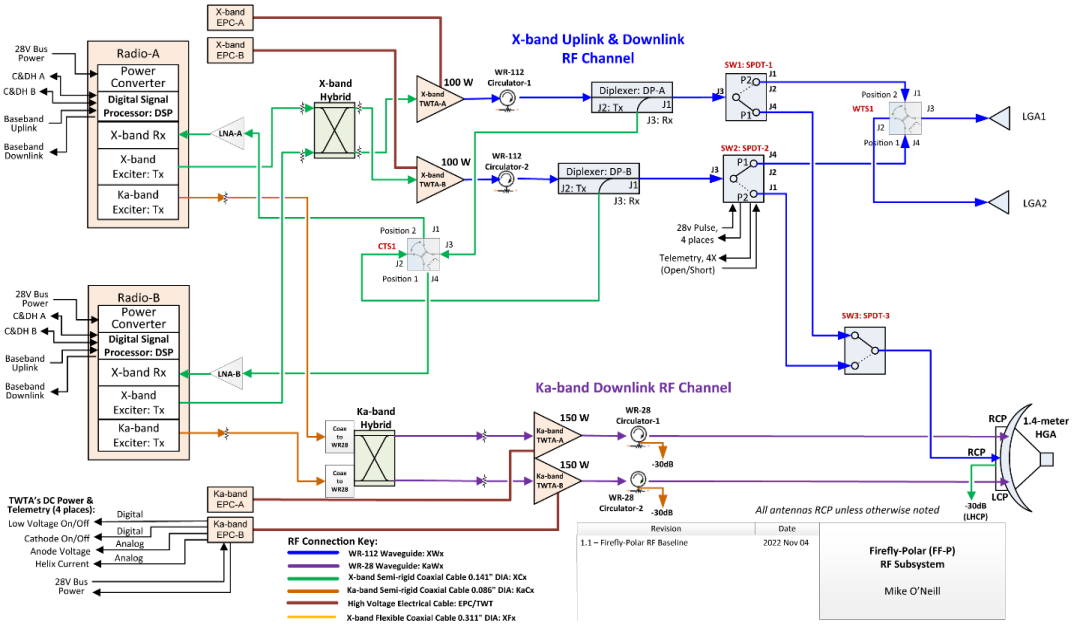

Exhibit 49. *FF-P Telecommunications Subsystem.*

70-m DSN station if pointing cannot be maintained. Numerous mission phases and conditions were evaluated to ensure links close with sufficient margin for FF-P. Exhibit 48 shows a summary of a few key rates for the FF-P spacecraft.

Two key trades defined the telecommunications subsystem. First, NASA directs all new missions to baseline Ka-band downlinks, which inherently offer more gain. For Firefly, the required data volume makes this extra Ka-band gain necessary. This adds mass, complexity, and more accurate pointing, however, accommodating these are within the scope of this mission. Second, because two spacecraft are launched on one rocket (each for FF-E and FF-P), fairing profiles limit the size of the HGA. Further, the relatively close Sun range means the power system is capable of accommodating higher power downlink amplifiers, so the HGA size is minimized in favor of higher power TWTAs.

Telemetry, tracking, and control (TT&C) is provided through redundant APL Frontier Radios. A next-generation version is under development to replace the current "Classic" version and would be available by the time 4π is underway. The Frontier Radio Classic has significant flight heritage on NASA's Van Allen Probes, Parker Solar Probe, and DART missions, as well as on the United Arab Emirates' Hope Mars mission, and by the time Firefly would launch, NASA's Europa Clipper and Dragonfly missions. The next-generation version will employ major reuse of the software-defined radio (SDR) algorithms and processing while taking advantage of more advanced modern hardware. All other components have flight heritage except for the 150-W Ka-band TWTA which a vendor has in development. It is based on flight heritage designs, and engineering models have been tested. It will have flight heritage by the time Firefly development would be underway. A block diagram details the subsystem in Exhibit 49. Just two notes indicated the difference between the FF-E and FF-P subsystems (TWTA power and HGA size).

3.2.3. Spacecraft Resources

Detailed mass and power equipment lists (MELs, PELs) were developed for each spacecraft and launch case. Exhibit 50 gives summary MEL and PEL tables for the FF-E spacecraft. Exhibit 51 gives these tables for the FF-P spacecraft. PEL tables for each spacecraft give power condition for science operations and for data downlink mode; other operating modes were examined, and all have robust margins.

Exhibit 50. *FF-E Flight System Element Mass and Power Summary Table.*

	FF-EA Mass			FF-EB Mass		
	CBE (kg)	% Cont.	MEV (kg)	CBE (kg)	% Cont.	MEV (kg)
Payload	78.9	13%	89.0	63.9	12.2%	71.7
Payload Accommodation	12.1	14.5%	13.8	12.1	14.5%	13.9
Avionics	30.7	8%	33.2	30.7	8%	33.2
Telecom	50.8	7%	54.4	50.8	7%	54.4
Guidance and Control	31.6	5%	33.2	31.6	5%	33.2
Power	199.7	8%	216.4	199.7	8%	216.4
Thermal	39.5	10%	43.5	39.5	10%	43.5
Chemical Propulsion	54.1	7%	57.7	54.1	7%	57.7
Structures and Mechanisms	203.0	15%	233.4	203.0	15%	233.4
Harness	59.5	10.6%	65.8	59.5	10.6%	65.8
Launch Adapter	5.4	10%	5.9	10.2	10%	11.2
Spacecraft Dry Mass	**765.3**	**10.6%**	**846.4**	**753.8**	**10.5%**	**832.9**
Chemical Propellant	**317.3**	**10%**	**349.0**	**329.5**	**10%**	**362.5**
Spacecraft Wet Mass	**1082.5**	**10%**	**1195.4**	**1083.3**	**10%**	**1195.4**
Combined Wet Mass	**2165.8**	**10.4%**	**2191.0**			
Max Launch Mass	3485.0					
Unallocated Margin	1094.2	129%				

				Science Mode		Downlink Mode	
FF-EA Power	CBE (W)	% Cont.	MEV (W)	Duty Cycle	MEV Avg (W)	Duty Cycle	MEV Avg (W)
Payload	84.1	14%	95.1	100%	95.1	0%	0.0
Payload Accommodation	94.0	15%	108.1	15%	16.1	85.1%	92.0
Avionics	28.4	10%	31.2	100%	31.2	100%	31.2
Telecom	428.5	5.4%	451.5	2.8%	12.6	54.5%	246.7
Guidance and Control	143.8	5%	151.0	33.6%	50.7	51%	77.0
Power	74.3	5%	78.0	100%	78.0	100%	78.0
Thermal	534.3	10%	587.7	15%	88.2	2%	11.8
Chemical Propulsion	371.7	5%	390.3	6.9%	26.7	6.9%	26.7
Harness Loss	70.4	7.6%	75.7	Loss	16.0	Loss	22.5
Spacecraft Total Power					**414.6**		**586.0**

				Science Mode		Downlink Mode	
FF-EB Power	CBE (W)	% Cont.	MEV (W)	Duty Cycle	MEV Avg (W)	Duty Cycle	MEV Avg (W)
Payload	70.1	14%	79.7	100%	79.7	0%	0.0
Payload Accommodation	94.0	15%	108.1	15%	16.1	85.1%	92.0
Avionics	28.4	10%	31.2	100%	31.2	100%	31.2
Telecom	428.5	5.4%	451.5	2.8%	12.6	54.5%	246.7
Guidance and Control	143.8	5%	151.0	33.6%	50.7	51%	77.0
Power	74.3	5%	78.0	100%	78.0	100%	78.0
Thermal	534.3	10%	587.7	15%	88.2	2%	11.8
Chemical Propulsion	371.7	5%	390.3	6.9%	26.7	6.9%	26.7
Harness Loss	69.8	7.6%	75.1	Loss	15.3	Loss	22.5
Spacecraft Total Power					**398.6**		**586.0**

Exhibit 51. *FF-Polar Flight System Element Mass and Power Summary Tables.*

	FF-EA Mass			FF-EB Mass		
	CBE (kg)	% Cont.	MEV (kg)	CBE (kg)	% Cont.	MEV (kg)
Payload	73.5	12%	83.0	32	14%	36.6
Payload Accommodation	14.1	15%	16.2	14.1	15%	16.2
Avionics	28.6	5%	30.1	28.6	5%	30.1
Telecom	54.1	8%	58.6	54.1	8%	58.6
Guidance and Control	36.2	5%	38.0	36.2	5%	38.0
Power	316.3	11%	349.5	316.3	11%	349.5
Thermal	61.0	10%	67.1	61.0	10%	67.1
Chemical Propulsion	21.2	8%	22.8	21.2	8%	22.8
Electric Propulsion	250.7	10%	276.0	250.7	10%	276.0
Structures and Mechanisms	274.2	15%	315.3	274.2	15%	315.3
Harness	96.0	11.2%	106.8	96.0	11.2%	106.8
Launch Adapter	1.2	10%	1.32	1.2	10%	1.32
Spacecraft Dry Mass	**1227.1**	**11.2%**	**1364.6**	**1182.1**	**11.2%**	**1314.3**
Chemical Propellant	**60.0**	**10%**	**66.0**	**62.0**	**10%**	**68.2**
Electric Propellant	**482.9**	**10%**	**531.2**	**482.9**	**10%**	**531.2**
Spacecraft Wet Mass	**1770.0**	**15%**	**1961.8**	**1727.0**	**15%**	**1913.7**
Combined Wet Mass	3497.0	10.8%	3875.0			
Dispenser	163.2	10%	180.0			
Total Launch Mass	**3660.1**		**4055.1**			
Max Launch Mass	5045.0					
Unallocated Margin	See Exhibit 52 for discussion of margin for EP systems.					

				Science Mode		Downlink Mode	
FF-PA Power	CBE (W)	% Cont.	MEV (W)	Duty Cycle	MEV Avg (W)	Duty Cycle	MEV Avg (W)
Payload	93.3	14%	106.4	100%	106.4	0%	0.0
Payload Accommodation	84.0	15%	96.6	16.7%	16.1	83.3%	80.5
Avionics	25.7	5%	26.9	100%	26.9	100%	26.9
Telecom	533.5	5%	561.7	2.2%	12.6	63.4%	357.0
Guidance and Control	459.8	5%	482.7	17.4%	83.9	34.6%	167.3
Power	135.9	7.4%	146.0	96.3%	140.5	96.3%	140.5
Thermal	120.0	10%	132.0	97.5%	128.7	8.3%	11.0
Chemical Propulsion	231.2	5%	242.8	6.8%	16.4	6.8%	16.4
Electric Propulsion	345.8	10%	380.6	36.7	139.6	5.5%	20.8
Harness Loss	81.2	7.2%	87.0	Loss	26.8	Loss	32.8
Spacecraft Total Power					**698.0**		**853.2**

				Science Mode		Downlink Mode	
FF-PB Power	CBE (W)	% Cont.	MEV (W)	Duty Cycle	MEV Avg (W)	Duty Cycle	MEV Avg (W)
Payload	31.8	14%	36.2	100%	36.2	0%	0.0
Payload Accommodation	84.0	15%	96.6	16.7%	16.1	83.3%	80.5
Avionics	25.7	5%	26.9	100%	26.9	100%	26.9
Telecom	533.5	5%	561.7	2.2%	12.6	63.4%	357.0
Guidance and Control	459.8	5%	482.7	17.4%	83.9	34.6%	167.3
Power	135.9	7.4%	146.0	96.3%	140.5	96.3%	140.5
Thermal	120.0	10%	132.0	97.5%	128.7	8.3%	11.0
Chemical Propulsion	231.2	5%	242.8	6.8%	16.4	6.8%	16.4
Electric Propulsion	345.8	10%	380.6	36.7	139.6	5.5%	20.8
Harness Loss	78.7	7.0%	84.2	Loss	24.0	Loss	32.8
Spacecraft Total Power					**625.0**		**853.2**

3.3. Mission Design & Concept of Operations

The Firefly trajectory design is split between the FF-E and FF-P spacecraft sets, as described in Exhibit 52. FF-E will ultimately enter solar orbit at 1 AU leading and trailing the Earth by 120 degrees. FF-P will orbit the Sun in elliptical orbits inclined by 65 degrees relative to the ecliptic, with aphelion of 2 AU and perihelion of 1 AU. Both FF-P spacecraft have the same right ascension of the ascending node (RAAN) and argument of perihelion (AOP), while 180 degrees apart in true anomaly at the end of the cruise phase. Details of the mission design for each spacecraft are provided in Exhibit 53.

Parameter	Value	Units
FF-P Science Orbit Parameters	R_p = 1 AU R_a = 2 AU INC = 65° RAAN = 45.38° AOP = 193.48°	AU, °
FF-E Science Orbit Parameters	R_p = 0.983 AU R_a = 1.016 AU INC = 4e-3° RAAN = 204.4° AOP = 257.4°	AU, °
Mission Lifetime	10	years
Maximum Eclipse Period	51 (FF-P) 54 (FF-E)	min
Launch Site	KSC	
FF-P #1 Mass **with** contingency (includes instruments)	1907	kg
FF-P #2 Mass **with** contingency (includes instruments)	1907	kg
FF-EA Mass **with** contingency (includes instruments)	1229.9	kg
FF-EB Mass **with** contingency (includes instruments)	1211.2	kg
Chemical Propellant Mass **without** contingency	60 (FF-P) 329.5 (FF-EA) 317.3 (FF-EB)	kg
Chemical Propellant contingency	10	%
Chemical Propellant Mass **with** contingency	66 (FF-P) 362.5 (FF-EA) 349 (FF-In-EB)	kg
EP Propellant Mass **without** contingency	482.9 (FF-P)	kg
EP Propellant contingency	10	%
EP Propellant Mass **with** contingency	531.2 (FF-P)	kg
Launch Adapter Mass **with** contingency	179.52 (FF-P) 5.94 (FF-E)	kg
Total Launch Mass	4861.3 (FF-P) 2441.1 (FF-E)	kg
Launch Vehicle (FF-P)	FH Expendable	Type
Launch Vehicle (FF-E)	F9 ASDS	Type
Launch Vehicle Lift Capability	5045 (FF-P) 3485 (FF-E)	kg
Launch Vehicle Mass Margin	183.7 (FF-P) 1043.9 (FF-E)	kg
Launch Vehicle Mass Margin (%)	3.6[2] (FF-P) 29.95 (FF-E)	%

Exhibit 52. *Mission Design Summary.*

[2]Mass margin for a mission employing solar electric propulsion must be assessed against the propulsion capability of both the launch vehicle and the spacecraft's propulsion system, not just the launch vehicle. This is because the SEP system must be capable of pushing the fully margined vehicle to its destination. Therefore, most of FF-P's mass margin is book-kept on the spacecraft, not the launch vehicle.

FF-E Launch & Cruise	FF-P Launch & Cruise	Science Operations
▪ Launch, Falcon 9 ASDS ▪ Phasing Orbits with Apogee/Perigee-Raise Maneuvers ▪ 1-2 Lunar Gravity Assists (LGA_{1-2}) ▪ Deep Space Maneuver (DSM)	▪ Launch, Falcon Heavy Expendable ▪ Jupiter Gravity Assist (JGA) ▪ 2 Earth Gravity Assists (EGA_{1-2})	▪ 4 years in Heliocentric Science Orbits

Exhibit 53. *Mission architecture with major events.*

FF-Ecliptic Launch & Cruise. The FF-E spacecraft use lunar flybys to escape the Earth-Moon system, and as a result, are significantly less launch constrained than the FF-E spacecraft. Given the Moon's relatively short orbit period about the Earth, LGA opportunities occur every month of the calendar year, as described in the Appendix. Therefore, assuming eclipse durations can be managed, the FF-E launch period is movable throughout the calendar year to fit best relative to the less plentiful FF-P launch opportunities.

Similar to the STEREO mission, phasing orbits are utilized to ensure the spacecraft can reach LGA1 for a 14-day primary launch period. A backup 7-day launch period that targets a subsequent LGA1 opportunity is used to satisfy the 21-day launch period requirement. To target an optimal LGA1, maneuvers can occur at perigee and apogee during the phasing orbits. These maneuvers change the spacecraft orbital period and are used to ensure the spacecraft performs LGA1 at the optimal location on the Moon's orbit regardless of where launch occurs within the launch period. As a result, the required phasing loop maneuvers and resulting trajectories vary across the launch period. To avoid potential impact due to orbit perturbations, the maneuvers are designed to ensure the phasing orbit perigee altitude remains above 500 km after launch. LGA1 places FF-EA on a cruise trajectory that escapes the Earth-Moon system with a heliocentric period less than that of the Earth. As a result, the spacecraft drifts ahead of the Earth in its orbit about the Sun. Conversely, FF-EB uses LGA1 to alter its Earth-centered orbit and reencounter the Moon for LGA2. LGA2 places it on an escape trajectory that has a heliocentric orbital period greater than 1 year and therefore lags behind the Earth in its heliocentric orbit. The phasing orbits and LGA escape sequence are depicted in Exhibit 54.

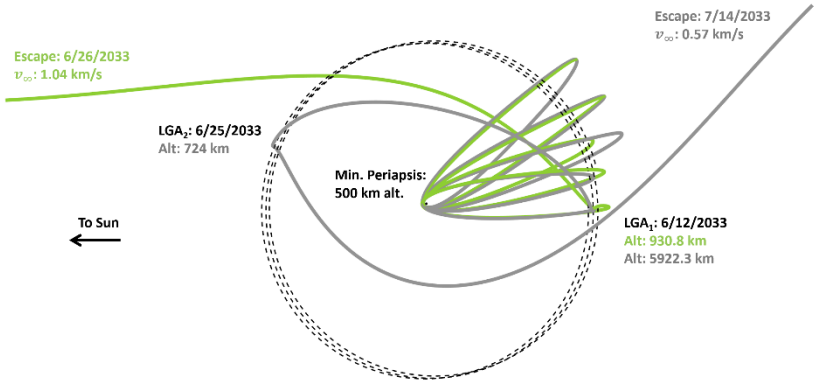

Exhibit 54. *FF-E phasing orbits and LGAs in the Sun-Earth rotating frame for a 16 Apr 2033 launch.*

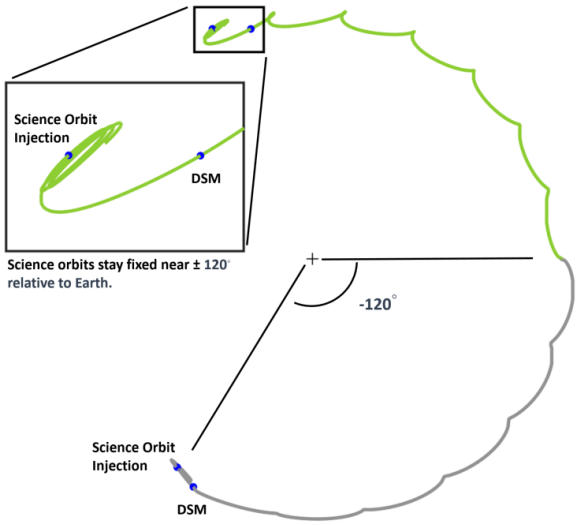

Exhibit 55. *FF-E cruise trajectories and science orbits in the Sun-Earth rotating frame.*

The lead/lag orbital drift allows the spacecraft to transfer significantly out of phase with the Earth and is critical to achieving solar coverage of the far side of the Sun. Once 120◦ out of phase with the Earth, each

Launch Period	S/C	Dates	C3 (km²/s²)	ΔV (m/s)	Propellant (kg)	Arrival
Primary	FF-EA (+120°)	16–29 Apr 2033	-1.8 to -1.7	515.8–638.4	251.0 – 317.9	7 Nov 2039 – 16 Apr 2040
Primary	FF-EB (-120°)	16–29 Apr 2033	-1.8 to -1.7	547.5–640.7	266.3 –317.3	27 Oct 2039 – 30 Jun 2040
Secondary	FF-EA (+120°)	22–28 Jun 2033	-1.8 to -1.5	552.3–658.8	270.5 – 329.5	6–10 Sep 2040
Secondary	FF-EB (-120°)	22–28 Jun 2033	-1.8 to -1.5	567.3–616.3	276.9 – 303.7	9 Jun 2040 – 23 Sep 2040

Exhibit 56. *FF-E launch period trajectory characteristics. Propellant values include 20 m/s allocated for TCMs but do not include contingency.*

spacecraft perform "braking burns" to stop the drift relative to the Earth and enter into their respective science orbits. Exhibit 55 shows the interplanetary cruise and final science orbits. Exhibit 56 describes the characteristics of the primary and secondary launch periods.

FF-Polar Launch and Cruise. The two FF-P spacecraft launch together on a single Falcon Heavy launch vehicle operating in the mode where boosters and core stage are expended, or another launch vehicle with equivalent performance. The 2032 baseline launches to a C3 of 51.9 km^2/s^2 with a total launch mass of 4861.3 kg including all margins. 163.2 kg are left behind as launch adapter mass, leaving a fly-away mass of 4698.1 kg. The optimal solution distributes this mass as 2349.9 kg to the first spacecraft (FF-PA) and 2348.2 kg to the second spacecraft (FF-PB). These masses are constant across the 21-day launch period from 10 Aug 2032 to 30 Aug 2032.

The two spacecraft coast for 60 days after launch in which checkout activities are performed. Each spacecraft then performs a sequence of thrust and coast arcs to target EGA_1. Thrusting is performed on a 14-day cycle with 90% duty cycle, i.e. 12.6 days of thrust followed by 1.4 days of coast. Thrust direction is held constant across each 12.6 day thrust period. The 1.4 days (33.6 hours) of coast are allocated as 8 hours for tracking and commanding and the rest for thrust contingencies. FF-PA performs EGA_1 on 6 May 2034 and FF-PB on 7 May 2034, both at 500-km altitude. A 6-week (42 day) forced coast period is allocated prior to EGA_1 to aid in tracking and corrections to ensure a safe EGA, and 14 days of forced coast are allocated after EGA1 for tracking and reconstruction of the trajectory. These coast margins may be reduced to make up for a loss of thrust or off-nominal EGA. EGA_1 increases the semi-major axes of both spacecraft and sends them out to the JGA on 12 Oct 2035 with an altitude of 9.2 R_j for FF-PA, and 14 Oct 2035 with an altitude of 8.8 R_j for FF-PB, respectively. Both spacecraft shut off their thrusters by the time they reach 3 AU from the Sun. There is still enough power to operate the thrusters at this time but we hold it in reserve to recover from missed thrust events. A ΔV of 20 m/s is book-kept for a statistical maneuver on the hydrazine thrusters to target the JGA b-plane 90 days out from the encounter because the ion thrusters will not operate near Jupiter.

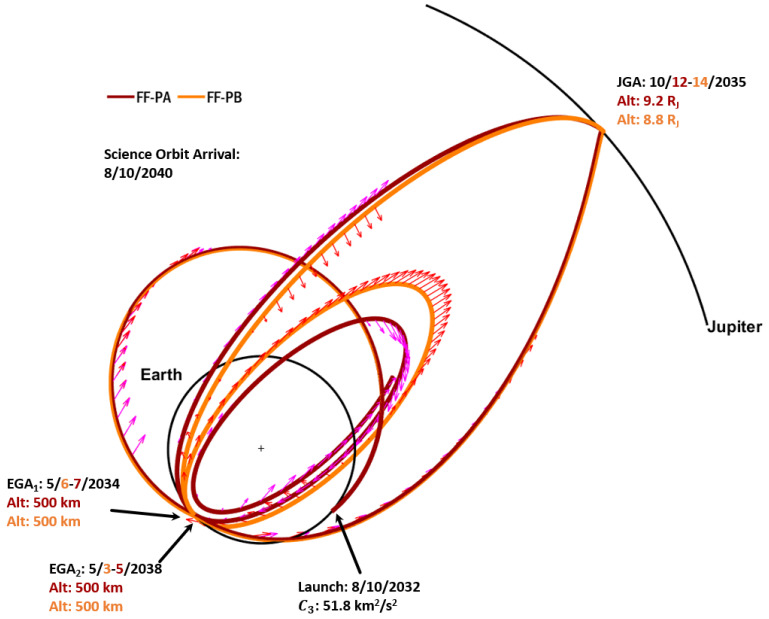

Exhibit 57. *FF-P heliocentric trajectories with mission events and thrust periods included.*

Event	Date		C3		Altitude (km)		Mass	
	FF-PA	FF-PB	FF-PA	FF-PB	FF-PA	FF-PB	FF-PA	FF-PB
Launch	8/10/2032	8/10/2032	51.9	51.9			2438.2	2438.2
EGA_1	5/7/2034	5/6/2034	144.0	149.4	500	500	2349.9	2346.2
JGA	10/12/2035	10/14/2035	135.7	132.8	643270	616210	2268.8	2272.9
EGA_2	5/5/2038	5/3/2038	1203.5	1112.3	500	500	2200.7	2188.1
Science Orbit Arrival	8/10/2040	8/10/2040					1955.3	1955.3

Exhibit 58. *FF-P Mission Events.*

The JGA changes the inclination of both FF-PA and FF-PB – almost all of the 65 degrees required plane change is accomplished by the JGA alone. Both spacecraft then proceed inward to EGA_2 on 3 May 2038 and 6 May 2038, both at an altitude of 500 km. The two spacecraft resume thrust at 3.2 AU. As in the case of EGA_1, 42 days of coast margin are allocated prior to the EGA and 14 days are allocated after EGA_2.

EGA_2 contracts the semi-major axis of the two spacecraft so that they are both near the 1 AU by 2 AU ellipse requirement but does not match the requirement exactly. This is because FF-PA and FF PB need to have different orbit periods at this time in order to end the cruise phase 180 degrees apart. The two spacecraft then perform a series of thrust and coast arcs terminating on 8/10/2040. At this time all science orbit constraints are met. FF-PA performs a total ΔV of 7.67 km/s on the SEP system and FF-PB performs a total ΔV of 7.88 km/s.

Exhibit 57 shows the FF-P cruise trajectories with thrust arcs marked with arrows. Exhibit 58 lists important events in the FF-P mission corresponding to the 2032 launch.

Science Coverage. The Firefly trajectories were designed to be feasible from an engineering standpoint while meeting science objectives. The FF-E spacecraft were chosen to travel to ±120 degrees relative to Earth because it is assumed that solar observations from the Earth-direction will be available from other observatories. As a result, placing the spacecraft ±120 degrees relative to Earth maximizes the coverage in the Ecliptic. Given that FF-E relies solely on chemical propulsion, there are no strict pointing requirements during cruise, and science observations can begin as soon as each spacecraft escapes the Earth-Moon system. It is assumed that each spacecraft will observe up to 60 degrees off nadir in all directions, so once in the science orbits, the observations from the FF-E spacecraft plus the Earth will provide constant coverage of the entire solar equator.

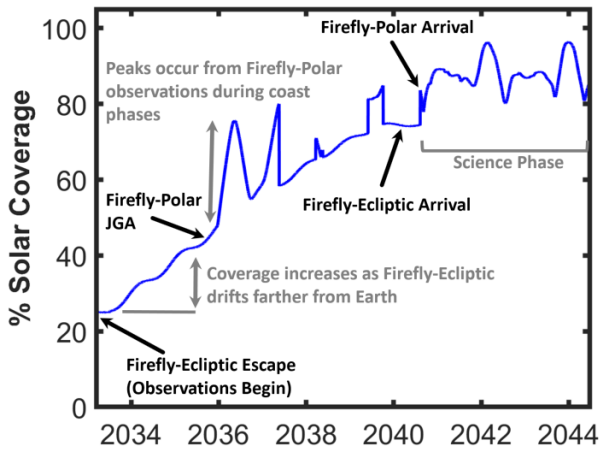

Exhibit 59. *Solar coverage throughout the Firefly mission.*

After the JGA, the FF-P spacecraft will be highly inclined relative to the ecliptic and thus can provide useful observations during cruise when possible. Due to pointing requirements during thrust periods, science observations are only available during coast phases until the science orbit is reached. Exhibit 59 shows the total solar coverage between the Firefly spacecraft and the Earth throughout the mission.

Concept of Operations. The goal of Firefly operations is to get all four spacecraft orbiting the sun in a primary science phase lasting 2 years. This section will detail operations common to all spacecraft first, then break down the aspects of the mission that are unique to the FF-E and FF-P pairs of spacecraft.

While the FF-E and FF-P spacecraft have different launch dates (with FF-P launching first), all four spacecraft will be operated using the established APL Mission Operations Center (MOC) infrastructure and NASA Deep Space Network (DSN) capabilities. The trajectory elements and critical events are similar to previous missions operated at APL, with APL personnel monitoring spacecraft health and status

during the mission lifetime with extra focus during critical events. Lessons learned for staffing and processes from previous APL dual-spacecraft missions, such as STEREO and Van Allen Probes, will be applied to operating this four-spacecraft mission.

The mission concept uses decoupled operations between spacecraft and instrument commanding. This means that mission operations will handle spacecraft commanding, control when the instruments are powered on, and manage the instrument command queues, but the individual instrument teams will be responsible for commanding and configuring their instruments. The CCSDS File Delivery Protocol (CFDP) will be used for nominal uplinks and downlinks, with both concepts used previously on Parker Solar Probe (PSP). Automation and unattended operations are expected to be utilized whenever possible after commissioning, to help cover the DSN passes for four spacecraft.

For DSN tracks, a single 34m antenna is baselined to support nominal operations outside of any planned critical events or navigation observations (e.g. Delta-Differential One-Way Ranging (DDOR) passes). All uplinks and beacon passes will be X-band, while Ka-band downlink will be used whenever possible. However, there may be certain timeframes during the mission where Ka-band is constrained, so X-band would be used in those periods. During the prime mission, continuous downlink of 0.02 MB per day of telemetry from each spacecraft, via HGA and either X- or Ka-band, will support space weather monitoring. Multiple Spacecraft per Aperture (MSPA) could potentially be used to reduce DSN antenna needs, but because Ka bandwidths are quite narrow, this would primarily be useful for any X-band passes.

FF-Polar. The FF-P spacecraft will have three major phases: launch and commissioning, cruise, and the prime science orbit. All discussions of track coverage in these phases are per spacecraft. Post-launch commissioning is expected to take approximately five weeks, with near-continuous coverage the first week and gradually decreasing to daily 8 hour shifts in weeks 3–5. The cruise phase will be subdivided into SEP thrusting and coasting periods, and will include two Earth gravity assists (EGAs) and a Jupiter flyby. The SEP thrusting periods will have one 8 hour telemetry pass as well as two 1 hour thrust verification beacons each week, so the majority of this period is devoted to thrusting. The coast periods will involve three 8 hour passes a week, with track coverage increasing around the EGAs, Jupiter flyby, and any trajectory correction maneuvers (TCMs). Finally, the prime science phase will consist of daily 8 hour passes for each spacecraft over a period of 2 years. It is estimated that each FF-P spacecraft will require 17,119 hours of DSN coverage, totaling 2,358 passes over the course of 8 years.

During the cruise phase for the FF-P spacecraft, the science instruments are off during the active EP thrust periods. Within 2 AU distance, while the spacecraft are coasting or using chemical propulsion, all the instruments will be collecting data. Beyond 2 AU, only the in-situ instrument suite will be collecting data. Once the FF-P spacecraft reach their prime mission solar orbit, in-situ instruments will collect data continuously, while the imaging instruments will gather data while the spacecraft is at ±10 degrees from the ecliptic plane. In all cases, the spacecraft design allows for instruments to operate during DSN contacts in order to minimize gaps in science data.

FF-Ecliptic. The FF-E spacecraft will also have three major phases: launch and commissioning, cruise, and the prime science orbit. However, the FF-E spacecraft stay much closer to Earth and do not require solar electric propulsion. Once again, all discussions of track coverage in these phases are per spacecraft. Post-launch commissioning is expected to take approximately five weeks, with near-continuous coverage during the first week and gradually decreasing to daily 8 hour shifts in weeks 3–5. The cruise phase will involve a single lunar gravity assist (LGA) for FF-EA and 2 LGAs for FF-EB, with both spacecraft having two planned deep space maneuvers (DSMs). The typical cruise period will involve three 8 hour passes a week, with increased tracking around the LGAs and DSMs. The prime science phase will consist of daily 8 hour passes for each spacecraft over a period of two years. It is estimated that each FF-E spacecraft will require approximately 19,516 hours of DSN coverage, totaling 2,214 passes over the course of 7.5 years.

During the cruise phase for the FF-E spacecraft, the science instruments collect data throughout, except for short periods during commissioning and TCMs. During the prime mission, all instruments collect data continuously, including during DSN contacts.

With this strategy, the prime science orbit data return for each of the FF-E and FF-P spacecraft is 4700 GB, with approximately 25% margin compared to available downlink capability.

3.4. Ground System

The Firefly Ground Data System (GDS) is based on proven ground data systems from previous decoupled instrument commanding missions including Parker Solar Probe and Van Allen Probes. The GDS will utilize the existing APL Mission Operations Center (MOC) infrastructure and APL's Mission Independent Ground Software (MIGS). No new GDS functionality has been identified for the 4π mission at this time.

The Firefly GDS supports all phases of the mission including: subsystem test, observatory I&T, hardware simulator control, and flight operations. Key GDS functionality includes:

1. Delivery of commands to the spacecraft and GSE
2. Acquisition, routing, processing, monitoring and archive of real-time telemetry
3. Supports CFDP (uplink/downlink)
4. Offline assessment processing, plotting and reporting of telemetry
5. Support interfaces to testbeds, navigation, DSN, etc.
6. Tools for on-board memory management
7. Tools for radiation monitoring
8. Timekeeping functions
9. Navigation tools

The same software and workstations with the same look and feel are used for all mission phases. Exhibit 60 illustrates the notional Firefly GDS architecture.

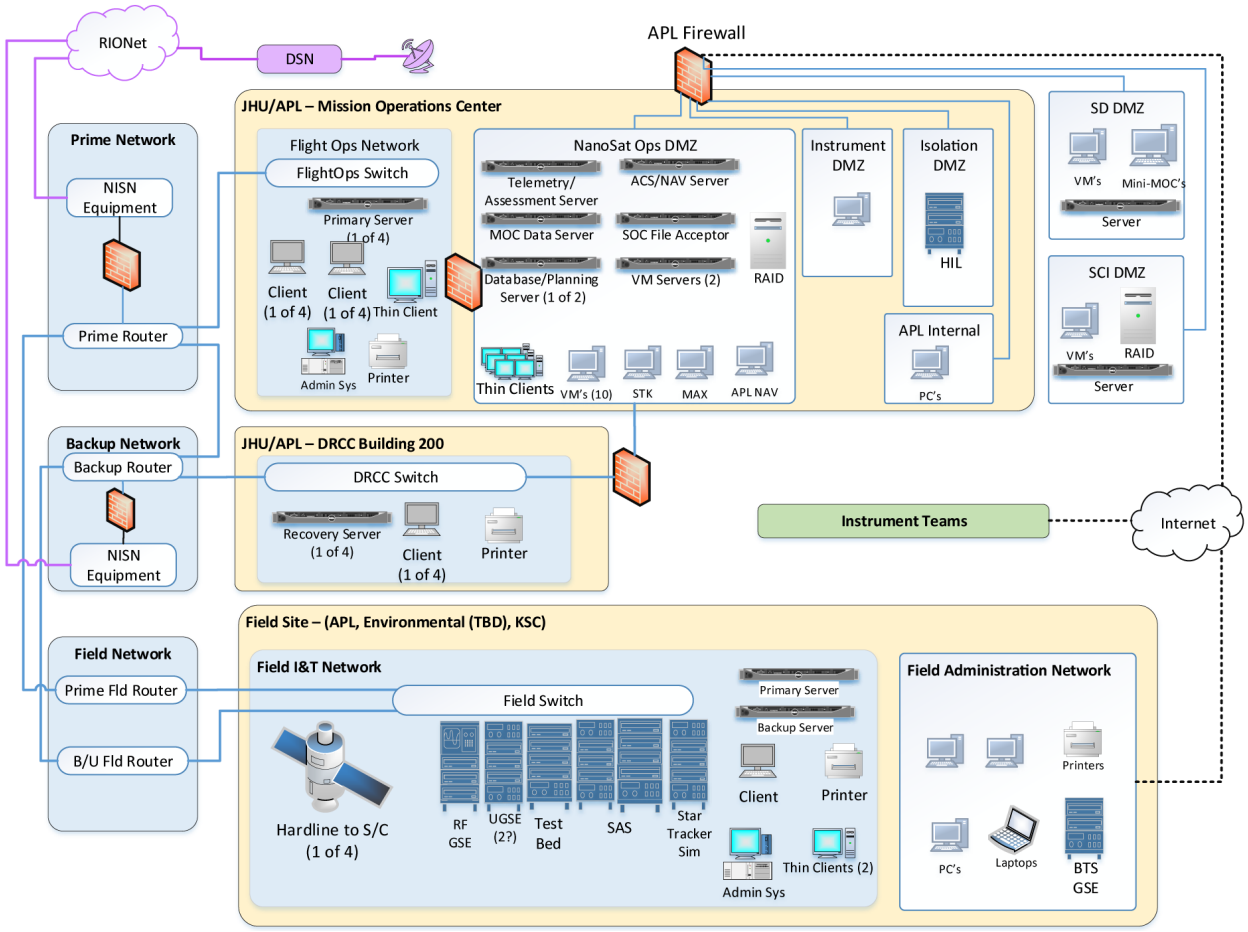

Exhibit 60. *Notional* ***Firefly*** *GDS Architecture.*

3.5. Risk List

The associated risks of the proposed baseline mission were assessed for both likelihood (L) and consequence (C) during this concept study. There are 5 notable risks outlined below, with their likelihood and consequence assessment rankings provided alongside their respective technical or cost/schedule classifications.

Risk	L × C	Risk	Response/Mitigation
A	3 × 3	**If** building, integrating and testing four spacecraft requires more than available manufacturing capability and/or test facilities, **then** the program may not be able to meet schedule. (Schedule)	Consider using multiple institutions or agencies to build the two types of spacecraft in parallel.
B	2 × 3	**If** the instrument development takes longer than anticipated, then schedule could be compromised. (Schedule/Cost)	Ensure technology development is funded early in the project.
C	2 × 3	**If** the electric propulsion for Firefly Polar system does not perform as expected, **then** the Firefly Polar orbit cannot be circularized, and so would impact the ability to accomplish science objectives. (Technical)	Ensure early design and testing of the electric propulsion system
D	1 ×3	**If** spacecraft-generated magnetic fields are higher than expected, **then** magnetometer measurements may be degraded. (Technical)	Develop magnetic cleanliness requirements early and make sure requirements are implemented in design.
E	1 ×2	**If** the mission downlink requirements exceed the DSN ability to meet, **then** the science return will be impacted. (Technical)	Reduce data volume to minimum required to meet science objectives.

Exhibit 61. *Summary of Firefly risks*

4. Development Schedule & Constraints

The high-level mission schedule for Firefly (Exhibit 62) is based upon previous missions such as Parker Solar Probe and STEREO. It is assumed that the two pairs of spacecraft (i.e., FF-Ecliptic and FF-Polar) will all be built in a single institution. As stated in the trade study in Section 2.3, developing FF-E and FF-P in different institutions might reduce the schedule and potentially save some cost. It is also possible that various agencies might collaborate to build the two pairs of spacecraft. For instance, two agencies (e.g., NASA and ESA) might agree to develop a pair of spacecraft each: one agency builds FF-E, and the other builds FF-P. This scenario will significantly impact the mission's cost and schedule.

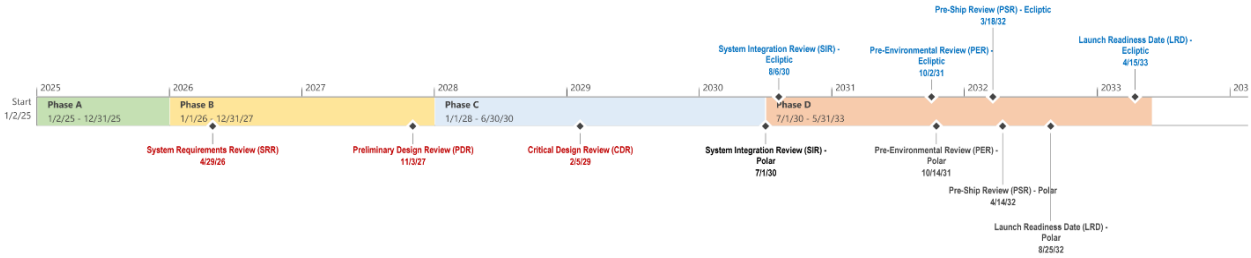

Exhibit 62. *High-Level development and operation timeline for the Firefly mission.*

Phase	Duration (months)	Start	Finish
Phase A	1.9	1/2/2025	12/31/2025
Phase B	24	1/1/2026	12/31/2027
Phase C	30	1/1/2028	6/30/2030
Phase D	35	7/1/2030	5/31/2033
Phase E	135.2	61/2033	8/312044
Phase F	6	9/1/204	3/1/2045

Requirements & Design	Date
System Rqmts Review (SRR)	4/28/2026
Preliminary Design Review (PDR)	11/1/2027
Critical Design Review (CDR)	2/1/2029

Firefly-Ecliptic	Date
System Integration Review (SIR)	7/1/2030
Pre-Environmental Rev (PER)	10/14/2031
Pre-Ship Review (PSR)	4/14/2032
Launch Readiness Review (LRR)	8/20/2032
Launch Readiness Date (LRD)	8/25/2032
Launch	8/26/2032

Firefly-Polar	Date
System Integration Review (SIR)	8/6/2030
Pre-Environmental Rev (PER)	10/2/2031
Pre-Ship Review (PSR)	3/18/2032
Launch Readiness Review (LRR)	3/17/2033
Launch Readiness Date (LRD)	3/22/2033
Launch	3/23/2033

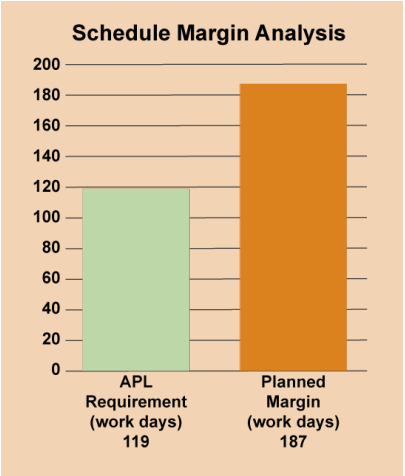

Exhibit 63. *(top-left) Phase A–F durations, start and end dates assuming a start date of 1 Feb 2025 for Phase A. (Bottom-left) Estimated dates for the SRR, PDR, and CDR reviews. (Middle) Review schedules and estimated launch dates for the FF-P (top) and FF-E (bottom). (Right) Study applied typical schedule margin.*

Detail schedules are provided for the development of each of the spacecraft in Exhibits 64–67, and the science timelines for each pair (ecliptic and polar) are provided in Exhibits 68–69.

Exhibit 64. *Development schedule for the Firefly-Ecliptic-A spacecraft.*

Exhibit 65. *Development schedule for the Firefly-Ecliptic-B spacecraft.*

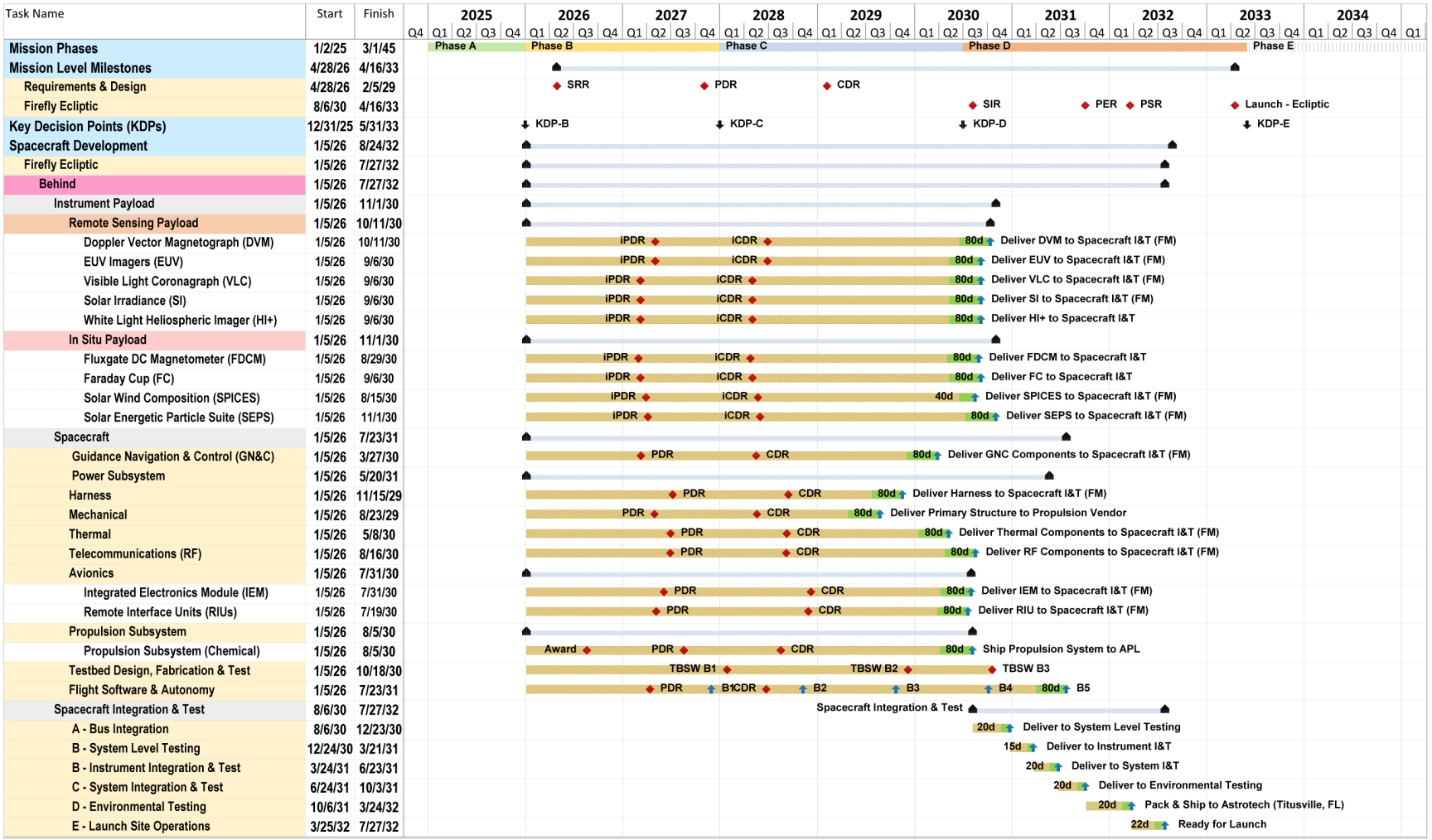

Exhibit 66. *Development schedule for the Firefly-Polar A spacecraft.*

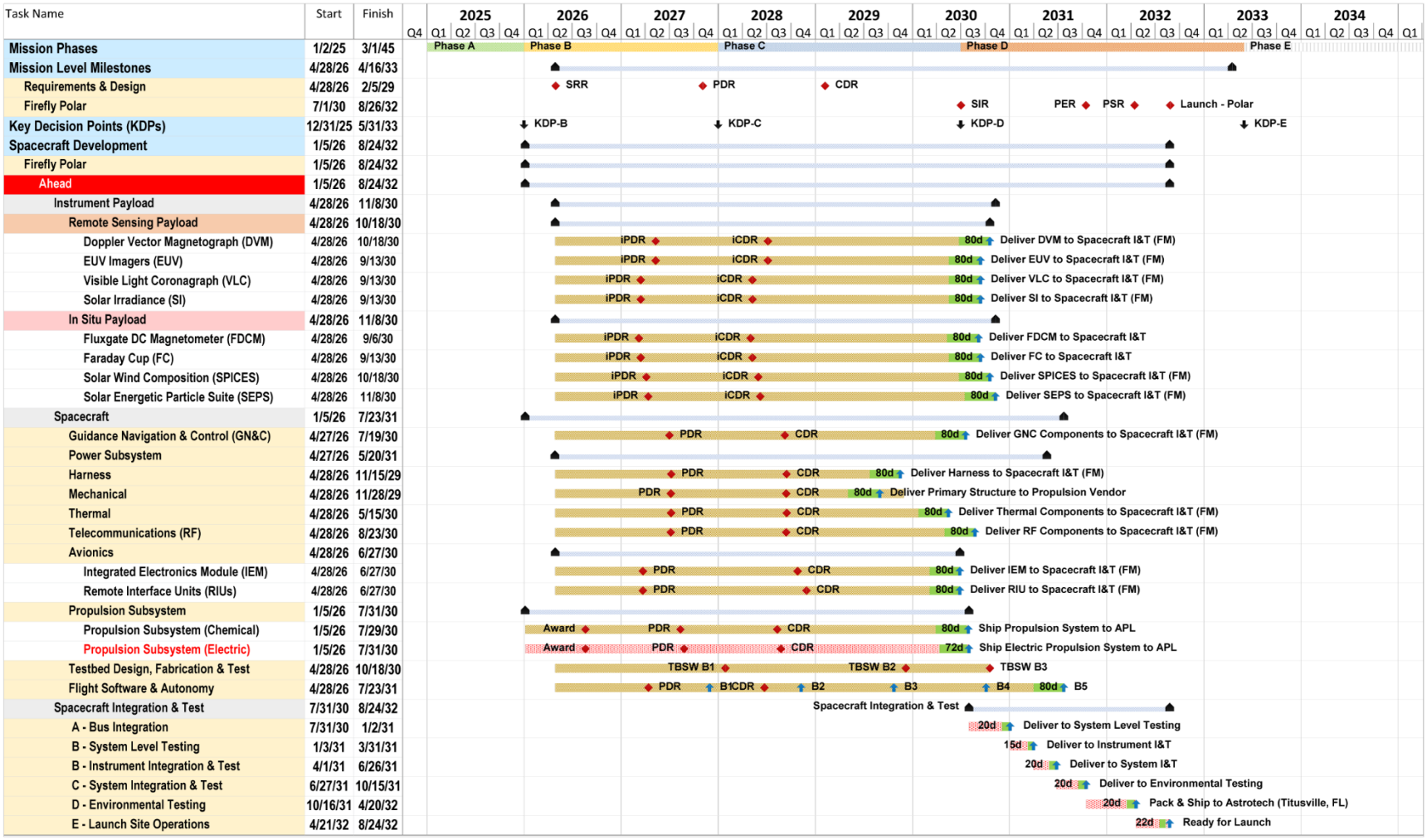

Exhibit 67. *Development schedule for the Firefly Polar-B spacecraft.*

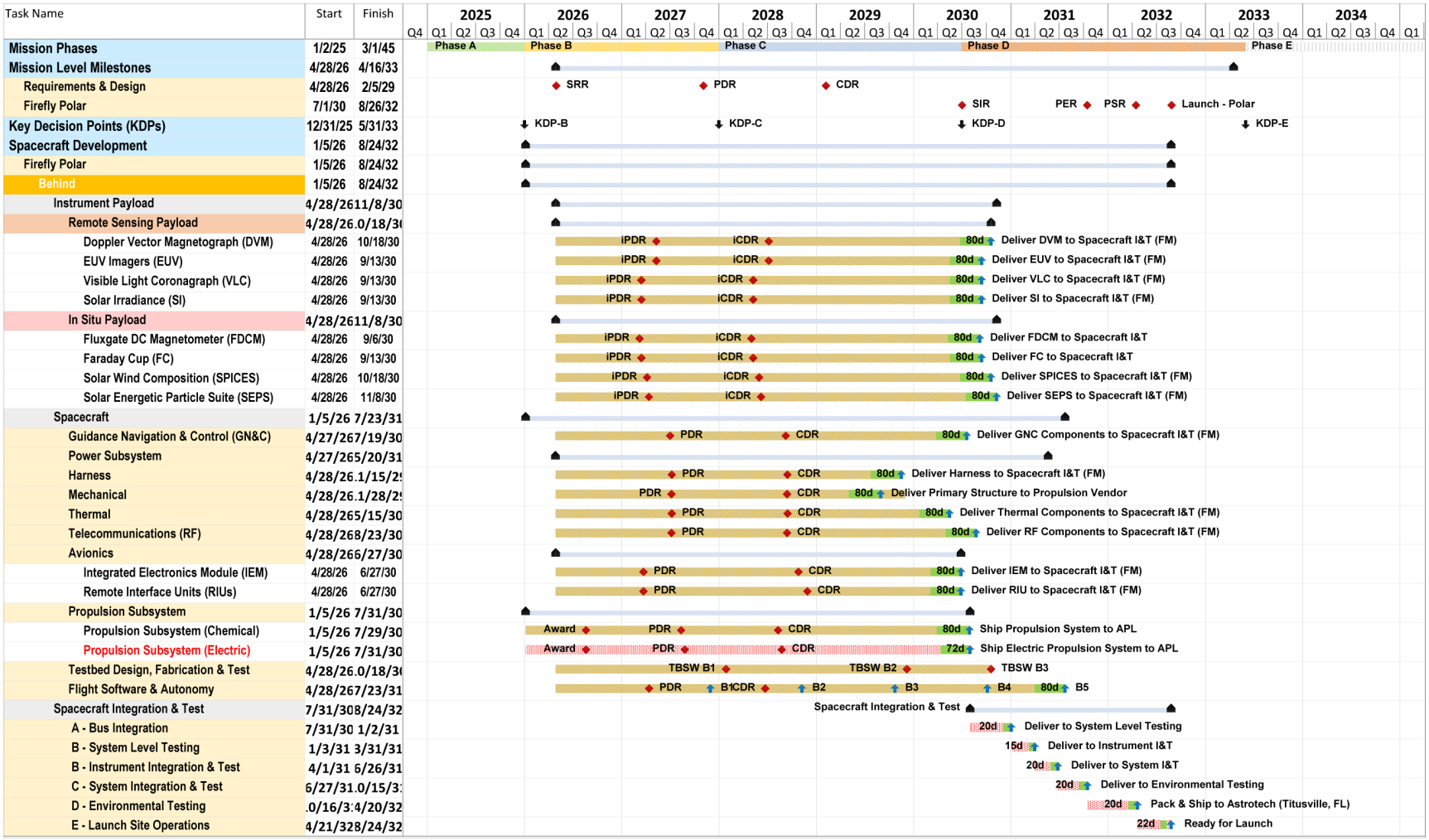

Exhibit 68. *Firefly Ecliptic Science Timeline.*

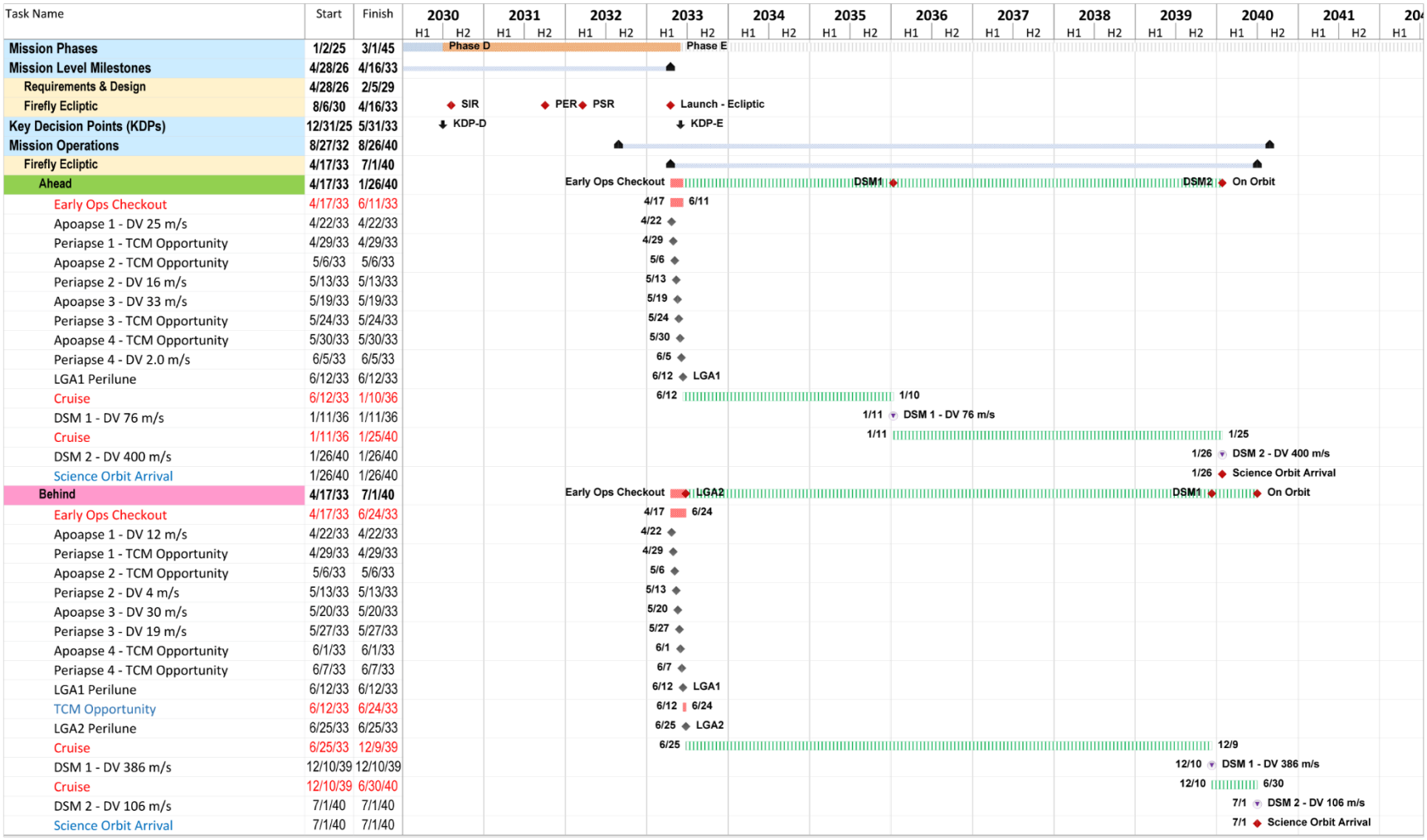

Exhibit 69. *Firefly Polar Science Timeline.*

5. Mission Life-Cycle Cost

5.1. Introduction

The Firefly mission cost estimate is of concept maturity level (CML) 4. The payload and spacecraft estimates capture the resources required for a preferred point design and take into account subsystem level mass, power, and risk. Our estimate also takes into account the technical and performance characteristics of components. Estimates for science, mission operations, and ground data system elements whose costs are primarily determined by labor take into account the Phase A–D schedule and Phase E timeline.

The result is a mission estimate that is comprehensive and representative of expenditures that might be expected if the Firefly mission is executed as described. The Firefly Phase A–F baseline mission cost, including launch vehicle (LV) and unencumbered reserves of 50% (A–D) and 25% (E–F), is $2.9B in fiscal year 2022 dollars (FY22$), as shown in Exhibit 70. Excluding all LV-related costs, the Firefly Phase A–D mission cost with reserves is $2.2B FY22. Exhibit 71 shows an estimated spend profile by phase and fiscal year for Phases A-D, excluding the LV costs. All tables and estimates below refer to the baseline mission configuration, with the exception of the enhancement and de-scope estimates, which are discussed in Section 5.5.

WBS	Description	Ph A–D	Ph E–F	Total	Notes
	Phase A	$6.0	—	$6.0	Assumption based on previous studies
1/2/3	PMSEMA	$193.1	—	$193.1	A-D: Wrap factor based recent NFs and APL missions. E-F: Bookkept with WBS 7
4	Science	$ 31.8	$148.7	$180.6	Cost per month of recent NFs and APL missions
5	Payload	$384.1	—	$384.1	Parametric and analogy based estimates
6	Spacecraft	$679.4	—	$679.4	Estimated via parametric models
7	Mission Operations	$24.1	$98.5	$122.7	Based on STEREO/VAP and recent proposal info
8	LV	$313.8	—	$313.8	Falcon 9 Reusable (FF-E) + Falcon Hvy Expendable (FF-P) Placeholder
9	Ground Data Systems	$16.7	$3.5	$20.2	Ground ROM from SME
10	I&T	$151.1	—	$151.1	APL historical I&T % of HW (incl testbeds)
	Total w/o Reserves	**$1,800.1**	**$250.8**	**$2,050.8**	
	Reserves	$740.1	$62.7	$802.8	50% B-D, 25% E-F, excludes launch services costs
	Total with Reserves	**$2,540.2**	**$313.5**	**$2,853.7**	
	Total without LV	**$2,226.3**	**$313.5**	**$2,539.8**	

Exhibit 70. *Estimated Phases A–F Firefly baseline mission cost by Level 2 WBS element.*

Phase A		Phase B			Phase C-D						
FY25	FY26	FY26	FY27	FY28	FY28	FY29	FY30	FY31	FY32	FY33	Total (FY22$M)
4.5	1.5	227.9	303.9	76.0	167.9	168.3	229.3	290.3	457.0	299.8	**$ 2,226.3**

Exhibit 71. *Estimated Phases A–D Spend Profile (excludes launch vehicle).*

5.2. Mission Ground Rules & Assumptions

Estimating ground rules and assumptions are derived from the "Ground Rules for Mission Concept Studies in Support of Heliophysics Decadal Survey" dated Jan 2022.

Mission costs are reported using the Level-2 (and Level-3 where appropriate) work breakdown structure (WBS) provided in NPR 7120.5F.

Cost estimates are reported in fiscal year 2022 (FY22) dollars.

The NASA New Start inflation index was used to adjust historical cost, price data, and parametric results to FY22 dollars if necessary.

The mission requires technology development (Pre-Phase A) to advance the Solar Wind Composition (SPICES) instrument to TRL 6. The technology development estimate is discussed in Section 5.4.3 and is outside of the total mission cost per the guidelines. All other mission components will be at or above TRL 6 when required.

A launch vehicle cost estimate of $314M is held in WBS 8 and assumes two launch vehicles: a SpaceX Falcon 9 reusable for the two FF-E spacecraft, and a Falcon Heavy Expendable for the two FF-P spacecraft.

A 40% cost to copy factor is applied to all copies of instruments and spacecraft [Whitley 2013].

Phase A–D cost reserves are calculated as 50% of the estimated costs of all components excluding the launch vehicle. Phase E–F cost reserves are calculated as 25% of the estimated costs of all Phase E elements excluding DSN aperture fees.

5.3. Cost Benchmarking

The cost and scope of the Firefly concept corresponds well with NASA Flagship-class missions (Exhibit 72). The estimated cost to develop Firefly compares favorably to current Flagship missions under development as well as past Flagship missions with an average cost of $2.94B, excluding launch vehicle costs, as shown by the grey line in the figure.

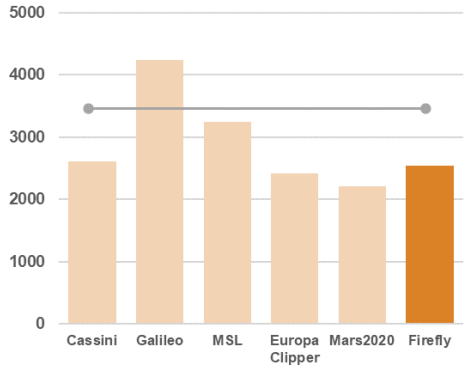

Exhibit 72. *Mission-level cost comparison to other Flagship class mission. Average shown by grey bar.*

5.4. Methodology & Basis of Estimate

The Firefly CML 4 mission cost estimate is a combination of high-level parametric and analog techniques and incorporates a wide range of uncertainty in the estimating process. No adjustments were made to remove the historical cost of manifested risk from the heritage data underlying the baseline estimate. Therefore, before reserves are applied, the estimated costs already include a historical average of the cost of risk. This approach is appropriate for capturing risk and uncertainty commensurate with early formulation stages of a mission. The following describes the basis of estimate for each element.

5.4.1. WBS 1, 2, 3 Project Management, Systems Engineering, Mission Assurance (PMSEMA)

Because these functions depend on multiple mission- and organization-specific characteristics [Hahn 2014], cost analogies to comparable historical missions are preferred over cost model output, which does not take the mission into account. Existing analyses demonstrate that hardware costs are a reliable predictor of these critical mission function costs. APL has conducted thorough and rigorous analyses of PMSEMA costs, both for historical APL missions and for analogous missions. Firefly's PMSEMA relies on APL's analysis of historical PMSEMA practices on Van Allen Probes (VAP), Parker Solar Probe (PSP), and New Horizons (NH). VAP and PSP in particular include costs associated with current NASA requirements (e.g., Earned Value Management System, 7120.5F). Firefly's total mission PMSEMA cost is 15.9% of the flight system (payload + spacecraft + I&T). This percentage is allowed to vary along with hardware costs as part of the mission cost risk analysis, discussed below, to capture uncertainty (particularly given CML-4-level design phase).

5.4.2. WBS 4 Science

This element covers the managing, directing, and controlling of the science investigation. It includes the costs of the Principal Investigator (PI), Project Scientist (PS), science team members, and activities. The Phase A–D and E–F science estimate is an analogous estimate based on the cost per month of NH, MESSENGER, Cassini, Dragonfly, OSIRIS-Rex, and Juno. The analogy costs are representative of expenditures for science on a typical New Frontiers or Flagship mission. The estimate reflects the manpower needed to create various data products as well as to ensure closure to science objectives.

5.4.3. WBS 5 Payload

The WBS 5 estimate includes a science payload of eight instruments plus the magnetometer boom, DPU, and payload-level PM/SE/MA. Cost shown in Exhibit 73 reflect the first unit instrument estimate, plus a 40% cost to copy factor for subsequent units [Whitley 2013]. The 8.2% cost-to-cost factor for estimating payload PMSEMA costs is based on the VAP, NH, MESSENGER, and PSP payload suite cost data with PMSEMA costs estimated as a percentage of the payload hardware. Technical management and systems engineering costs for individual instruments are carried in their respective instrument development costs.

WBS	Description	Ph A–D	Notes	Qty.
5	**Payload**	**$384.1**	**Parametric and analogy based estimates**	
5.1	PL PM/SE/MA	$27.6	Based on VAP, NH, MESSENGER, PSP	
5.2	Doppler Vector Magnetograph (DVM)	$90.7	NICM 9 and SEER Space Average	4
5.3	Extreme Ultraviolet Imager (EUVI)	$77.9		3
5.4	White Light Coronagraph (mini-COR)	$15.5		4
5.5	White Light Heliospheric Imager (HI+)	$33.1		1
5.6	Flux Gate Magnetometer (FGM)	$16.5		4
5.7	Faraday Cup	$27.3		4
5.8	Solar Wind Composition (SPICES)	$38.4		1
5.9	Solar Energetic Particle Suite (SoIO/EPD)	$36.8		3
5.A	Magnetometer Boom, 4 m	$5.9	PSP/VAP Boom Analogy	4
5.B	Payload Data Processing Unit (DPU)	$14.2	PSP DPU Analogy	4
5.C	Payload Survival Heaters / Thermostats	$0.1	SEER Estimate	4

Exhibit 73. *WBS 5 costs in FY$22M.*

Given the early design phase, multiple approaches are used to estimate each instrument to capture the potential range in cost. This includes two parametric estimates that rely on different sets of input variables (SEER Space and NICM 9), and historical analogous costs to specific heritage instruments where available. An average of the two parametric estimates is used as the point estimate to prevent estimate bias (high or low). These estimates are subject to a cost risk analysis (discussed below) to further quantify uncertainty.

There is technology development required for the Solar Wind Composition (SPICES) instrument. This technology development will occur prior to Phase A, and is estimated to be $12.6M. This estimate is kept outside of the cost table shown here per the study report guidelines.

5.4.4. WBS 6 Spacecraft

The WBS 6 estimate includes the spacecraft (SC) bus, flight software, and component engineering (Exhibit 74). Spacecraft PMSEMA is carried in WBS 1, 2, and 3 consistent with APL in-house builds

WBS	Description	First Unit	Copy	Total	Notes
6	**Spacecraft Total**	**$465.2**	**$214.1**	**$679.4**	**Estimated via parametric models**
6.1	**FF-E**	**$229.8**	**$91.9**	**$321.7**	**2 S/C, 40% copy factor**
6.1.1	Avionics	$24.6	$9.8	$34.5	All subsystem estimates use the average of SEER Space and PRICE Trueplanning model outputs with the exception of three. The propulsion estimate is a ROM from the subsystem lead. FSW and component engineering are analogy estimates from the PSP mission.
6.1.2	Telecommunications	$36.1	$14.5	$50.6	
6.1.3	Guidance & Control	$19.4	$7.7	$27.1	
6.1.4	Power	$59.2	$23.7	$82.8	
6.1.5	Thermal	$ 2.7	$1.1	$ 3.8	
6.1.6	Propulsion	$13.5	$5.4	$19.0	
6.1.7	Mechanical	$23.7	$9.5	$33.2	
6.1.8	Harness	$3.5	$1.4	$4.9	
6.1.9	FSW	$24.2	$9.7	$33.8	
6.1.A	Component Engineering	$22.9	$9.1	$32.0	
6.2	**FF-P**	**$235.5**	**$122.2**	**$357.7**	**2 S/C, 40% copy factor, 1st unit common savings in subsystems noted**
6.2.1	Avionics	$9.4	$9.4	$18.7	Same notes as FF-E on the basis of estimate. FF-P does realize some savings in the first unit due to commonalities in the avionics, telecom, G&C, Thermal, and mechanical subsystems. In these cases the copy factor is applied to the average cost model output.
6.2.2	Telecommunications	$15.0	$15.0	$30.0	
6.2.3	Guidance & Control	$8.2	$8.2	$16.4	
6.2.4	Power	$87.5	$35.0	$122.5	
6.2.5	Thermal	$1.9	$1.9	$ 3.9	
6.2.6	Propulsion	$49.1	$19.6	$ 68.8	
6.2.7	Mechanical	$12.2	$12.2	$24.4	
6.2.8	Harness	$5.1	$2.1	$ 7.2	
6.2.9	FSW	$24.2	$9.7	$33.8	
6.2.A	Component Engineering	$ 22.9	$9.1	$32.0	

Exhibit 74. *WBS 6 costs in FY$22M.*

[Hahn 2015]. The basis of estimate relies primarily on parametric models. The exception to this is the spacecraft propulsion systems, estimated via a ROM by a propulsion subject-matter expert. Flight software and component engineering are analogy estimates based on the PSP mission. An average of two parametric estimates is used as the point estimate to mitigate estimate bias (high or low). SEER Space is one of the primary estimating methodologies because it was designed specifically for missions in early formulation stages. PRICE TruePlanning is also utilized as it provides a cost estimate at the component level. No major technology development is required for the SC. The two parametric estimates are within 8% of each other. A 40% cost to copy factor is applied for the second SC units [Whitley 2013]. In the case of the first FF-P unit, there are some savings realized due to commonalities between subsystems with the FF-E spacecraft (avionics, telecom, G&C, mechanical, and thermal). In these cases, the 40% copy factor is applied to the average cost model output.

5.4.5. WBS 7 & 9 Mission Operations (MOps) and Ground Data Systems (GDS)

The Firefly mission operations estimate includes mission operations planning and development, network security, data processing, and mission management. The pre- and post-launch mission operations estimates are based on STEREO and VAP analogies (both missions combined), with insight from recent proposal submittals for items like navigation and DSN set up fees. DSN aperture fees are excluded and discussed below. These missions represent expenditure on pre and post-launch MOps for projects of comparable scope and complexity. The GDS estimate is a BUE from a ground data systems subject matter expert. The Firefly ground data system provides full life cycle support for subsystem test, observatory I&T, hardware simulator control, & flight operations. The cost estimate is based on extensive reuse of PSP, IMAP, and DART Ground software via APL's mission independent ground software (MIGS) as well as use of the existing Mission Operations Center (MOC).

5.4.6. WBS 8 Launch Vehicle & Services

The mission requires a launch vehicle that does not correspond with any of the options currently described in the Decadal Survey Ground Rules. As such, the figures used in this estimate are based on an evaluation of current best estimates of the cost of the capability that will be required. The price of a LV with Falcon 9 Reusable (FF-E), and Falcon Heavy Expendable (FF-P) type capabilities would be approximately $314M for a launch using a standard sized fairing. This is based on past pricing to NASA missions of EELVs and most current LV cost information available.

5.4.7. WBS 10 System Integration & Testing (I&T)

This element covers the efforts to assemble and test the spacecraft and instruments. The Firefly I&T effort is estimated as 12.7% of the hardware. This percentage is based on a detailed analysis of cost actuals from previous APL missions, including MESSENGER, NH, STEREO, VAP, and PSP. This percentage is allowed to vary along with hardware costs as part of the mission cost risk analysis to capture the risk historically manifested during I&T.

5.4.8. Deep Space Network (DSN) Aperture Fees

This element provides for access to the DSN infrastructure needed to transmit and receive mission and scientific data. Mission charges are estimated at $67M using the Jet Propulsion Laboratory (JPL) DSN Aperture Fee tool. The DSN cost estimate covers pre- and post-contact activity for each linkage. The DSN aperture fee estimate is excluded from the mission budget and the cost tables in this report. Estimates for DSN set up fees are included in WBS 7.

5.4.9. Confidence & Cost Reserves

The cost risk ranges by major WBS element as inputs for the Firefly probabilistic cost risk analysis to quantify total cost risk are found in Exhibit 75 and are described below.

PMSEMA. Given the use of cost-to-cost factors to estimate these functions, both the CER and underlying cost drivers are allowed to range so that all sources of uncertainty can be quantified.

Science, GDS & MOps. These are low-risk cost elements but are subject to cost growth as part of the cost risk analysis.

Payload. The 70th percentile cost model estimate is used to inform the Firefly payload risk model to capture the uncertainty given the CML-4-level design phase.

Spacecraft. Each subsystem is subject to a data-driven risk analysis based on historical APL cost growth. Mass input also varies in the SEER model consistent with early design programs to 30% over current best estimate.

I&T. I&T as a percentage of the payload and spacecraft from the point estimate is used to inform the risk analysis, allowing I&T to vary with hardware cost.

WBS	Cost Element	Point Estimate	High
1,2,3	Mission PMSEMA	$193	$ 268
4	Science	$32	$ 40
5	Payload	$384	$523
6	Spacecraft	$ 679	$970
7	Mission Ops	$24	$ 30
9	GDS	$17	$ 21
10	I&T	$151	$190

Exhibit 75. *Inputs to cost distributions in FY$22M.*

Description	Value (FY$22M)	Confidence Level
Point Estimate	$1,800.1	48.7%
Mean	$2,056.2	
Standard Deviation	$964.0	
Reserves	$740.1	
Total w. Reserves	$ 2,540.2	76.6%

Exhibit 76. *Cost risk analysis.*

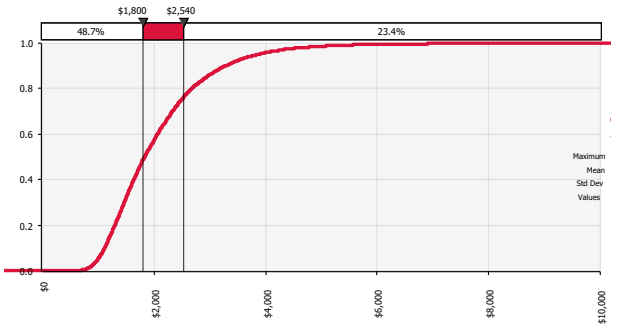

Exhibit 77. *S-curve summary.*

The estimate includes unencumbered cost reserves of 50% of the estimated costs of all Phase A–D elements except for the launch vehicle. A probabilistic cost risk analysis shows 76.6% confidence that the Phase A–D mission is achievable within the estimated costs of this study (Exhibits 76 and 77). The high confidence level is driven primarily by the large cost reserves for this pre-proposal concept. Given a typical competitive pre-Phase A NASA environment with 25% reserves on Phase A–D elements, the probabilistic cost risk analysis shows 64.2% confidence that the Phase A–D mission would be achievable. A 50th- to 70th-percentile confidence level is expected and reasonable for a pre-Phase A concept with this level of reserves.

A coefficient of variation (standard deviation/mean) of approximately 46% indicates appropriate levels of conservatism given the early formulation phase. The model confirms the point estimate and provides a reasonable basis for the Firefly CML-4 study.

5.5. Enhancement & De-Scope Options

The following describes the Firefly mission enhancement and de-scope options. The same estimating methodologies for the baseline mission were applied to the enhancement and De-Scope options. Exhibit 78 summarizes the total Phase A–F estimates both excluding and including the launch vehicle cost estimates.

Options Description	Phase A-D	Phase E-F	Res.*	Launch Vehicle	Total w. Res./excl. LV	Total w. Res. & LV
1	1,133.3	250.8	626.3	246.9	2,010.4	2,257.3
2	1,336.2	250.8	727.8	313.8	2,314.8	2,628.6
3	1,182.2	250.8	650.8	246.9	2,083.8	2,330.7
4	1,385.2	250.8	752.3	313.8	2,388.2	2,702.0
5	1,283.3	250.8	701.3	246.9	2,235.4	2,482.3
6 (Baseline)	1,486.3	250.8	802.8	313.8	2,539.8	2,853.7
7	1,510.7	250.8	815.0	313.8	2,576.5	2,890.4
8	1,522.3	250.8	820.8	313.8	2,593.9	2,907.7
9	1,606.2	250.8	862.8	313.8	2,719.7	3,033.5

Exhibit 78. *Enhancement and De-Scope Option summary estimates (FY22$M).*
*Reserves: 50% Phase B-D, 25% Phase E-F, exclude launch services costs.

5.5.1. Enhancement 3: Option 9

Enhancement 3 takes the baseline mission and adds one EUVI, HI+, SEP, and three SPICES instruments. The summary cost estimate for Enhancement 3 is shown in Exhibit 79.

Instrument	FF-EA	FF-EB	FF-PA	FF-PB
Doppler Vector Magnetograph (DVM)	✓	✓	✓	✓
EUV Imager/Solar Spectral Irradiance (EUV/SSI)	✓	✓	✓	✓
White Light Coronagraph (WLC)	✓	✓	✓	✓
White Light Heliospheric Imager (WL HI)	✓	✓		
Fluxgate Magnetometer (FGM)	✓	✓	✓	✓
Faraday Cup (FC)	✓	✓	✓	✓
Solar Wind Composition (SWC)	✓	✓	✓	✓
Solar Energetic Particle Suite (EPS)	✓	✓	✓	✓

Exhibit 79. *Enhancement 3 summary instrument complement, adding one EUVI, HI+, SEP and three SPICES instruments.*

WBS	Description	Phase A-D	Phase E-F	Total
	Phase A	$6.0	—	$6.0
1/2/3	**PMSEMA**	$209.6	—	$209.6
4	**Science**	$31.8	$148.7	$180.6
5	**Payload**	$475.9	—	$475.9
6	**Spacecraft**	$679.4	—	$679.4
7	**Mission Operations**	$24.1	$98.5	$122.7
8	**LV**	$313.8	—	$313.8
9	**Ground Data Systems**	$16.7	$3.5	$20.2
10	**I&T**	$162.7	—	$162.7
	Subtotal	**$1920.0**	**$250.8**	**$2170.7**
	Reserves	$800.1	$62.7	$862.8
	Total with Reserves	**$2720.0**	**$313.5**	**$3033.5**
	Total without LV	**$2406.2**	**$313.5**	**$2719.7**

Exhibit 80. *Enhancement 3 summary estimate (FY22$M).*

5.5.2. Enhancement 2: Option 8

Enhancement 2 takes the baseline mission and adds one EUVI and SEP instrument (Exhibit 81). The summary cost estimate for Enhancement 2 is shown in Exhibit 82.

Instrument	FF-EA	FF-EB	FF-PA	FF-PB
Doppler Vector Magnetograph (DVM)	✓	✓	✓	✓
EUV Imager/Solar Spectral Irradiance (EUV/SSI)	✓	✓	✓	✓
White Light Coronagraph (WLC)	✓	✓	✓	✓
White Light Heliospheric Imager (WL HI)	✓			
Fluxgate Magnetometer (FGM)	✓	✓	✓	✓
Faraday Cup (FC)	✓	✓	✓	✓
Solar Wind Composition (SWC)			✓	
Solar Energetic Particle Suite (EPS)	✓	✓	✓	✓

Exhibit 81. *Enhancement 2 summary instrument complement, adding one EUVI and one SEP instrument.*

WBS	Description	Phase A-D	Phase E-F	Total
	Phase A	$6.0	—	$6.0
1/2/3	**PMSEMA**	$198.1	—	$198.1
4	**Science**	$31.8	$148.7	$180.6
5	**Payload**	$411.7	—	$411.7
6	**Spacecraft**	$679.4	—	$679.4
7	**Mission Operations**	$24.1	$98.5	$122.7
8	**LV**	$313.8	—	$313.8
9	**Ground Data Systems**	$16.7	$3.5	$20.2
10	**I&T**	$154.6	—	$154.6
	Subtotal	**$1,836.1**	**$250.8**	**$2,086.9**
	Reserves	$758.1	$62.7	$820.8
	Total with Reserves	**$2,594.2**	**$313.5**	**$2,907.7**
	Total without LV	**$2,280.4**	**$313.5**	**$2,593.9**

Exhibit 82. *Enhancement 2 summary estimate (FY22$M).*

5.5.3. Enhancement 1: Option 7

Enhancement 1 takes the baseline mission and adds one EUVI instrument (Exhibit 83). The summary cost estimate for Enhancement 1 is shown in Exhibit 84.

Instrument	FF-EA	FF-EB	FF-PA	FF-PB
Doppler Vector Magnetograph (DVM)	✓	✓	✓	✓
EUV Imager/Solar Spectral Irradiance (EUV/SSI)	✓	✓	✓	
White Light Coronagraph (WLC)	✓	✓	✓	✓
White Light Heliospheric Imager (WL HI)	✓			
Fluxgate Magnetometer (FGM)	✓	✓	✓	✓
Faraday Cup (FC)	✓	✓	✓	✓
Solar Wind Composition (SWC)			✓	
Solar Energetic Particle Suite (EPS)	✓	✓	✓	

Exhibit 83. *Enhancement 1 summary instrument complement, adding one EUVI, HI+, SEP and three SPICES instruments.*

WBS	Description	Phase A-D	Phase E-F	Total
	Phase A	$6.0	—	$6.0
1/2/3	**PMSEMA**	$196.5	—	$196.5
4	**Science**	$31.8	$148.7	$180.6
5	**Payload**	$402.8	—	$402.8
6	**Spacecraft**	$679.4	—	$679.4
7	**Mission Operations**	$24.1	$98.5	$122.7
8	**LV**	$313.8	—	$313.8
9	**Ground Data Systems**	$16.7	$3.5	$20.2
10	**I&T**	$153.4	—	$153.4
	Subtotal	**$1,824.5**	**$250.8**	**$2,075.3**
	Reserves	$752.3	$62.7	$815.0
	Total with Reserves	**$2,576.9**	**$313.5**	**$2,890.4**
	Total without LV	**$2,263.0**	**$313.5**	**$2,576.5**

Exhibit 84. *Enhancement 1 summary estimate (FY22$M).*

5.5.4. Descope 1: Option 5

The first descope option takes the baseline mission and removes one of the FF-P spacecraft (Exhibit 85). The launch vehicle assumption changes to a Falcon Heavy Reusable for the single FF-P spacecraft. The summary cost estimate for Descope 1 is shown in Exhibit 86.

Instrument	FF-EA	FF-EB	FF-PA	FF-PB
Doppler Vector Magnetograph (DVM)	✓	✓	✓	
EUV Imager/Solar Spectral Irradiance (EUV/SSI)	✓	✓	✓	
White Light Coronagraph (WLC)	✓	✓	✓	
White Light Heliospheric Imager (WL HI)	✓			
Fluxgate Magnetometer (FGM)	✓	✓	✓	
Faraday Cup (FC)	✓	✓	✓	
Solar Wind Composition (SWC)			✓	
Solar Energetic Particle Suite (EPS)	✓	✓	✓	

Exhibit 85. *Descope 1 summary instrument complement, removes one Firefly Polar spacecraft and changes to a Falcon Heavy Reusable launch vehicle.*

WBS	Description	Phase A-D	Phase E-F	Total
	Phase A	$6.0	—	$6.0
1/2/3	**PMSEMA**	$165.3	—	$165.3
4	**Science**	$31.8	$148.7	$180.6
5	**Payload**	$350.9	—	$350.9
6	**Spacecraft**	$557.2	—	$557.2
7	**Mission Operations**	$24.1	$98.5	$122.7
8	**LV**	$246.9	—	$246.9
9	**Ground Data Systems**	$16.7	$3.5	$20.2
10	**I&T**	$131.3	—	$131.3
	Subtotal	**$1,530.2**	**$250.8**	**$1,781.0**
	Reserves	$638.6	$62.7	$701.3
	Total with Reserves	**$2,168.8**	**$313.5**	**$2,482.3**
	Total without LV	**$1,921.9**	**$313.5**	**$2,235.4**

Exhibit 86. *Descope1 summary estimate (FY22$M).*

5.5.6. Descope 2: Option 4

The second descope option takes the baseline mission and removes the White Light Heliospheric Imager and Solar Wind Composition Instrument from the payload (Exhibit 87). The summary cost estimate for Descope Option 2 is shown in Exhibit 88.

Instrument	FF-EA	FF-EB	FF-PA	FF-PB
Doppler Vector Magnetograph (DVM)	✓	✓	✓	✓
EUV Imager/Solar Spectral Irradiance (EUV/SSI)	✓	✓	✓	
White Light Coronagraph (WLC)	✓	✓	✓	✓
White Light Heliospheric Imager (WL HI)				
Fluxgate Magnetometer (FGM)	✓	✓	✓	✓
Faraday Cup (FC)	✓	✓	✓	✓
Solar Wind Composition (SWC)				
Solar Energetic Particle Suite (EPS)	✓	✓	✓	

Exhibit 87. *Descope 2 removes the White Light Heliospheric Imager and Solar Wind Composition instrument from the payload.*

WBS	Description	Phase A-D	Phase E-F	Total
	Phase A	$6.0	—	$6.0
1/2/3	**PMSEMA**	$179.2	—	$179.2
4	**Science**	$31.8	$148.7	$180.6
5	**Payload**	$306.7	—	$306.7
6	**Spacecraft**	$679.4	—	$679.4
7	**Mission Operations**	$24.1	$98.5	$122.7
8	**LV**	$313.8	—	$313.8
9	**Ground Data Systems**	$16.7	$3.5	$20.2
10	**I&T**	$141.2	—	$141.2
	Subtotal	**$1,699.0**	**$250.8**	**$1,949.8**
	Reserves	$689.6	$62.7	$752.3
	Total with Reserves	**$2,388.5**	**$313.5**	**$2,702.0**
	Total without LV	**$2,074.7**	**$313.5**	**$2,388.2**

Exhibit 88. *Descope 2 summary estimate (FY22$M).*

5.5.7. Descope 3: Option 3

The third descope option takes the baseline mission, and removes one of the FF-P spacecraft and removes the White Light Heliospheric Imagers, and the Solar Wind Composition Instrument from the payload (Exhibit 89). The launch vehicle assumption changes to a Falcon Heavy Reusable for the single FF-P spacecraft. The summary cost estimate for Descope Option 3 is shown in Exhibit 90.

Instrument	FF-EA	FF-EB	FF-PA	FF-PB
Doppler Vector Magnetograph (DVM)	✓	✓	✓	
EUV Imager/Solar Spectral Irradiance (EUV/SSI)	✓	✓	✓	
White Light Coronagraph (WLC)	✓	✓	✓	
White Light Heliospheric Imager (WL HI)				
Fluxgate Magnetometer (FGM)	✓	✓	✓	
Faraday Cup (FC)	✓	✓	✓	
Solar Wind Composition (SWC)				
Solar Energetic Particle Suite (EPS)	✓	✓	✓	

Exhibit 89. *Descope 3 removes one FF-P spacecraft, and also removes the White Light Heliospheric Imagers and the Solar Wind Composition Instruments.*

WBS	Description	Phase A-D	Phase E-F	Total
	Phase A	$6.0	—	$6.0
1/2/3	**PMSEMA**	$151.4	—	$151.4
4	**Science**	$31.8	$148.7	$180.6
5	**Payload**	$273.5	—	$273.5
6	**Spacecraft**	$557.2	—	$557.2
7	**Mission Operations**	$24.1	$98.5	$122.7
8	**LV**	$246.9	—	$246.9
9	**Ground Data Systems**	$16.7	$3.5	$20.2
10	**I&T**	$121.5	—	$121.5
	Subtotal	**$1,429.1**	**$250.8**	**$1,679.9**
	Reserves	$588.1	$62.7	$650.8
	Total with Reserves	**$2,017.2**	**$313.5**	**$2,330.7**
	Total without LV	**$1,770.3**	**$313.5**	**$2,083.8**

Exhibit 90. *Descope 3 summary estimate (FY22$M).*

5.5.8. Descope 4: Option 2

The fourth descope option takes the baseline mission and removes the White Light Heliospheric Imager and Solar Wind Composition Instrument from the payload (same as Descope Option 2), plus it removes the single EUVI from the FF-P spacecraft (Exhibit 91). The summary cost estimate for Descope Option 4 is shown in Exhibit 92.

Instrument	FF-EA	FF-EB	FF-PA	FF-PB
Doppler Vector Magnetograph (DVM)	✓	✓	✓	✓
EUV Imager/Solar Spectral Irradiance (EUV/SSI)	✓	✓		
White Light Coronagraph (WLC)	✓	✓	✓	✓
White Light Heliospheric Imager (WL HI)				
Fluxgate Magnetometer (FGM)	✓	✓	✓	✓
Faraday Cup (FC)	✓	✓	✓	✓
Solar Wind Composition (SWC)				
Solar Energetic Particle Suite (EPS)	✓	✓	✓	

Exhibit 91. *Descope 4 removes the White Light Heliospheric Imager, Solar Wind Composition instrument, and the EUV Imager.*

WBS	Description	Phase A-D	Phase E-F	Total
	Phase A	$6.0	—	$6.0
1/2/3	**PMSEMA**	$172.5	—	$172.5
4	**Science**	$31.8	$148.7	$180.6
5	**Payload**	$269.2	—	$269.2
6	**Spacecraft**	$679.4	—	$679.4
7	**Mission Operations**	$24.1	$98.5	$122.7
8	**LV**	$313.8	—	$313.8
9	**Ground Data Systems**	$16.7	$3.5	$20.2
10	**I&T**	$136.5	—	$136.5
	Subtotal	**$1,650.0**	**$250.8**	**$1,900.8**
	Reserves	$665.1	$62.7	$727.8
	Total with Reserves	**$2,315.1**	**$313.5**	**$2,628.6**
	Total without LV	**$2,001.3**	**$313.5**	**$2,314.8**

Exhibit 92. *Descope 4 summary estimate (FY22$M).*

5.5.9. Descope 5: Option 1

The fifth descope option takes the previous (Descope 4) configuration, and removes one of the FF-P spacecraft (Exhibit 93). The launch vehicle assumption changes to a Falcon Heavy Reusable for the single FF-P spacecraft. The summary cost estimate for Descope Option 5 is shown in Table Exhibit 94.

Instrument	FF-EA	FF-EB	FF-PA	FF-PB
Doppler Vector Magnetograph (DVM)	✓	✓	✓	
EUV Imager/Solar Spectral Irradiance (EUV/SSI)	✓	✓		
White Light Coronagraph (WLC)	✓	✓	✓	
White Light Heliospheric Imager (WL HI)				
Fluxgate Magnetometer (FGM)	✓	✓	✓	
Faraday Cup (FC)	✓	✓	✓	
Solar Wind Composition (SWC)				
Solar Energetic Particle Suite (EPS)	✓	✓	✓	

Exhibit 93. *Descope 5 assumes Descope 4, plus the removal of one of the FF-P spacecraft; launch vehicle changes to Falcon Heavy Reusable.*

WBS	Description	Phase A-D	Phase E-F	Total
	Phase A	$6.0	—	$6.0
1/2/3	**PMSEMA**	$144.7	—	$144.7
4	**Science**	$31.8	$148.7	$180.6
5	**Payload**	$236.1	—	$236.1
6	**Spacecraft**	$557.2	—	$557.2
7	**Mission Operations**	$24.1	$98.5	$122.7
8	**LV**	$246.9	—	$246.9
9	**Ground Data Systems**	$16.7	$3.5	$20.2
10	**I&T**	$116.7	—	$116.7
	Subtotal	**$1,380.2**	**$250.8**	**$1,630.9**
	Reserves	$563.6	$62.7	$626.3
	Total with Reserves	**$1,943.8**	**$313.5**	**$2,257.3**
	Total without LV	**$1,696.9**	**$313.5**	**$2,010.4**

Exhibit 94. *Descope 5 summary estimate (FY22$M).*

Appendix A. Mission Design Analysis

A.1 Physical Models

All mission design work for Firefly was performed using the Evolutionary Mission Trajectory Generator (EMTG), a trajectory optimization and design tool maintained by APL's Space Astrodynamics and Controls group. EMTG was originally developed at Goddard Space Flight Center and later the development team moved to APL. EMTG has flight heritage from OSIRIS-REx and Lucy, and is used in the development of Europa Clipper, Dragonfly, DAVINCI, Lunar IceCube, LunaH-Map, and Janus, as well as many proposal and concept studies involving both chemical and low-thrust electric propulsion, and has been verified against JPL's MONTE tool and the legacy navigation tool ODP/DPTRAJ. EMTG is capable of low-fidelity design (patched conic flybys, Kepler propagation, Sims-Flanagan approximation for low-thrust electric propulsion), as well as high-fidelity design (integrated trajectory, non-spherical gravity, finite burns). A high-fidelity model of the NEXT-C propulsion system and the spacecraft's power system is used. Initial trade studies and trajectory design were performed using low-fidelity trajectory modeling that leveraged Kepler propagation and patched conic flybys. The final Firefly mission trajectories were optimized in high-fidelity using the setup described in Exhibit A-1

Perturbing-Bodies	Flyby Model	Integrator	Integrator Tolerance	Optimizer	Feasibility Tolerance
Earth, Moon, Sun, Jupiter point mass	Integrated	Variable-step, Variable order Adams-Moulton	1e-10	SNOPT	1e-6

Exhibit A-1. *Dynamics and optimization models used during trajectory optimization.*

The FF-P power system was modeled using a polynomial fit to available power during the 8-year cruise phase. This function takes into account non-propulsion spacecraft power and LILT effects.

$$P(r) = \frac{22.487}{r^2} E(r)$$

$$E(r) = 0.0179\, r^4 - 0.2509\, r^3 + 1.3045\, r^2 - 3.0422\, r + 2.8008$$

The NEXT-C propulsion system is modeled using a Heaviside smooth-stepped fit [Knittel 207] to the NEXT-C Throttle Table 11 data set [Woytach 2017]. Throttle levels 38, 39, and 40 are removed from the set to meet open circuit voltage requirements.

A.2 FF-P Launch Flexibility

The FF-P trajectories depend on the 13-month synodic period of Earth and Jupiter. However, some opportunities are better than others because of Jupiter's inclination. When Jupiter is at its farthest displacement from the Ecliptic plane, the combination of Falcon Heavy, EGA, and SEP is not sufficient to reach the mission orbit with positive neutral mass margin. Accordingly, launch opportunities exist in 2031, 2032, 2033, 2034, and 2036 but not 2035 as shown in Exhibit A-2. Increasing the flight time upper bound from 8 years to 9 years does not enable 2035. Each dot in Exhibit A-2 represents the worst case neutral mass across a 21-day launch period. The out-year trajectories were

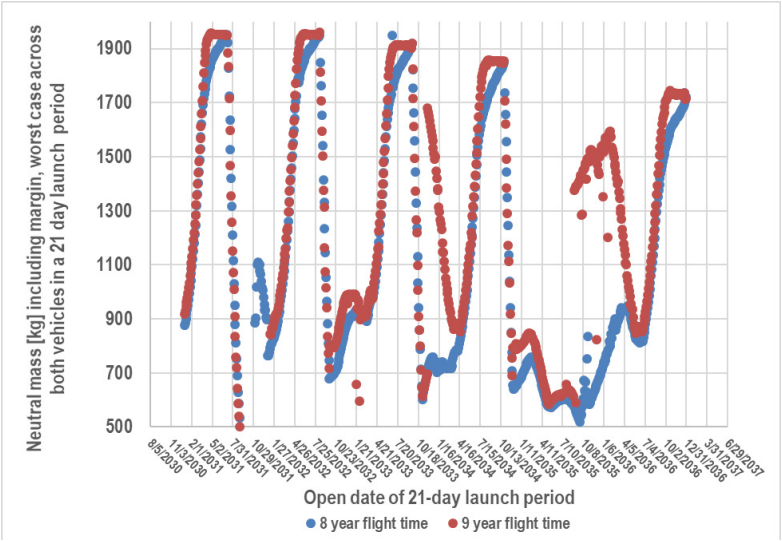

Exhibit A-2*: FF-P can launch in any year from 2031 to 2034. 2035 is not viable due to Jupiter being at its maximum out-of-plane position but launch opportunities will repeat in the late 2030s and 2040s.*

designed in a lower fidelity model than the reference trajectory, using the Sims-Flanagan approximation to low-thrust and patched conic flybys.

A.2 FF-E Launch Flexibility

Exhibit A-3 shows the best LGA_1 date for a launch each day during the 2032, 2033, and 2034 possible launch years. The solutions in Exhibit A-3 were produced using low-fidelity Kepler propagation and the patched-conic flyby model and are optimized to minimize the ΔV between the two spacecraft. There are clear discrete groupings of the LGA_1 occurrences occurring within the lunar cycles. Phasing orbits were used to provide flexibility and maneuvering to target the LGA_1 that best reduces ΔV for both FF-E spacecraft. The low-fidelity solutions represented in Exhibit A-3 are relatively ΔV invariant across the three launch years considered, with the ΔV ranging between 500 and 620 m/s for each spacecraft. As a result, the FF-E launch is extremely flexible throughout the calendar year from a ΔV standpoint and can be chosen to best satisfy budget and operational constraints relative to the FF-P launch. It should be noted that the orientation of the phasing loops varies in the Sun-Earth frame throughout the calendar year and can result in very long eclipses when the Sun-Earth line intersects the orbit near apogee.

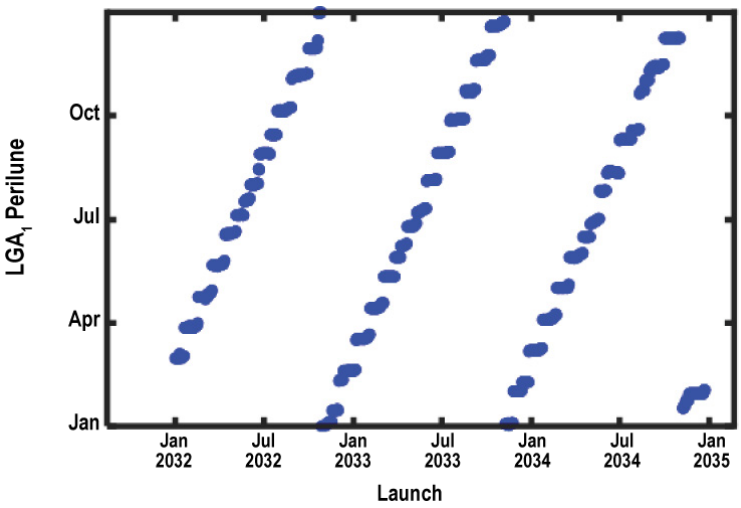

Exhibit A-3. *FF-E LGA_1 occurrence relative to launch date in 2032, 2033, and 2034.*

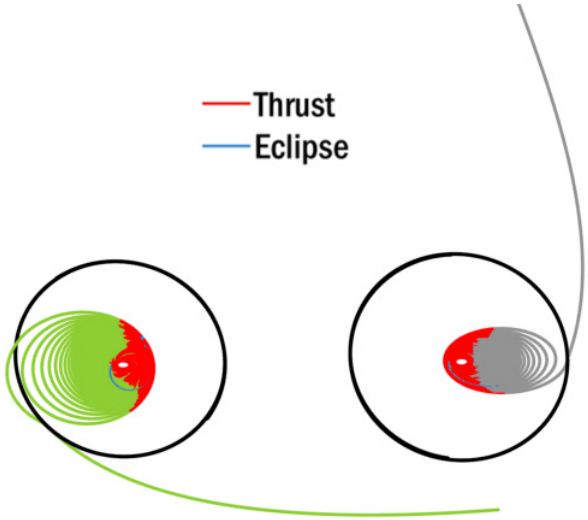

Exhibit A-4. *Sample FF-E low-thrust rideshare trajectories to +120 deg (left) and -120 deg (right) relative to Earth represented in the Earth-centered inertial frame.*

A.3 FF-E Rideshare Opportunity

The FF-E science orbits could also be achieved by low-thrust smallsats leveraging a geostationary transfer orbit (GTO) rideshare and lunar flyby. In this scenario, each of the FF-E spacecraft ride as secondary payloads to GTO. Depending on the available rideshare opportunities, the two spacecraft could either launch together or on separate launch vehicles. Once in orbit, their low-thrust propulsion systems raise the spacecraft orbit to encounter the Moon for a flyby, placing each spacecraft on an escape trajectory leading to their respective science orbits. The low-thrust orbit raising phase of the mission can last many months and allows each spacecraft to target different LGA epochs and locations, resulting in only one LGA needed for each spacecraft. Sample rideshare trajectories are shown and described in Exhibit A-4 and Exhibit A-5, respectively.

Destination	Departure	Initial Orbit Parameters (a km, e, inc°, ω°, Ω°, θ°)	M_0 (kg)	M_f (kg)	Spiral Duration(days)	Arrival
+120°	1 Jan 2030	24364, 0.73, 27, 180, 0, 0	500	395	328	22 Nov 2037
-120°	1 Jan 2030	24364, 0.73, 27, 180, 0, 0	500	405	282	28 Feb 2036

Exhibit A-5. *Sample FF-E orbit parameters to +120 degree and -120 degree relative to Earth.*

Appendix B: Acronyms & Abbreviations

3D	Three Dimensional
ACE	APL Concurrent Engineering
ACS	Attitude Control System
AO	Announcement of Opportunity
APL	(Johns Hopkins) Applied Physics Laboratory
ARC	Avionics Redundant Controller
AU	Astronautical Unit
BOE	Basis of Estimate
BOL	Beginning of Life
BUE	Bottom-Up Estimate
BWG	Beam Waveguide
C/A	Close (Closest) Approach
C&DH	Command and Data Handling
Catbed (Heaters)	Catalyst Bed (Heaters)
CBE	Current Best Estimate
CDM	Compact Doppler Magnetograph
CDR	Critical Design Review
CER	Cost Estimating Relationship
cFE	Core Flight Executive
CFD	Computational Fluid Dynamics
CFDP	CCSDS File Delivery Protocol
CG	Center of Gravity
CIR	Corotating Interaction Regions
CM	Center of Mass
CME	Coronal Mass Ejection
CML	Concept Maturity Level
CMOS	Complementary Metal Oxide Semiconductor
COTS	Commercial Off the Shelf
CP	Center of Pressure
CR	Carrington Rotation
ΔV	Delta (Change in) Velocity
DART	Double Asteroid Redirection Test
DC/DC	Direct-Current to Direct-Current (Converter Card)
DCO	Data Cutoff
DD	Dust Detector
DDOR	Delta Differential One-Way Ranging
DMA	Direct Memory Access
DOE	Department of Energy
DOR	Differential One-Way Ranging
DPLR	Data Parallel Line Relaxation
DPU	Data Processing Unit
DSM	Deep Space Maneuver
DSN	Deep Space Network
DSS	Digital Sun Sensor
DTE	Direct to Earth
DVM	Doppler Vector Magnetograph
EC	Electrical Conductivity
EDS	Entry & Descent System

EELV	Evolved Expendable Launch Vehicle
EFH	Expendable Falcon Heavy
EIT	Extreme ultraviolet Imaging Telescope
EOL	End of Life
EOM	End of Mission
EPC	Electronic Power Conditioner
EPS	Electrical Power Subsystem
EPS	Solar Energetic Particle Suite
ESI	Engineering Science Investigation
ESA	European Space Agency
EUV	Extreme Ultraviolet
EUVI	Extreme Ultraviolet Imager
EVMS	Earned Value Management System
FC	Faraday Cup
FF-E	Firefly-Ecliptic (spacecraft)
FF-P	Firefly-Polar (spacecraft)
FGM	Fluxgate Magnetometer
FIAT	Fully Implicit Ablation and Thermal response
FIPS	Fast Imaging Plasma Spectrometer
FOV	Field of View
FPGA	Field-Programmable Gate Array
FSS	Fine Sun Sensor
FSW	Flight Software
FY	Fiscal Year
G&C	Guidance and Control
GCR	Galactic Cosmic Ray
GDS	Ground Data System
GFE	Government Furnished Equipment
GIC	Geomagnetically Induced Current
GNC	Guidance, Navigation & Control
GOES	Geostationary Operational Environmental Satellite
GOLF	(VIRGO) Global Oscillations at Low Frequencies
GONG	(NSF) Global Oscillation Network Group
GPS	Global Positioning System
GSE	Geocentric Solar Ecliptic System
HAO	High Altitude Observatory
HF	High Frequency
HGA	High-Gain Antenna
HMI	Helioseismic and Magnetic Imager
HSS	High Speed Stream
I&T	Integration and Test
I^2C	Inter-Integrated Circuit
IBR	Integrated Baseline Review
IEM	Integrated Electronics Module
IIF	Instrument Interface (Card)
IMF	Interplanetary Magnetic Field
IMU	Inertial Measurement Unit
INMS	Ion & Neutral Mass Spectrometer
IR	Infrared
IT	Information Technology
IVO	Io Volcano Explorer (Proposed Discovery Mission in Step 2)

JGA	Jupiter Gravity Assist
JHU	Johns Hopkins University
JPL	Jet Propulsion Laboratory
JSC	Johnson Space Center
KBO	Kuiper Belt Object
L/W	Launch Window
LASCO	Large Angle and Spectrometric COronagaph
LASCO C2	LASCO Coronagraph 2
LFF	Linear Force-Free
LEOP	Launch and Early Operations Phase
LGA	Low-Gain Antenna
LGA	Lunar Gravity Assist
LNA	Low-Noise Amplifiers
LOI	(VIRGO) Luminosity Oscillations Imager
LOS	Line of Sight
LPW	(MAVEN) Langmuir Probe & Waves (Instrument)
LRD	Launch Readiness Date
LRM	Low-Reflectance Material
LRR	Launch Readiness Review
LV	Launch Vehicle
LVS	Low-Voltage Sensor
Ma	Million Years
MA	Mission Assurance
MAG	Magnetometer
MDI	Michelson Doppler Imager
MEL	Master Equipment List
MEOP	Maximum Expected Operating Pressure
MER	Mars Exploration Rovers
MEV	Maximum Expected Value
MGA	Medium-Gain Antenna
MHD	Magnetohydrodynamic
MiSC	Mission-Specific Cards
MIGS	Mission Independent Ground Software
MIMU	Miniature Inertial Measurement Unit
MLI	Multi-Layer Insulation
MMH	Monomethylhydrazine
MMRTG	Multi-Mission Radioisotope Thermal Generator
MOC	Mission Operations Center
MOCET	(Aerospace Corp.) Mission Cost Estimating Tool
MON-3	Mixed Oxides of Nitrogen (Nitrogen Tetroxide)
MOps	Mission Operations
MOR	Mission Operations Review
MPV	Maximum Possible Value
MRAM	Magnetoresistive Random-Access Memory
MRR	Mission Readiness Review
MSC	(TRACERS) Search Coil Magnetometer
MSL	Mars Science Laboratory
MUX	Multiplexer
MY	Million Years
NAC	Narrow Angle Camera
NASA	National Aeronautics and Space Administration

NCAR	National Center for Atmospheric Research
NEPA	National Environmental Policy Act
NGRTG	Next-Generation (RTG)
NH	New Horizons
NICM	NASA Instrument Cost Model
NIR	Near Infrared
NLFF	Non-Linear Force-Free
NOI	Neptune Orbit Insertion
NPR	NASA Procedural Requirement
NRC	National Research Council
NRE	Non-Recurring Engineering
OPAG	Outer Planets Assessment Group
ORR	Operational Readiness Review
OSIRIS-REx	Origins, Spectral Interpretation, Resource Identification, Security-Regolith EXplorer
PAF	Payload Adapter Fitting
PBP	Polar Bright points
PCF	Polar Crown Filament
PDB	Propulsion Diode Boxes
PDR	Preliminary Design Review
PDU	Power Distribution Unit
PER	Pre-Environmental Review
PFSS	Potential-Field Source Surfac
PIMMC	Principal Investigator Managed Mission Cost
PIMS	Plasma Instrument for Magnetic Sounding
PM	Project Management
PMCS	Planetary Mission Concept Studies
PMSEMA	Project Management, Systems Engineering, Mission Assurance
POST2	Program to Optimize Simulated Trajectories II
PPS	Pulse Per Second
PPU	Power Processing Unit
PRM	Periapsis Reduction Maneuver
PSP	Parker Solar Probe
PSR	Pre-Ship Review
PSI	Predictive cience In.c
PSU	Power Switching Unit
Q&A	Question & Answer
RCS	Reaction Control System
RDM	Radiation Design Model
RF	Radio Frequency
RHU	Radioisotope Heater Unit
RIO	Remote Input/Output
RIU	Remote Interface Unit
ROM	Rough Order of Magnitude
RPM	Rotations/Revolutions per Minute
RPS	(NASA) Radioisotope Power System(s)
RS	Radio Science
RTG	Radioisotope Thermoelectric Generator
RW	Reaction Wheel
S/C	Spacecraft
S&MA	Safety & Mission Assurance
SBC	Single Board Computer

SCIF	Spacecraft Interface
SDO	Solar Dynamic Observatory
SE	Systems Engineering
SECCHI	Sun-Earth Connection Coronal and Heliospheric Investigation
SEE	Single Effect Effects
SEER	System Evaluation and Estimation of Resources
SEIS-SP	Seismic Experiment for Internal Structure-Short Period
SEP	Solar Electric Propulsion
SEP	Solar Energetic Particle
SIR	Stream Interaction Region
SIR	System Integrations Review
SLS	Space Launch System
SMSR	Safety and Mission Success Review
SOC	Science Operations Center
SOHO	Solar and Heliospheric Observatory
SOLPEX	SOLar Polar EXplorer
SOR	Science Operations Review
SPHERE	Spectro-Polarimetric High-contrast Exoplanet REsearch
SPICE	Space Interferometer for Cosmic Evolution
SPOC	Solar Polar Observing Constellation
SPS	Sun Pulse Sensor
SRAM	Static Random-Access Memory
SRP	Solar Radiation Pressure
SRR	System Requirements Review
SRU	Shunt Regulator Unit
SSI	Solar Spectral Irradiance
SSIRU	Scalable Space Inertial Reference Unit
SSPA	Solid State Power Amplifier
SSR	Solid-State Recorder
STEREO	Solar Terrestrial Relations Observatory
STM	Science Traceability Matrix
STP	Solar Terrestrial Probes
SWAP	(New Horizons) Solar Winds Around Pluto
SWAPI	(IMAP) Solar Winds and Pickup Ions
SWC	Solar Wind Composition
SWOOPS	Solar Win Observations Over the Poles of the Sun
TAC	Thruster/Actuator Card
TCM	Trajectory Correction Maneuver
TID	Total Ionizing Dose
TNID	Total Non-Iodizing Dose
TOF	Time of Flight
TPS	Thermal Protection System
TRACERS	Tandem Reconnection and Cusp Electrodynamics Reconnaissance Satellites
TRL	Technology Readiness Level
TT&C	Tracking, Telemetry and Control
TVC	Thrust Vector Control
TVC	Thrust Vector Control Assembly
TWTA	Travelling Wave Tube Amplifier
UHF	Ultra-High Frequency
UMOD	Uranian Model
USO	UltraStable Oscillator

UV	Ultraviolet
UVIS	Ultraviolet Imaging Spectrometer
V&V	Validation & Verification
VAP	Van Allen Probes
VDA	Vacuum Deposited Aluminum
VIRGO	(SOHO) Variability of solar Irradiance and Graity Oscillations
Vis/NIR	Visible and Near-Infrared (Imaging Spectrometer Instrument)
VLT	Very Large Telescope
WAC	Wide-Angle Camera
WBS	Work Breakdown Structure
WL	White Light
WLC	White Light Coronagraph (see also mini-COR)
WT	Traveling Wave Tube

Appendix C: Institutions Involved in the Mission Concept Study

Academy of Athens Research Center for Astronomy and Applied Mathematics
Catholic University of America
Harvard-Smithsonian Center for Astrophysics
High Altitude Observatory
Johns Hopkins Applied Physics Laboratory (APL)
National Aeronautics and Space Administration (NASA)
Southwest Research Institute (SwRI)
Stanford University
University of California Los Angeles (UCLA)
University of Colorado Boulder
University of Michigan
US Naval Research Laboratory

Appendix D: References

Aerts, C., Christensen-Dalsgaard, J., & Kurtz, D.W. 2010, "*Asteroseismology*," Astronomy and Astrophysics Library. ISBN 978-1-4020-5178-4. Springer Science+Business Media B.V.

Amari, T., Canou, A. and Aly, J.-J. 2014 "Characterizing and predicting the magnetic environment leading to solar eruptions," Nature, 514(7523), pp.465–469. doi: 10.1038/nature13815

Appourchaux, T., Belkacem, K., Broomhall, A.-M., et al. 2010, "*The Quest for the Solar g modes*," Astron. Astrophys. Rev., 18, 197. doi: 10.1007/s00159-009-0027-z

Appourchaux, T. & Pallé, P.L. 2013, "*The History of the g-mode Quest*," in Fifty Years of Seismology of the Sun and Stars. Eds. K. Jain, S.C. Tripathy, F. Hill, J.W. Leibacher, and A.A. Pevtsov. ASP Conference Proceedings, vol. 478, p.125

Appourchaux, T. & Corbard, T. 2019, "*Searching for g modes II. Unconfirmed g-mode detection in the power spectrum of the time series of round-trip travel time*," A&A, 624, A106. doi: 10.1051/0004-6361/201935196

Archontis, V. & Hood, A.W. 2012, "*Magnetic flux emergence: a precursor of solar plasma expulsion*," A&A, 537, 62. doi: 10.1051/0004-6361/201116956

Archontis, V. & Török, T. 2008, "*Eruption of magnetic flux ropes during flux emergence*," A&A, 492(2), L35. doi: 10.1051/0004-6361:200811131

Aschwanden, M.J., Schrijver, C.J. & Malanushenko, A. 2015, "*Blind stereoscopy of the coronal magnetic field*," Sol. Phys., 290(10), pp.2765-2789. doi: 10.1007/s11207-015-0791-z

Bale, S.D., Badman, S.T., Bonnell, J.W., et al. 2019, "*Highly structured slow solar wind emerging from an equatorial coronal hole*," Nature, 576, 237-242. doi: 10.1038/s41586-019-1818-7

Basu, S. 2016, "*Global Seismology of the Sun*," Liv. Rev. Sol. Phys., 13, 2. doi: 10.1007/s41116-016-0003-4

Burkepile, J.T., Hundhausen, A.J., Stanger, A.L., et al. 2004, "*Role of projection effects on solar coronal mass ejection properties: 1. A study of CMEs associated with limb activity*," JGR: Space Physics, 109(A3) . doi: 10.1029/2003JA010149

Charbonneau, P. 2020, "*Dynamo models of the solar cycle*," Liv. Rev. Sol. Phys., 17:4. doi: 10.1007/s41116-020-00025-6

Cranmer, S.R., Gibson, S.E., & Riley, P. 2017, "*Origins of the ambient solar wind: Implications for Space Weather*," Space Sci. Rev., 212, 1345-1384. doi: 10.1007/s11214-017-0416-y

Dalmasse, K., Savcheva, A., Gibson, S.E., et al. 2019, "*Data-optimized Coronal Field Model. I. Proof of Concept*," ApJ, 877(2), 111. doi: 10.3847/1538-4357/ab1907

DeRosa, M.L., Schrijver, C.J., Barnes, G., et al. 2009, "*A critical assessment of nonlinear force-free field modeling of the solar corona for active region 10953*," ApJ, 696(2), 1780. doi: 10.1088/0004-637X/696/2/1780

Desai, M. & Giacalone, J. 2016, "*Large gradual solar energetic particle events*," Liv. Rev. Sol. Phys., 13, 3. doi: 10.1007/s41116-016-0002-5

Dikpati, M., Gilman, P.A., de Toma, G., et al. 2010, "*Impact of changes in the Sun's conveyor-belt on recent solar cycles*," Geophys. Res. Lett., 37, L14107. doi: 10.1029/2010GL044143

Dikpati, M. 2014, "*Generating the Sun's global meridional circulation from differential rotation and turbulent Reynolds stresses*," MNRAS, 438, 2380. doi: 10.1093/mnras/stt2353

Dikpati, M., Cally, P.S., McIntosh, S.W., et al. 2017, "*The Origin of the "Seasons" in Space Weather*," Scientific Reports, 7, 14750. doi: 10.1038/s41598-017-14957-x

Drake, J.F. & Swisdak, M. 2012, "*Ion Heating and Acceleration During Magnetic Reconnection Relevant to the Corona*," Space Sci. Rev., 172, 227. doi: 10.1007/s11214-012-9903-3

Elliott, H.A., Henney, C.J., McComas, D.J., et al. 2012, "*Temporal and radial variation of the solar wind temperature-speed relationship*," JGR, 117, A09102. doi: 10.1029/2011JA017125

Fan, Y. & Gibson, S.E. 2007, "*Onset of coronal mass ejections due to loss of confinement of coronal flux ropes*," ApJ, 668, 1232. doi: 10.1086/521335

Fan, Y. 2017, "*MHD simulations of the eruption of coronal flux ropes under coronal streamers*," ApJ, 844, 26. doi: 10.3847/1538-4357/aa7a56

Fan, Y. & Liu, T. 2019, "*MHD simulation of prominence-cavity system*," Front. Astron. Space Sci., 6, 27. doi: 10.3389/fspas.2019.00027

Feynman, J. & Martin, S.F. 1995, "*The initiation of coronal mass ejections by newly emerging magnetic flux*," JGR, 100, 3355. doi: 10.1029/94JA02591

Forbes, T.G. 2000, "*A review on the genesis of coronal mass ejections*," JGR: Space Physics, 105(A10), 23153. doi: 10.1029/2000JA000005

Gallet, F., Charbonnel, C., Amard, L., et al. 2017, "*Impacts of stellar evolution and dynamics on the habitable zone: The role of rotation and magnetic activity*," A&A, 597, A14. doi: 10.1051/0004-6361/201629034

Giacalone, J. 2010, "*Energetic particle transport*," Heliophysics: Space Storms and Radiation: Causes and Effects. Eds. C. J. Schrijver and G. L. Siscoe, p233. ISBN: 9780521760515

Gibson, S.E., Kucera, T.A., White, S.M., et al. 2016, "*FORWARD: A toolset for multiwavelength coronal magnetometry*," Front. Astron. Space Sci., 3, 8. doi: 10.3389/fspas.2016.00008

Gibson, S.E., Vourlidas, A., Hassler, D.M., et al. 2018, "*Solar Physics from Unconventional Viewpoints*," Front. Astron. Space Sci., 5, 32. doi: 10.3389/fspas.2018.00032

Gibson, S.E., de Toma, G., Malanushenko, A., et al. 2020, "*The Science Case for a 4π Perspective: A Polar/Global View of Space Weather Origins*," Helio2050 White Papers #4059

Goldstein, B.E., Smith, E.J., Balogh, A., et al. 1995, "*Properties of magnetohydrodynamic turbulence in the solar wind as observed by Ulysses at high heliographic latitudes*," GRL, 22, 3393. doi: 10.1029/95GL03183

Gopalswamy, N., Dal Lago, A., Yashiro, S., et al. 2009, "*The expansion and radial speeds of coronal mass ejections*," Cent. Eur. Astrophys. Bull. 33, 115

Hassler, D.M., Wilhelm, K., Lemaire, P., et al. 1997, "*Observations of Polar Plumes with the Sumer Instrument on SOHO*," Sol. Phys., 175, 375. doi: 10.1023/A:1004959324214

Hathaway, D.H., & Upton, L.A. 2021, "*Hydrodynamic Properties of the Sun's Giant Cellular Flows*," ApJ, 908, 160. doi: 10.3847/1538-4357/abcbfa

Howe, R. 2009, "*Solar I*nterior Rotation and its Variation," Liv. Rev. Sol. Phys., 6, 1. doi: 10.12942/lrsp-2009-1

Karna, M.L., Karna, N., Saar, S.H., et al. 2020, "*A study of equatorial coronal holes during the maximum phase of four solar cycles*," ApJ, 901, 124. doi: 10.3847/1538-4357/abafae

Kliem, B. & Török, T. 2006, "*Torus instability*," PRL, 96, 255002. doi: 10.1103/PhysRevLett.96.255002

Knittel, J., Englander, J. Ozimek, M., Atchison, J. and Gould, J. , "*Improved Propulsion Modeling for Low-Thrust Trajectory Optimization*," in *Space Flight Mechanics Meeting*, San Antonio, TX, 2017

Kramar, M., Inhester, B. & Solanki, S.K. 2006, "*Vector tomography for the coronal magnetic field-I. Longitudinal Zeeman effect measurements*", A&A, 456, 665. doi: 10.1051/0004-6361:20064865

Kramar, M., Airapetian, V. & Lin, H. 2016, "*3D global coronal density structure and associated magnetic field near solar maximum*," Front. Astron. Space Sci., 3, p.25. doi: 10.3389/fspas.2016.00025

Lee, M.A., Mewaldt, R.A. & Giacalone J. 2012, "*Shock acceleration of ions in the heliosphere*," Space Sci. Rev. 173, 247. doi: 10.1007/s11214-012-9932-y

Lee, C.O., Arge, C.N., Odstrčil, D., et al. 2013, "*Ensemble modeling of CME propagation*," Sol. Phys., 285, 349. doi: 10.1007/s11207-012-9980-1

Linker, J.A., Caplan, R.M., Downs, C. et al. 2017 "The Open Flux Problem," ApJ, 848(1), 70. doi: 10.3847/1538-4357/aa8a70

Löptien, B., Gizon, L., Birch, A.C., et al. 2018, "Global-scale equatorial Rossby waves as an essential component of solar internal dynamics," Nature Astronomy, 2, 568. doi: 10.1038/s41550-018-0460-x

Lüftinger, T., Güdel, M., & Johnstone, C. 2015, "*Stellar magnetic activity and their influence on the habitability of exoplanets*," in Polarimetry: From the Sun to Stars and Stellar Environments, Proceedings IAU Symposium 305, 333–339, K.N. Nagendra, S. Bagnulo, R. Centeno, & M. J. Martínez González, eds. doi: 10.1017/S1743921315005001

Malanushenko, A., Schrijver, C.J., DeRosa, M.L., et al. 2014, "*Using coronal loops to reconstruct the magnetic field of an active region before and after a major flare*," ApJ, 783, 102. doi: 10.1088/0004-637X/783/2/102

Marsden, R.G. 2001, "*The heliosphere after Ulysses*," Astrophys. Space Sci., 277, 337. doi: 10.1023/A:1012260014646

McComas, D.J., Ebert, R.W., Elliott, H.A., et al. 2008, "Weaker solar wind from the polar coronal holes and the whole Sun," Geophys. Res. Lett, 35, L18103. doi: 10.1029/2008GL034896

McIntosh, S.W., Cramer, W.J., Pichardo M., et al. 2017, "*The Detection of Rossby-Like Waves on the Sun*," Nature Astronomy, vol. 1, id. 0086. doi: 10.1038/s41550-017-0086

Mewaldt, R.A. 2006, "*Solar Energetic Particle Composition, Energy Spectra, and Space Weather*," Space Sci. Rev., 124, 303. doi: 10.1007/s11214-006-9091-0

Nandy, D., Muñoz-Jaramillo, A., & Martens, P.C.H. 2011, "*The unusual minimum of sunspot cycle 23 caused by meridional plasma flow variations*," Nature, 471, 80. doi: 10.1038/nature09786

Pevtsov, A.A., Bertello, L., MacNeice, P., et al. 2016, "*What if we had a magnetograph at Lagrangian L5?*," Space Weather, 14, 1026. doi: 10.1002/2016SW001471

Pizzo, V. 1978, "*A three-deminsional model of corotating streams in the solar wind 1. Theoretical foundations*,"J. Geophys. Res., 83, 5563. doi: 10.1029/JA083iA12p05563

Poduval, B., Petrie, G., & Bertello, L. 2020, "*Uncertainty estimates of solar wind prediction using HMI photospheric vector and spatial standard deviation maps*," Sol. Phys., 295, 138. doi: 10.1007/s11207-020-01704-1

Raymond, J.C., Krucker, S., Lin, R.P., et al. 2012, "*Observational Aspects of Particle Acceleration in Large Solar Flares*," Space Sci. Rev., 173, 197. doi: 10.1007/s11214-012-9897-x

Reames, D.V. 1999, "*Particle acceleration at the Sun and in the heliosphere*," Space Sci. Rev., 90, 413. doi: 10.1023/A:1005105831781

Riley, P., Ben-Nun, M., Linker, J.A., et al. 2014, "*A multi-observatory inter-comparison of line-of-sight synoptic solar magnetograms*," Sol. Phys., 289, 769. doi: 10.1007/s11207-013-0353-1

Riley, P., Linker, J.A., Mikić, Z., et al. 2019, "Can an unobserved concentration of magnetic flux above the poles of the Sun resolve the open flux problem?," ApJ, 884, 18. doi: 10.3847/1538-4357/ab3a98

Rouillard, A.P. 2011, "*Relating white light and in situ observations of coronal mass ejections: a review*," J. Atmos. Solar-Terr. Phys. 73, 1201. doi: 10.1016/j.jastp.2010.08.015

Savcheva, A.S., Pariat, E., van Ballegooijen, A.A. et al. 2013, "*A Topological View at CME/flare Features with Application to 3D Reconnection*," Solar Heliospheric and INterplanetary Environment (SHINE 2013), p.143. doi:

Schrijver, C.J. & Title, A.M. 2011, "*Long-range magnetic couplings between solar flares and coronal mass ejections observed by SDO and STEREO*," JGR: Space Physics, 116, A04108. doi: 10.1029/2010JA016224

Schwenn, R., dal Lago, A., Huttunen, E., et al. 2005, "*The association of coronal mass ejections with their effects near the Earth*," Ann. Geophys., 23, 1033. doi: 10.5194/angeo-23-1033-2005

Sterling, A.C. 2018, "*Coronal jets and the jet-CME connection*," J. Phys. Conf. Ser., 1100, 012024. doi: 10.1088/1742-6596/1100/1/012024

Temmer, M., Preiss, S. & Veronig, A.M. 2009. "*CME projection effects studied with STEREO/COR and SOHO/LASCO*," Sol. Phys., 256, 183. doi: 10.1007/s11207-009-9336-7

Thompson, M.J., Christensen-Dalsgaard, J., Miesch, M.S., et al. 2003, "*The Internal Rotation of the Sun*," ARAA, 41, 599. doi: 10.1146/annurev.astro.41.011802.094848

Titov, V.S., Mikic, Z., Török, T., et al. 2012, "*2010 August 1-2 sympathetic eruptions. I. Magnetic topology of the source-surface background field*," ApJ, 759, 70. doi: 10.1088/0004-637X/759/1/70

Titov, V.S., Mikić, Z., Török, T., et al. 2017, "*2010 August 1–2 Sympathetic Eruptions. II. Magnetic Topology of the MHD Background Field*," ApJ, 845, 141. doi: 10.3847/1538-4357/aa81ce

Török, T., Panasenco, O., Titov, V.S., et al. 2011, "*A model for magnetically coupled sympathetic eruptions*," ApJL, 739, L63. doi: 10.1088/2041-8205/739/2/L63

Tsuneta, S., Ichimoto, K., Katsukawa, Y., et al. 2008, "*The Magnetic Landscape of the Sun's Polar Region*," ApJ, 688, 1374. doi: 10.1086/592226

Tziotziou, K., Georgoulis, M.K., & Raouafi, N.E. 2012, "*The Magnetic Energy-Helicity Diagram of Solar Active Regions*," ApJL, 759, L4. doi: 10.1088/2041-8205/759/1/L4

Verbanac, G., Vršnak, B., Veronig, A., et al. 2011, "*Equatorial coronal holes, solar wind high-speed streams, and their geoeffectiveness*," A&A, 526, 13. doi: 10.1051/0004-6361/201014617

Vourlidas, A., Lynch, B.J., Howard, R.A., et al. 2013, "*How Many CMEs Have Flux Ropes? Deciphering the Signatures of Shocks, Flux Ropes, and Prominences in Coronagraph Observations of CMEs*," Sol. Phys., 284, 179. doi: 10.1007/s11207-012-0084-8

Webb, D.F., & Howard, T.A. 2012 "*Coronal mass ejections: Observations*," Living Reviews in Solar Physics, 9, 3. doi: 10.12942/lrsp-2012-3

Woytach, J., Patterson, M., Soulas, G., Aulisio, M. and Shastry, R., "*NASA's Evolutionary Xenon Thruster - Commercial (NEXT-C): Throttle Table Baseline*," NASA Glenn Research Center, Cleveland, OH, 2017.

Yeates, A.R. & Mackay, D.H. 2012, "*Chirality of High-latitude Filaments over Solar Cycle 23*," ApJL, 753, L34. doi: 10.1088/2041-8205/753/2/L34

Appendix E: Additional Details

See separate file for Appendix D details.